ON THE ELECTRONIC STRUCTURE AND THERMODYNAMICS OF ALLOYS

CHRISTOPHE H. SIGLI

Submitted in partial fulfillment of the
requirements for the degree
of Doctor of Philosophy
in the Graduate School of Art and Sciences

COLUMBIA UNIVERSITY
1986

ABSTRACT

ON THE ELECTRONIC STRUCTURE AND THERMODYNAMICS OF ALLOYS

CHRISTOPHE H. SIGLI

A free energy formalism is developed in order to describe phase equilibria in binary alloys. The proposed phenomenological approach uses a limited number of experimental data to provide a global thermodynamic description of a system including its equilibrium and metastable phase diagrams. Emphasis is placed on the description of short range order by means of the cluster variation method.

A microscopic theory is also developed in order to predict the enthalpies of formation of transition metal alloys as well as the short range order dependence of these enthalpies. The theory uses a tight-binding Hamiltonian together with the generalized perturbation method. Off-diagonal disorder is taken into account, and charge transfer is treated self-consistently in the random alloy. All input parameters to the theory are obtained from ab-initio calculations for the pure elements. In this regard, the model can be considered parameter free.

The phenomenological approach has been used to analyzed the Al-Ni, Ni-Cr, and Al-Li systems. It is found that the vibrational entropy of formation plays an important role in the thermodynamics of the Al-Li

and Ni-Cr alloys. The approach allows an accurate description of stable and metastable order-disorder or order-order equilibria existing in the Ni-Al or AL-Li systems. The model is used to predict a metastable clustering tendency in Al-Li alloys which appears to have been recently confirmed by experiment.

The microscopic theory has been applied to the VB-VIB and IVB-VIIIB (Ni, Pt, Pd) alloys. The calculations are in good agreement with the available experimental data and phase diagram information. It is shown that off-diagonal disorder and electronic self-consistency play a crucial role in the accuracy of the results.

TABLE OF CONTENTS

LIST OF FIGURES

LIST OF TABLES

ACKNOWLEDGEMENTS

This thesis work has been carried out at the Henry Krumb School of Mines in the division of Metallurgy and Material Science.

I would like to express my gratitude to Professor Juan Sanchez, my research adviser, for the guidance and encouragement I have received from him throughout my thesis work. His precious scientific knowledge that he has shared with me has been greatly appreciated.

My gratitude is extended to the French Government and the National Science Foundation for funding this work.

I am indebted to the members of my examination board, Professors Gertrude Neumark, Juan Sanchez, Jim Skinner, Ulrich Stimming, and John Tien.

I would also like to thank all the students of the department for their friendship and their support. They have made my stay at Columbia very enjoyable.

I am indebted to my parents, Paul and Paulette, who have always supported and encouraged me in all aspects of my life.

Finally, let a very special thought go to my wife, Katrine.

à Katrine,

à Paul et Paulette.

1. INTRODUCTION

An important factor in the development of new alloys is the detailed knowledge of phase diagrams of stable and metastable phases. Until the beginning of this century, a considerable amount of effort has been invested in increasing the body of experimental thermodynamic data on phase diagrams. However, experimental phase diagram determination is cumbersome, and many systems are not yet well characterized. For example, the lack of experimental data has led to the proposal of five different phase diagrams for the Cr-Ni system. A theoretical approach is therefore recognized to be a very important complementary tool to guide, understand and unify the experimental data.

The main objective of this thesis is to develop reliable phenomenological methods for the calculation of thermodynamic potentials and phase diagrams in binary alloys. In addition, microscopic electronic theories are investigated and used to compute the energy of alloy formation for transition metals.

By far, most investigations of phase equilibria performed in the past are based on phenomenological models which rely heavily on existing phase diagrams and thermochemical data. A semi-empirical approach along such lines has been successfully implemented by Kaufman et al. [1-4] who developed an extensive free energy data-base for transition metal alloys. The general procedure consists in using a subregular solution model to fit experimental thermodynamic data and

available phase diagram information. In addition to equilibrium free energies, the data-base provides lattice stability energies for the pure elements in their metastable phases. With the exception of ordered phases, which are treated by Kaufman and co-workers as stoichiometric compounds, the overall agreement between experimental phase diagrams and those obtained from the semi-empirical free energies is excellent. The subregular solution model and its generalization to ordered compounds, the Bragg-Williams approximation, has also been used extensively to characterize alloy free energies and to compute equilibrium phase diagrams [5-9]. This semi-empirical approach tends to produce a more realistic description of non-stoichiometric ordered compounds due to the improved treatment of the configurational entropy of ordered phases by means of sublattices [5,7].

A feature common to free energy functions based on the subregular solution model and/or the Bragg-Williams approximation is that Short Range Order (SRO) is not explicitly included in the configurational entropy. It must be emphasized that SRO plays a significant role on phase equilibria although its contribution to the alloy's total free energy of mixing is usually small. Thus, SRO effects are commonly incorporated into the Bragg-Williams models by means of a phenomenological expansion of the excess free energy in powers of temperature and composition. This essentially empirical approach to the description of the configurational free energy has, however, some important limitations. Among the most significant of such limitations is the fact that the configurational entropy cannot be properly

approximated by a polynomial expansion over extended temperature and composition ranges. In addition, the Bragg-Williams approximation, when applied to a simple FCC model alloy with nearest neighbor interactions, fails to describe general features of the equilibrium phase diagram [10,11]. Consequently, free energy functions obtained by fitting equilibrium data in binary alloys cannot be extrapolated with confidence to treat, for example, metastable phases or multicomponent systems.

A relatively straightforward and computationally efficient way of introducing SRO in the description of binary and multicomponent alloys is by means of the Cluster Variation Method (CVM) [12]. The CVM, investigated extensively over the last ten years or so, has been shown to be a reliable and powerful statistical mechanics approximation for the study of short- and long-range order in alloys [13-22]. The method has also been used to compute phase diagrams for model binary [11,19,20] and ternary [21,22] systems. Most of the implementations of the CVM, however, are based on internal energy approximations in which pair and many-body interactions are assumed to be concentration independent. Thus, the resulting ordering phase diagrams can only describe equilibrium between superstructures based on a unique crystal lattice. Recently, the more general problem of incoherent equilibrium, i.e. equilibrium between phases based on different crystal structures, has been investigated with the CVM by Sigli and Sanchez using lattice parameter dependent pair potentials [20].

First principle characterization of the internal energy of alloys,

and in particular of the effect of SRO in alloy cohesion, has also been the subject of considerable interest during the last decade. Some techniques are based on truly ab-initio electronic structure calculations. For example, Connolly and Williams [23] have deduced pair and many-body interactions from the cohesive energies of ordered compounds calculated using the density-functional theory. These interactions could then be used to describe the enthalpy of formation of disordered alloys. This approach, which relies strictly on localized interactions for the description of the enthalpy of formation, has not been put to a quantitative test against experimental thermodynamic data or phase diagram calculations. Another ab-initio approach has been proposed which consists in calculating the energy of the random alloy by means of the Korringa-Kohn-Rostoker Coherent-Potential-Approximation (KKR-CPA). The KKR-CPA approach uses a muffin-tin potential [24] and has recently been made charge self-consistent within the framework of the local density functional theory [25]. Although the KKR-CPA appears to be a very promising method for future applications, it still needs further improvement in order to achieve sufficient accuracy in the calculation of the enthalpy of formation. Recently, Hawkins, Robbins, and Sanchez have used the Cluster-Bethe-Lattice Method (CBLM) together with a model tight-binding Hamiltonian (TB-CBLM) in order to investigate the thermodynamic properties of the bcc based systems Cr-Mo, Cr-W and Mo-W [26-27]. Their results are in general agreement with the experiments and have shown that, in order to obtain accurate enthalpies of formation, one must include off-diagonal disorder in the tight-binding Hamiltonian and, in addition, carry out a self-consistent treatment of

charge transfer. The CBLM, however, replaces the real lattice by a fictitious topological structure (Cayley Tree) that reflects the actual coordination number of the lattice but has no closed rings [26-30].

An alternative way of describing SRO in alloys has been proposed by Gautier, Ducastelle and co-workers, who describe the ordering energy of transition metal alloys by expanding the energy of the random mixture, calculated with a tight-binding Hamiltonian and the single site Coherent Potential Approximation (TB-CPA), in power of concentration fluctuations. This approach, known as the Generalized Perturbation Method (GPM), suggests that the alloy enthalpy of formation may be conveniently written as the sum of a non-local energy term (associated with the random alloy) plus a strictly local ordering energy contribution which itself can be accurately approximated in terms of localized pair and/or many-body interactions [31-36]. Unlike the TB-CBLM, the TB-CPA-GPM method can be applied to the actual structure of the alloy and should provide a more accurate description of the bulk thermodynamic properties of alloys. The enthalpies of formation calculated with the TB-CPA-GPM have been, until now, too inaccurate to be used in the calculation of a phase diagram. It should be noticed, however, that the effects of off-diagonal disorder and electronic self-consistency have been generally neglected in such calculations. In the light of the recent TB-CBLM results [26-27], the inaccuracies observed in the TB-CPA-GPM calculations should be explained, in most cases, by off-diagonal disorder and electronic self-consistency effects.

2. OBJECTIVES AND STRATEGY

The main objective of this thesis is to develop a realistic model for the free energy functions of solid phases in binary alloys. The emphasis is placed on the calculation of phase diagrams and on the description of order-disorder reactions. For the reasons mentioned in the introduction, the free energy formalism must include explicitly short- and long-range order. In general, the free energy of a binary alloy is given by:

$$F = x_1 F_1 + x_2 F_2 + \Delta H_f - T \Delta S_f \qquad (1)$$

where x_i and F_i are, respectively, the atomic concentration and the free energy of pure element "i", where ΔH_f is the alloy enthalpy of formation (function of SRO), and where ΔS_f is the alloy entropy of formation (function of SRO). In addition, ΔS_f can be written as the sum of a configurational entropy (ΔS_{conf}) plus a vibrational entropy of formation (ΔS_{vib}):

$$\Delta S_f = \Delta S_{conf} + \Delta S_{vib} \qquad (2)$$

The cluster variation method, which provides an accurate description of short- and long-range order in alloys, has been used to calculate the configurational entropy. The other terms in Eq.(1) can be determined from experimental data by means of a phenomenological model, or they can be calculated from first principles. A first principle calculation has advantages over a phenomenological approach since it does not rely on the existence and the accuracy of experimental data, and it gives deep physical insights into the

different contributions to the free energy.

The first part of this thesis is devoted to the global description of binary alloy phase diagrams. Due to the major difficulties involved in a first principle calculation of all the energy contributions to the free energy, we have used a strictly phenomenological approach where the energy parameters are determined by reproducing a few experimental data points. Some typical applications of the approach are given for the Li-Al, Al-Ni, Ni-Cr systems for which the complete equilibrium phase diagram is calculated. In addition, the method is used to describe metastable equilibria in the Al-Li system where a metastable clustering reaction is predicted at low temperature.

As already mentioned, a first principle calculation of all the energy parameters entering the free energy expression of Eq.(1) is a very difficult task. However, the recent results obtained by Hawkins et al. have shown that it is feasible, using a TB Hamiltonian, to calculate enthalpies of formation for the VIB binary alloys which are in fair agreement with experiments. In the second part of this thesis, we present calculations of the enthalpy of formation of transition metal alloys based on the TB-CPA-GPM method. The local electronic density of states is obtained by means of the recursion method. We show that accurate enthalpies of formation can be calculated by treating electronic self-consistency and off-diagonal disorder in the TB-CPA-GPM approach.

3. FREE ENERGY FORMALISM

3.1 Free Energy of The Pure Elements

The free energy of a pure element in a given structure ζ is written as a linear function of temperature (T):

$$F_i^{\zeta} = H_i^{\zeta} - T\, S_i^{\zeta} \tag{3}$$

where both the enthalpy H_i^{ζ} and the vibrational entropy S_i^{ζ} are temperature independent. It is convenient to refer F_i^{ζ} to the free energy of the same element in a reference structure θ:

$$F_i^{\theta->\zeta} = H_i^{\theta->\zeta} - T\, S_i^{\theta->\zeta} \tag{4}$$

where:

$$H_i^{\theta->\zeta} = H_i^{\zeta} - H_i^{\theta} \tag{5}$$

$$S_i^{\theta->\zeta} = S_i^{\zeta} - S_i^{\theta} \tag{6}$$

The reference structure is generally chosen to be a structure for which the element is stable in a given range of temperature. Note that the reference structure does not need to be the same for the two elements "1" and "2". Values of $H_i^{\theta->\zeta}$ and $S_i^{\theta->\zeta}$ are generally available; they can be taken from experimental data (see for example Hultgren et al [37]) when the pure element is in a stable structure, or from the data base of Kaufman and Nesor [31,36] when it is in a metastable or unstable structure.

3.2 Energy of Formation

The form for the alloy enthalpy of formation to be adopted in this work has been suggested by the recent CPA-GPM calculations of Gautier, Ducastelle and co-workers [31-36]. In this approach, the total enthalpy of formation is written as the sum of the random alloy enthalpy of formation (E_{rand}) plus the ordering energy (E_{ord}) which includes both short- and long-range order. The ordering energy takes the form of a cluster expansion involving concentration dependent effective interactions for pairs, triplets, etc... [33,36]. Thus, the energy of alloy formation per lattice point, ΔH_f, is written as:

$$\Delta H_f = E_{rand} + E_{ord} \tag{7}$$

Although the total enthalpy of formation of transition metal alloys cannot be expressed as a sum of pair and/or many-body interactions, the GPM results indicate that the ordering energy may be approximated very accurately in terms of localized interactions. Moreover, for the case of the non magnetic transition metals, the leading contributions to the ordering energy are given by pair interactions which extend to first nearest neighbors in the FCC lattice [33,34,36] and to first and second nearest neighbors in the BCC lattice [34,36].

In what follows, only pair interactions will be included in the expression of the ordering energy [34]. The ordering energy takes then the form:

$$E_{ord} = (1/2) \sum_{k} \sum_{ij} \omega_k \, (y_{ij}^{(k)} - x_i \, x_j) \, V_{ij}^{(k)} \qquad (8)$$

where ω_k is the coordination number for the k^{th} nearest neighbor pair, and where $y_{ij}^{(k)}$ and $V_{ij}^{(k)}$ are respectively the pair probability and the pair interaction of the k-pair in the configuration $\{ij\}$ (i,j=1,2). Note that for a random alloy, we have:

$$y_{ij}^{(k)} = x_i \, x_j \qquad (9)$$

and, as expected, the ordering energy vanishes. Eq.(8) can be written in a more compact form using correlation functions [15,38].

$$\Delta E_{ord} = (1/2) \sum_{k} \omega_k \, V_k \, (\xi_2^{(k)} - \xi_1^{\,2}) \qquad (10)$$

where the pair correlation function $\xi_2^{(k)}$ and the point correlation function ξ_1 are defined respectively by:

$$\xi_2^{(k)} = y_{11}^{(k)} + y_{22}^{(k)} - 2 \, y_{12}^{(k)} \qquad (11)$$

$$\xi_1 = x_1 - x_2 \qquad (12)$$

and where the effective pair interaction (EPI), V_k, for the k^{th} nearest neighbor pair is defined by:

$$V_k = (1/4) \, (V_{11}^{(k)} + V_{22}^{(k)} - 2 \, V_{12}^{(k)}) \qquad (13)$$

The magnitude of the EPIs decreases very rapidly as the inter-atomic distance increases, and accordingly, only a few neighbor pair interactions must be considered in Eq.(10). In practice, the first nearest neighbor EPI will be retained for FCC-based phases (A_1,

$L1_2$, $L1_0$, ...), whereas first and second nearest neighbor EPIs will be considered for BCC-based phases (A_2, B_2, B_{32},...).

For a given concentration, the relative magnitude and sign of the EPIs determine which ordered structure is the most stable at 0 K [39-43]. For finite temperature calculations, the alloy entropy of formation must also be taken into account in the analysis. It should be noticed that in the absence of second nearest neighbor pair interaction (V_2), the $L1_2$ and DO_{22} structures are degenerate in energy since, as shown by the ground state analysis [39,40], these phases are stable for, respectively, $V_2/V_1 < 0$ and $0 < V_2/V_1 < 1/2$. This degeneracy, however, is lifted at non zero temperatures by the configurational entropy, and the $L1_2$ phase is the stable structure.

The random alloy enthalpy of formation, E_{rand}, can be expressed using the following polynomial expansion in the point correlation ξ_1 :

$$E_{rand} = (1 - \xi_1^2) \left[\sum_{n=0,p} h_n \xi_1^n \right] \qquad (14)$$

The phenomenological expansion of Eq.(14) is such that E_{rand} vanishes when ξ_1 equals 1 (pure component 1) or -1 (pure component 2).

3.3 Vibrational Entropy of Formation

The vibrational entropy of formation is, in general, a function of both short range order (SRO) and long range order (LRO) [44-46]. However, the concentration dependence of ΔS_{vib} is expected to be

predominant and will be the only one considered in our treatment. In practice, we will express ΔS_{vib} by the following phenomenological expansion in powers of the point correlation:

$$\Delta S_{vib} = (1 - \xi_1^2) \left[\sum_{n=0,p} s_n \xi_1^n \right] \quad (15)$$

3.4 Configurational Entropy

In the present model, different approximations will be used for the configurational entropy depending on the nature of the phase being studied. Three families of phases are distinguished: the strictly stoichiometric compounds for which the configurational entropy is taken equal to zero, the liquid phase for which an ideal entropy of mixing is used, and solid solutions or ordered phases stable over extended concentration range. For the latter phases, which is referred to as SRO-phases, the configurational entropy is described by means of the CVM.

3.4.1 Stoichiometric Compounds

A stoichiometric compound (C) will be assumed to be perfectly ordered. Within this approximation, the compound configurational entropy is equal to zero, and the compound free energy is written as:

$$F^{(C)} = A_c + B_c T \quad (16)$$

where the coefficients A_c and B_c are temperature independent.

3.4.2 Liquid Phase

In our analysis, we neglect SRO in the liquid phase, which implies:

$$\xi_2^{(k)} = \xi_1^2 \tag{17}$$

Accordingly, the ordering energy of the liquid phase vanishes (see Eq.(10)) and the configurational entropy of the liquid ($S^{(L)}$) is given by:

$$S_{conf}^{(L)} = - k_B \{x_1 \ln(x_1) + x_2 \ln(x_2)\} \tag{18}$$

where k_B is the Boltzmann's constant.

3.4.3 SRO-Phases

The configurational entropy of SRO-phases is calculated via the CVM. In the CVM, the entropy is written as a function of the probabilities of arranging different atomic species on a set of lattice points included in one or several maximum clusters. Although the accuracy of the CVM increases with the size of the maximum cluster, reliable results are obtained with relatively small clusters. In this study, we will use the tetrahedron approximation of the CVM, i.e. the maximum cluster is a compact tetrahedron. The derivation of the configurational entropy equation within the CVM formalism has been the subject of numerous articles in the literature [12,15,47-49]. We will simply give here, without any derivation, the equations of the configurational entropy in the tetrahedron approximation for the BCC

and FCC solid solutions. In the BCC structure, the tetrahedron (irregular) is composed of four first nearest neighbor pairs and two second nearest neighbor pairs (see Fig.3.1.a), whereas, in the FCC structure the tetrahedron (regular) contains six nearest neighbor pairs (see Fig.3.1.b).

In the tetrahedron approximation, the configurational entropy per lattice point of a disordered FCC structure is given by [12]:

$$\Delta S_{conf}^{(FCC)} = -k_B \{ 2 \sum_{ijkl} L(z_{ijkl}) - 6 \sum_{ij} L(y_{ij}^{(1)}) + 5 \sum_{i} L(x_i) \} \qquad (19)$$

where z_{ijkl} is the probability of finding a regular tetrahedron in the configuration {ijkl} (i,j,k and l take values 1 or 2 as we are dealing with binary alloys), and $L(x) = x \ln(x)$.

For a BCC structure, the configurational entropy takes the form [50]:

$$\Delta S_{conf}^{(BCC)} = -k_B \{ 6 \sum_{ijkl} L(z_{ijkl}) - 12 \sum_{ijk} L(t_{ijk}) + 4 \sum_{ij} L(y_{ij}^{(1)}) + 3 \sum_{ij} L(y_{ij}^{(2)}) - \sum_{i} L(x_i) \} \qquad (20)$$

where t_{ijk} is the probability of finding an irregular triangle in the configuration {ijk}.

The cluster probabilities are related by the following consistency relations:

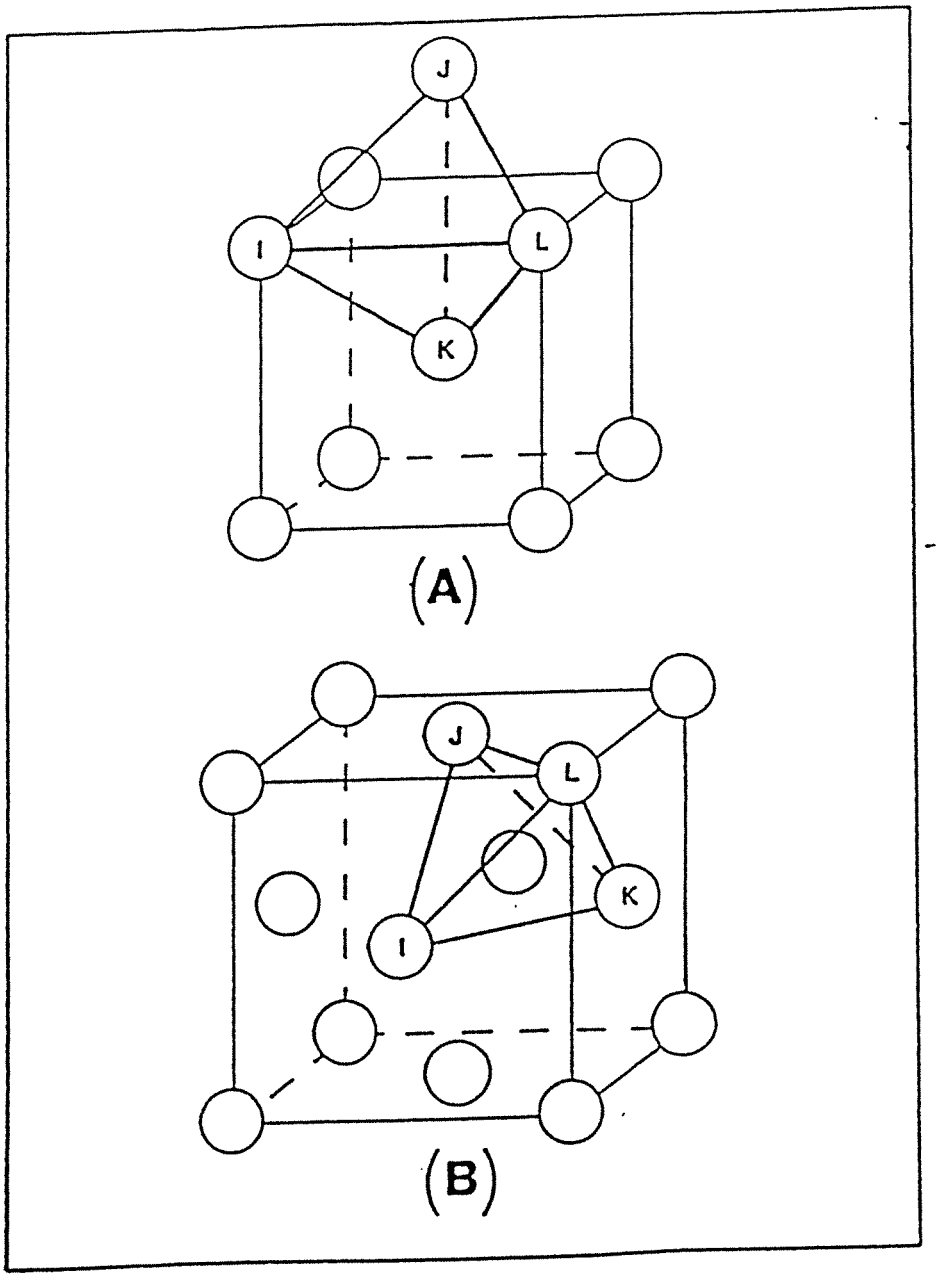

Fig. 3.1 : The basic tetrahedron cluster for the BCC (A), and FCC (B) structures.

$$t_{ijk} = \sum_{l} z_{ijkl} \qquad (21)$$

$$y_{ij} = \sum_{k} t_{ijk} \qquad (22)$$

$$x_{i} = \sum_{j} y_{ij} \qquad (23)$$

The equilibrium state of the system and the degree of SRO in the alloy is obtained at any given concentration and temperature by minimizing the total free energy with respect to a set of independent configurational variables. In the case of the tetrahedron approximation, the minimization is conveniently carried out using the Natural Iteration (NI) method developed by Kikuchi [14,27]. A brief summary of this method is given in section 3.6.

3.4.4 Ordered Phases

In the case of an ordered phase (FCC- or BCC- based), long range order is described in the usual manner by means of sublattices reflecting the symmetry of the ordered structure. In a Cu_3Au compound, for example, Cu atoms occupy preferentially a given sublattice α, whereas Au atoms are located preferentially on a different sublattice β.

For ordered phases, a given cluster may strand points in the crystal belonging to different sublattices, and its probabilities must be distinguished accordingly (see for example Ref.[14]). Concerning the point probability for example, we distinguish the point

probability on a α sublattice (x_i^α), i.e. the probability of finding an "i" atom on a sublattice α, and the point probability on a β sublattice (x_i^β). For an ordered phase, x_i^α is different from x_i^β, and the long range order parameter may be defined as:

$$\eta = x_i^\beta - x_i^\alpha \tag{24}$$

3.5 Grand Potential and Effective Chemical Potential

In order to determine a phase equilibrium, it is convenient to introduce the grand potential Ω. In what follows, we give some useful equations relating the grand potential to the more commonly used free energy and chemical potentials.

For a given temperature and pressure, the equilibrium conditions between two phases α and β are given in terms of the chemical potentials by the equations:

$$\mu_1^\alpha = \mu_1^\beta \tag{25}$$

$$\mu_2^\alpha = \mu_2^\beta \tag{26}$$

where μ_i^α is the chemical potential of element "i" in phase α. We recall that μ_i can be written as:

$$\mu_i = F_i + k_B T \, \mathrm{Ln}(a_i) \tag{27}$$

where a_i is the activity of element "i" . Note that F_i and a_i are, in general, temperature and concentration dependent.

As already mentioned, it is convenient to refer the free energy of a pure metal in the structure of phase α to the free energy of the same element in a reference structure θ. The chemical potential of element "i" is then written as:

$$\mu_i^\alpha = F_i^\alpha - F_i^\theta + k_B T \, Ln(a_i^\alpha) \qquad (28)$$

Defining the grand potential Ω and the effective chemical potential μ_o as:

$$\Omega^\alpha = (1/2)\ (\mu_1^\alpha + \mu_2^\alpha) \qquad (29)$$

$$\mu_o^\alpha = (1/2)\ (\mu_2^\alpha - \mu_1^\alpha)\ , \qquad (30)$$

the equilibrium conditions become:

$$\Omega^\alpha = \Omega^\beta \qquad (31)$$

$$\mu_o^\alpha = \mu_o^\beta \qquad (32)$$

We will now relate Ω and μ_o to the free energy of formation F_f. By definition of the chemical potential, we have:

$$\mu_1 = F_f + \frac{dF_f}{dx_1}\,(1-x_1) \qquad (33)$$

$$\mu_2 = F_f - \frac{dF_f}{dx_1}\,x_1 \qquad (34)$$

where the free energy of formation, F_f, is obtained by subtracting from the total alloy free energy the free energy of the pure elements in their reference structures weighted by their respective atomic concentrations. Combining Eqs.(29, 30, 33, 34), we obtain the following relations for μ_o and Ω:

$$\mu_o = - (1/2) \frac{dF_f}{dx_1} \tag{35}$$

$$\Omega = F_f + \mu_o (x_1 - x_2) \tag{36}$$

For a given phase α, the activities of each element can be expressed in terms of Ω and μ_o. Taking the reference structure of the pure elements to be the structure of phase α, it follows from Eq.(28) that:

$$\mu_i^\alpha = k_B T \ln(a_i^\alpha) \tag{37}$$

and the activities are given by (see Eqs.(29-30)):

$$a_1^\alpha = \exp[(\Omega^\alpha - \mu_o^\alpha)/k_B T] \tag{38}$$

$$a_2^\alpha = \exp[(\Omega^\alpha + \mu_o^\alpha)/k_B T] \tag{39}$$

3.6 Natural Iteration Method

The Natural Iteration (NI) Method [14] is used to minimize the grand potential at a given temperature, T, and effective chemical potential, μ_o. In this method, the minimization is carried out with respect to the maximum cluster probabilities (here the tetrahedron probabilities z_{uvws}). A Lagrange multiplier, λ, is introduced in order to take into account the normalization constraint:

$$\sum_{ijkl} z_{ijkl} = 1 \tag{40}$$

Accordingly, the equation to be solved is:

$$\frac{\partial}{\partial z_{uvws}} \{ F + \mu_o \xi_1 + \lambda (\sum_{ijkl} z_{ijkl} - 1) \} = 0 \tag{41}$$

3.6.1 FCC solid solution

In order to write the NI equations for an **FCC solid solution**, it is convenient to define M such that:

$$F = M - T\,\Delta S_{conf} \tag{42}$$

It can then be shown that Eq.(41) becomes:

$$z_{uvws} = C\ \exp[-(\beta/2)\ E_{uvws}]\ \ Y^{1/2}\,X^{-5/8} \tag{43}$$

where C is a normalization constant, and where:

$$\beta = 1/(k_B\,T) \tag{44}$$

$$Y = y_{uv}^{(1)}\ y_{uw}^{(1)}\ y_{us}^{(1)}\ y_{vw}^{(1)}\ y_{vs}^{(1)}\ y_{ws}^{(1)} \tag{45}$$

$$X = x_u\,x_v\,x_w\,x_s \tag{46}$$

$$E_{uvws} = V_1\,(P_{uv}+P_{uw}+P_{us}+P_{vw}+P_{vs}+P_{ws}-6) + \mu\,(P_u+P_v+P_w+P_s)/4 \tag{47}$$

$$\mu = \mu_o + \partial M/\partial \xi_1 \tag{48}$$

$$P_u = (-1)^{(u+1)} \tag{49}$$

$$P_{uv} = P_u\,P_v \tag{50}$$

3.6.2 BCC Solid Solution

For a BCC solid solution Eq.(41) becomes:

$$z_{uvws} = C\ \exp[-(\beta/6)\,E_{uvws}]\ \ T^{1/2}\,Y_s^{-1/6}\,Y_1^{-1/4}\,X^{1/24} \tag{51}$$

where:

$$T = t_{uvw}\,t_{uvs}\,t_{uws}\,t_{vws} \tag{52}$$

$$Y_s = y_{uv}^{(1)}\ y_{uw}^{(1)}\ y_{sv}^{(1)}\ y_{sw}^{(1)} \tag{53}$$

$$Y_1 = y_{us}^{(2)}\ y_{vw}^{(2)} \tag{54}$$

$$E_{uvws} = V_1\,(P_{uv}+P_{uw}+P_{sv}+P_{sw}-4) + V_2\,(P_{us}+P_{vw}-2)\,(3/2) + \mu\,(P_u+P_v+P_w+P_s)/4 \tag{55}$$

In order to find the set of tetrahedron probabilities that minimize the free energy, it is necessary to iterate Eq.(43) or Eq.(51). After each iteration step, the consistency equations (21-23) are used to deduce the triplet, pair, and point probabilities entering Eqs.(43,51). The iteration process is stopped when the values of the tetrahedron probabilities do not change appreciably from one iteration to another.

4. PHENOMENOLOGICAL APPROACH

4.1 Preamble

In general, the experimental information needed to evaluate the effective pair interactions (EPIs) is not available. This fact underlines the need for a microscopic theory which gives information about the EPIs. We return to that consideration in the second part of the thesis where we present a microscopic theory based on the generalized perturbation method (GPM) that enables the calculation of pair interactions. Although the GPM indicates that the EPIs are, in general, concentration dependent, we have assumed in the phenomenological approach that, within the concentration range of stability of a given phase, the concentration dependence of the pair interactions can be neglected.

4.2 Determination of The Energy Parameters

The free energy parameters that must be evaluated for a phase diagram calculation are the EPIs, the coefficients h_n and s_n in the phenomenological expansions of Eqs.(14-15), and the compound parameters A_c and B_c in Eq.(16). These parameters are obtained according to the following procedure. We begin by estimating trial values of the effective pair interactions for each SRO-phase. The estimation of an EPI can be done using an experimental ordering energy (generally not available) or a congruent order-disorder temperature in the phase diagram. Selected isothermal two-phase boundary points (i.e.

concentrations for each pair of phases in equilibrium at a given temperature), experimental enthalpies of formation and experimental entropies of formation are then used, as explained in subsection 4.2.2, in order to determine values of the other unknown energy parameters (h_n, s_n, A_c, B_c). Finally, the phase diagram as well as the thermodynamic potentials are calculated and compared with experimental results. If necessary, the guessed values of the EPIs are readjusted and the complete fitting procedure is repeated until a satisfactory global agreement is obtained with the experimental phase diagram and thermodynamic data.

4.2.1 Effective pair interactions

In general, the effective pair interactions cannot be uniquely obtained from the phase diagram. However, knowledge of the equilibrium low temperature phases (ground states) provides important information concerning the range of values that such effective pair interactions may take [39-43]. In addition, if the phase of interest presents an experimental congruent order-disorder transformation with no structural change, it is possible to obtain accurate estimates of the effective pair interactions from the order-disorder temperature. Under such conditions, it is reasonable to assume that the energy parameters for the alloy enthalpy of formation (h_n,V_k) are the same for the ordered and disordered phases. We further assume in this study that the vibrational entropies of formation of the disordered and ordered phases are identical. This approximation is rather crude but appears to produce results which are in good agreement with experimental data

(i.e. phase diagram and energies of formation). For more details, the reader is referred to the studies involving the Al_3Li and Ni_3Al phases which are presented in sections 4.3.1 and 4.5.4 .

As a result, the investigation of the equilibrium between an ordered phase and the corresponding disordered phase at the order-disorder congruent point is reduced to the study of an Ising model for which the relation between the effective pair interactions and the ordering temperature T_o is well known. For example, the ordering temperature of an FCC lattice with first nearest neighbor interactions V_1 ($V_1 > 0$) is given by:

$$k_B T_o = \tau V_1 \tag{56}$$

where the constant τ equals 1.9248 and 1.8924 for, respectively, the $L1_2$ and $L1_0$ transitions in the tetrahedron approximation of the CVM [51].

4.2.2 Random Energy, Vibrational Entropy of Formation and Compound Parameters

The values of h_n, s_n, A_c, and B_c defined in Eqs.(13-16) are determined by fitting a limited set of isothermal equilibrium two-phase boundary points, experimental energies, and/or vibrational entropies of formation. As mentioned in section 3.5, the equilibrium condition between two phases α and β is given by the equality of the effective chemical potential μ_o and the grand potential Ω in each phase. The expressions for the energy of formation, vibrational

entropy of formation, effective chemical potential, and grand potential are linear in h_n, s_n, A_c, and B_c. Accordingly, the determination of these parameters is simply reduced to solving a system of linear equations. We recall in Table 4.1 the expressions of the enthalpy and entropy of formation for each type of phase (SRO-phase, liquid, compound).

As will be shown in section 4.3-5, the introduction of SRO into the free energy formalism via the Cluster Variation Method allows an accurate description of stable and metastable order-disorder equilibria in binary alloys. It should be emphasized here that a subregular solution model applied to solid phases would not provide the accuracy needed to investigate stable and metastable order-disorder equilibria. The phenomenological approach presented in this chapter has been used to investigate the Ni-Al, Ni-Cr and Al-Li systems and we report hereafter the results of this investigation. Aside from their metallurgical importance, these alloys provide good test studies for the approach.

The **Ni-Al system** includes the three different types of phases we have distinguished (liquid, compound, and SRO-phase) but presents a negligible vibrational entropy of formation at all concentrations. As a result, the Ni-Al phase diagram is relatively complicated in shape, but can be modeled with a minimum number of energy parameters.

The **Ni-Cr system** has a simple phase diagram which includes a liquid phase, a Ni-rich FCC solid solution and a Cr-rich BCC solid

Table 4.1

Equations of the enthalpies and entropies of formation.

SRO-PHASE
$\Delta H_f = \sum_{i=1}^{2} x_i H_i^{\theta->\zeta} + (1-\xi_1^2) \{ \sum_{n=0}^{p} h_n \xi_1^n \} + \sum_{k=1}^{Q} (\omega_k V_k/2) (\xi_2^{(k)} - \xi_1^2)$
$\Delta S_f = \sum_{i=1}^{2} x_i S_i^{\theta->\zeta} + (1-\xi_1^2) \{ \sum_{n=0}^{p'} s_n \xi_1^n \} + \Delta S_{conf}$
LIQUID
$\Delta H_f = \sum_{i=1}^{2} x_i H_i^{\theta->L} + (1-\xi_1^2) \{ \sum_{n=0}^{p} h_n \xi_1^n \}$
$\Delta S_f = \sum_{i=1}^{2} x_i S_i^{\theta->L} + (1-\xi_1^2) \{ \sum_{n=0}^{p'} s_n \xi_1^n \} - k_B \sum_{i=1}^{2} x_i \ln(x_i)$
COMPOUNDS
$\Delta H_f = A_c$
$\Delta S_f = - B_c$

solution. In contrast to the Ni-Al alloys, the Ni-Cr alloys show, experimentally, a non-negligible vibrational entropy of formation.

The **Al-Li system** includes in its phase diagram the three different types of phases we have distinguished, metastable order-disorder equilibria, and a non negligible vibrational entropy of formation. Accordingly, this system is a typical case for which we can test the power and the accuracy of the proposed phenomenological approach.

4.3 Ni-Al System [52]

In what follows, we describe five intermediate phases observed in the equilibrium phase diagram of the Ni-Al system. In the commonly used structurbericht notation, these phases are called the DO_{20} (Al_3Ni), $D5_{13}$ (Al_3Ni_2), B2 (AlNi), $L1_2$ ($AlNi_3$), and A1 (FCC solid solution) phases [53]. The DO_{20} phase is found experimentally to be a stoichiometric compound and consequently, it is treated as such in the present work. Although the $D5_{13}$ phase is experimentally reported to be stable over a small concentration range, it is described as a stoichiometric compound in the present analysis. The A1, B2 and $L1_2$ phases are stable over an extended concentration range and are described as SRO-phases.

4.3.1 A1 and $L1_2$ Phases

The effective pair interaction of the A1 and $L1_2$ phases has been evaluated by extrapolating the A1-$L1_2$ two phase boundary into the liquid high temperature region. A metastable congruent point at 1857 K was estimated which corresponds to an effective pair interaction of 1.92 kcal/g-at. This result is in very good agreement with the values of 1.85 kcal/g-at [19] and 2.11 kcal/g-at [20] previously estimated using 8-4 Lennard-Jones pair interactions. The values of h_0, h_1, and h_2 (see Table 4.2) were calculated by reproducing the experimental enthalpy of formation {-9.1 kcal/g-at, for $x_{Ni} = 0.75$} of the $L1_2$ phase measured at 298 K [53], and a set of two equilibrium concentrations at 800 K belonging to the A_1-$L1_2$ two-phase boundary.

Table 4.2

Energy parameters caracterizing the Ni-Al system. The lattice stability parameters H_i and S_i refer to the fcc structure. They are taken from ref.[37] for the liquid phase, and from ref.[2] for the B2 phase. Energies are expressed in kcal/g-at.

PHASE	V_1	V_2	h_0	h_1	h_2	H_{Ni}	S_{Ni} 10^3	H_{Al}	S_{Al} 10^3
A1	1.92	-----	- 9.60	3.56	-2.07	0.00	0.00	0.00	0.00
$L1_2$	1.92	-----	- 9.60	3.56	-2.07	0.00	0.00	0.00	0.00
B2	2.11	1.05	- 9.42	-.44	0.00	1.33	0.25	2.41	1.15
Liquid	-----	-----	-10.03	0.00	2.37	4.17	2.42	2.58	2.76

	COMPOUND PARAMETERS	
	A_c	B_c 10^3
DO_{20}	- 9.89	1.24
$D5_{13}$	-13.83	1.10

In Fig.(4.1) we present a detailed comparison between the calculated A1-$L1_2$ two phase boundary (full line) and the compilation of experimental data taken from ref.[19] (dashed line). As can be seen, the present model closely reproduces the phase equilibrium between the A1 and $L1_2$ phases, a fact particularly remarkable since both phases are described by a unique free energy function which itself depends on only four physical parameters (V_1, h_0, h_1, h_2).

4.3.2 B2 Phase

For the B2 phase, values of 2.11 kcal/g-at and 1.05 kcal/g-at for, respectively, the first and second nearest neighbor effective pair interactions, were found to give a good overall agreement between the calculated and the experimental phase diagrams. The agreement can be seen in Fig.(4.2) where the calculated phase diagram is indicated in full line, and the experimental phase diagram [53] is indicated in dashed line. For the sake of clarity, the same calculated phase diagram is presented alone in Fig.(4.3). The parameters h_0 and h_1 have been determined by reproducing the experimental equilibrium concentrations of the B2-$L1_2$ two phase-boundary at 1000 K. The vibrational entropy of the B_2 phase was found to be negligible.

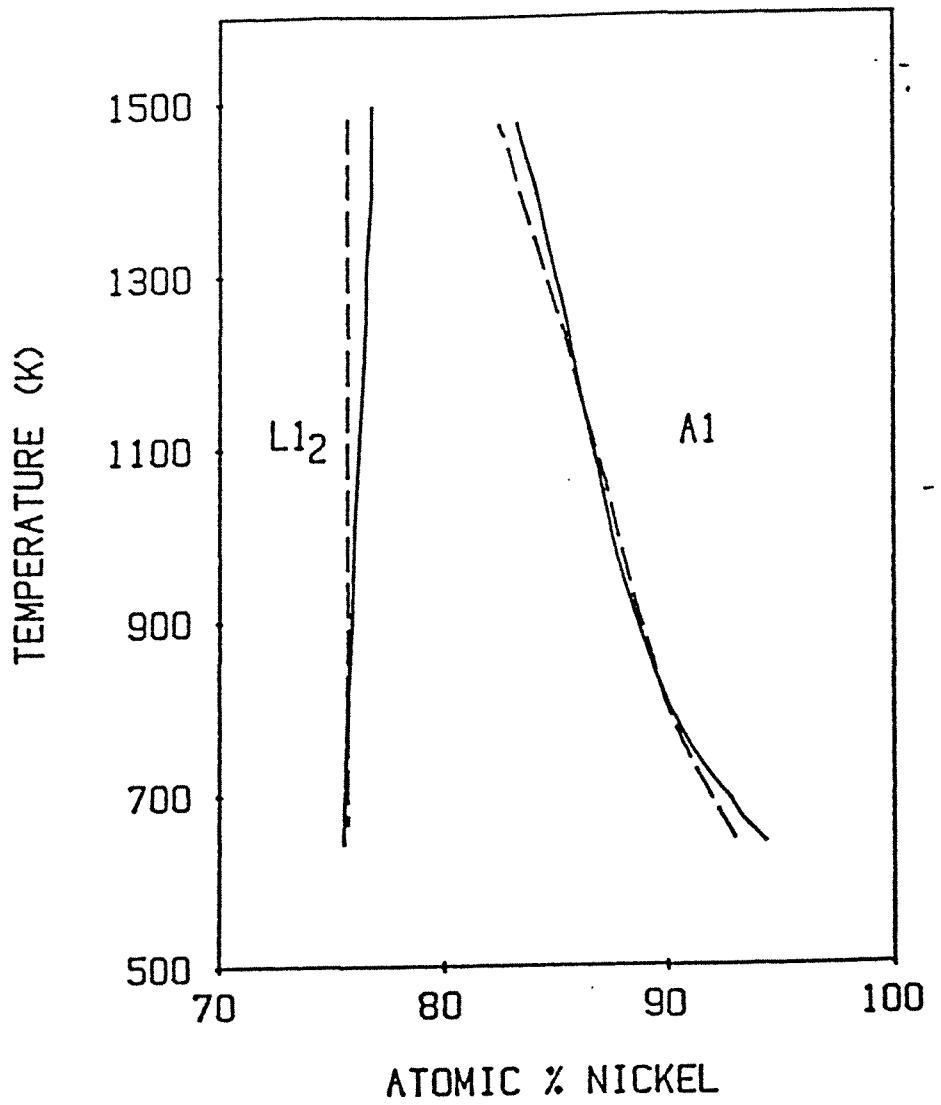

Fig. 4.1 : Detailed comparison between the calculated (full line) and the experimental [19] (broken line) $L1_2$-A1 two-phase boundary in the Ni-Al system.

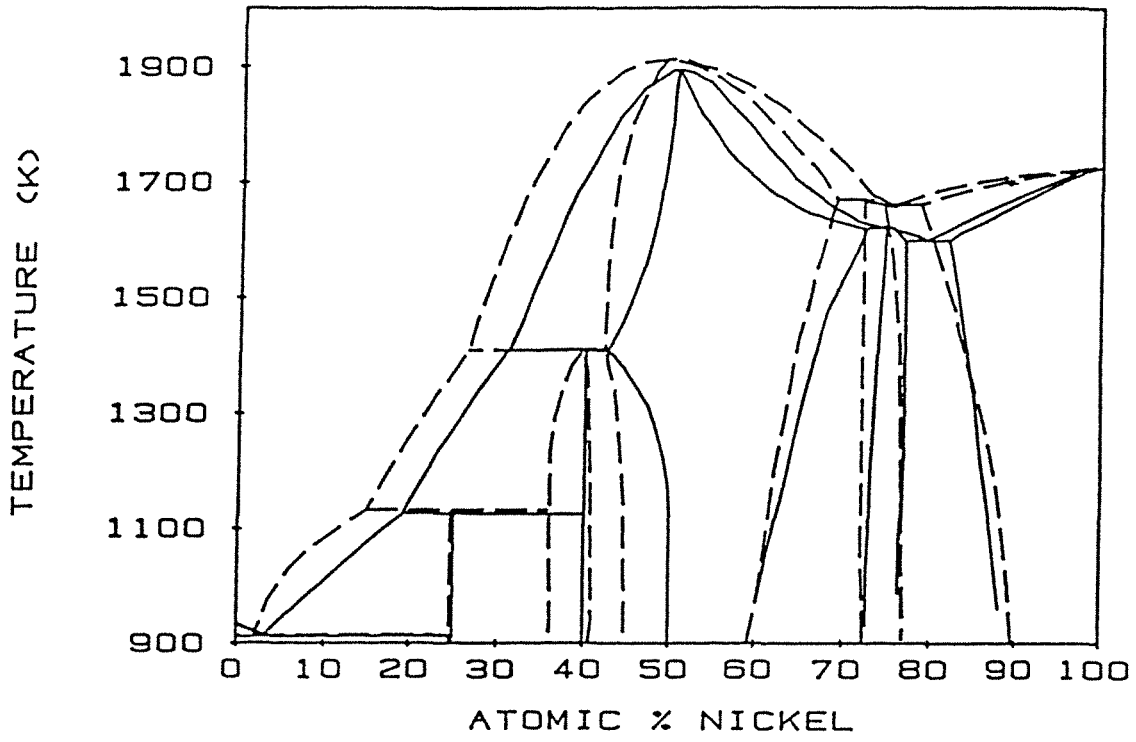

Fig. 4.2 : Comparison between the calculated (full line) and the experimental [53] (broken line) phase diagram for the Ni-Al system. The parameters used in the phase diagram calculation are shown in Table 4.2.

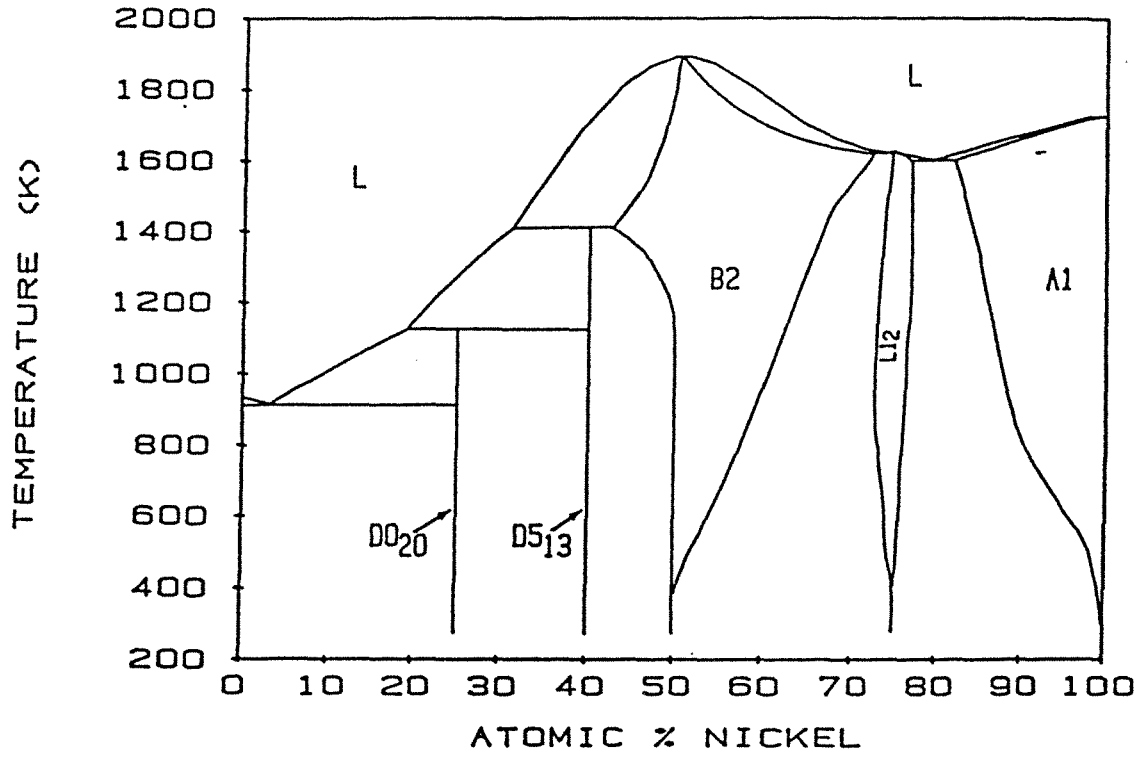

Fig. 4.3 : The calculated Ni-Al phase diagram using the energy parameters of Table 4.2.

4.3.3 Liquid Phase and Compounds

For the liquid phase, the value of h_0 was obtained by reproducing the congruent temperature between the liquid phase and the B2 phase at 1900K. The value of h_1 was set equal to zero and the value of h_2 was obtained by reproducing the equilibrium concentration of the B2 phase with the liquid phase at 1400 K. The excess entropy of the liquid phase was found to be negligible.

The energy parameters of the $D5_{13}$ compound have been obtained by reproducing the peritectic temperature at 1406 K, and the experimental enthalpy of formation at 298 K (-13.5 kcal/g-atom) [53]. The energy parameters of the DO_{20} compound were determined by reproducing the peritectic temperature at 1127 K and the eutectic temperature (913K).

4.3.4 Comparison With Experimental Results

The calculated and experimental [53] enthalpies of formation of the ordered phases stable at 298 K are reported in Table 4.3. We also give in Table 4.4 a comparison between the predicted and the experimental free energy of formation of the phases stable at 1273 K. The energy parameters describing the thermodynamic potentials of the Ni-Al system are given in Table 4.2.

Note that the enthalpies of formation of the A1 and $D5_{13}$ phases are the only thermodynamic potentials used as input in the calculations, the remaining enthalpies of formation in Table 4.3 are a

Table 4.3

Comparison of the available experimental enthalpies of formation for the intermediate phases of the Ni-Al system (T=298 K) [53], with the values calculated by Kaufman and Nesor [3], and with the values calculated in the present work .

phase	atomic concentration of Ni	enthalpy of formation based on fcc Ni and fcc Al (kcal/g-at)		
		experimental [53]	present work	ref.[3]
$L1_2$	0.725	- 9.80	------	------
	0.750	------	- 9.10*	- 9.79
	0.770	- 8.25	------	------
B2	0.500	-14.05	-13.03	-13.45
$D5_{13}$	0.400	-13.50	-13.50*	-12.45
DO_{20}	0.250	- 9.00	- 9.50	- 8.50

* : used as input data for the analysis

Table 4.4

Comparison of the available experimental free energies of formation for the Ni-Al system (T=1273 K) [53], with the values calculated by Kaufman and Nesor [3], and with the values calculated in the present work.

phase	atomic concentration of Ni	free energy of formation based on fcc Ni and fcc Al (kcal/g-at)		
		experimental [53]	present work	ref.[3]
A1	0.950	- 2.13	- 2.11	------
	0.900	- 3.85	- 4.00	- 5.07
	0.857	- 5.09	------	------
	0.851	------	- 5.73	------
$L1_2$	0.770	- 7.38	------	------
	0.765	------	- 8.65	------
	0.750	------	------	-11.52
	0.725	- 8.51	- 9.59	------
B2	0.643	------	-11.40	------
	0.637	-10.56	------	------
	0.600	-11.38	-12.20	------
	0.550	-12.35	-13.10	------
	0.500	-12.96	-13.71	-11.05
	0.445	-12.46	------	------
	0.439	------	-12.82	------
$D5_{13}$	0.410	-11.99	------	------
	0.400	------	-12.43	-11.95
	0.396	-11.77	------	------

prediction of the model resulting from the fitting of ten points in the phase diagram.

As can be seen from Table 4.3-4 and Fig.(4.1-3), our results closely reproduce the experimental phase diagram as well as the experimental thermodynamic data. The study of the Ni-Al system has shown that it is possible to describe complex phase equilibrium with a small number of physically meaningful parameters (V_k, h_n). Furthermore, the study has shown that SRO plays an important role in the description of order-disorder reactions (A1-$L1_2$) and order-order reactions (B2-$L1_2$).

In the Ni-Al system, we have found that the vibrational entropy of formation is negligible. This is not always the case, and in general one must include a vibrational entropy of formation in order to obtain a reliable description of the alloy thermodynamic potentials and phase diagram. This point is illustrated in the next sections which are devoted to the thermodynamic investigation of the Ni-Cr and Al-Li systems.

4.4 Cr - Ni System

4.4.1 Introduction

The commonly accepted Ni-Cr phase diagram is presented in Fig.(4.4). This phase diagram includes a solid BCC solid solution (A2) and an FCC solid solution (A1) with a eutectic transformation at 1618 K [54,55]. A $CrNi_2$ phase having a Pt_2Mo structure is also reported to exist below 830 K [54,56-58]. Three other proposed phase diagrams can be found in the literature. One includes the presence of a high temperature allotropic form (β) for pure chromium above 2100 K which leads to the presence of an additional eutectoid reaction [59-60]. Another alternative includes, in addition to β chromium, the presence of a sigma phase at about 0.60 Cr. As a result, the proposed phase diagram [61] contains one eutectic, two eutectoids and one peritectic reaction. A phase diagram including one eutectic and four eutectoids can also be found in the literature [62].

Following Raynor and Rivlin [63], we have ignored the controversial β chromium as well as the sigma phase, and we have concentrated our attention on the thermodynamic investigation of the A1, A2, and liquid phases above 900 K. For reasons explained in the next sub-section, the $CrNi_2$ phase is not analyzed in this study.

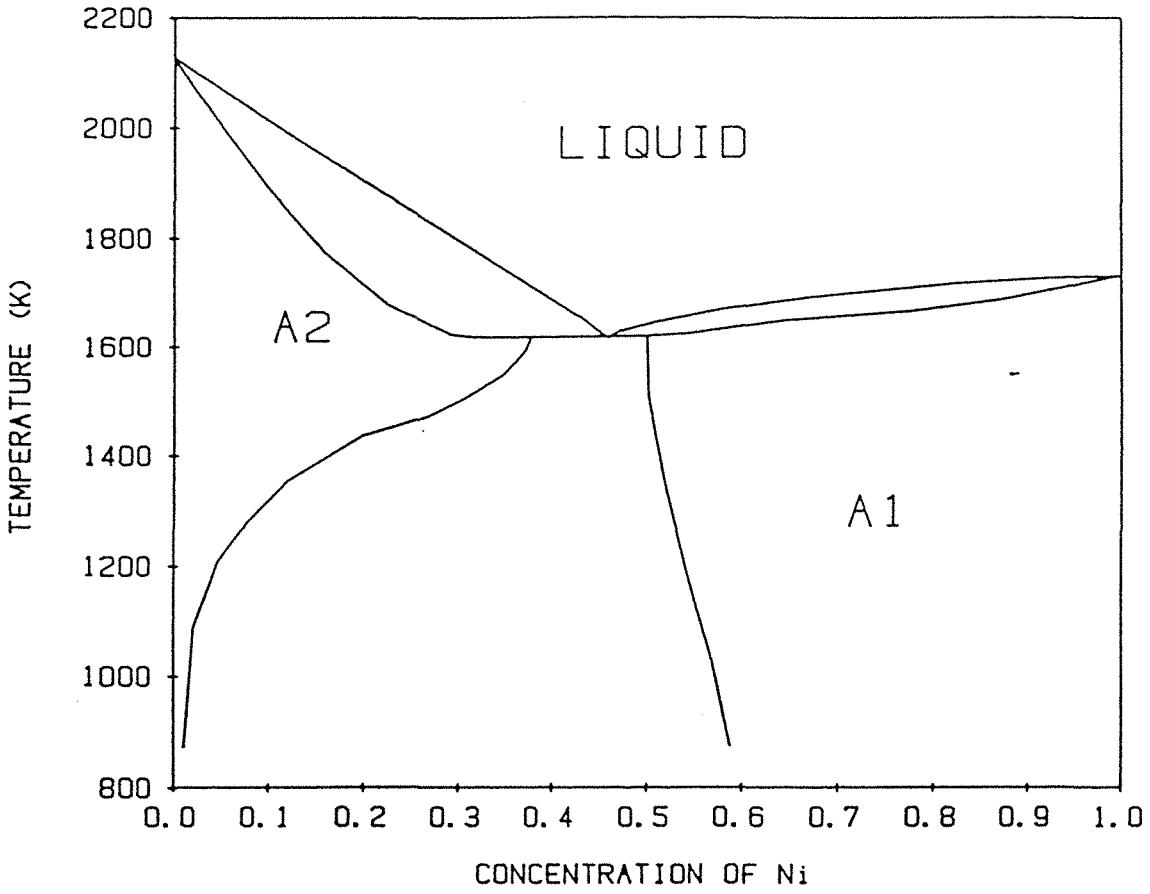

Fig. 4.4 : Experimental Cr-Ni phase diagram [54].

4.4.2 FCC Solid Solution (A1)

The existence of the $CrNi_2$ phase indicates an ordering tendency in the FCC solid solution at a Ni concentration of 0.66. The $CrNi_2$ phase has a Pt_2Mo structure which is stable for { $0 \leq V_1$ and $0 \leq V_2 \leq V_1/2$ }. The approach adopted in this study uses the tetrahedron approximation of the CVM to model the alloy configurational entropy. In that case, the ordering energy does not include the second neighbors required for the stability of $CrNi_2$, and the $CrNi_2$ phase is degenerate with a mixture of the $L1_2$ and $L1_0$ phases. It would therefore be necessary to use a larger cluster approximation in order to describe correctly the $CrNi_2$ phase.

The value of V_1 was set equal to 0.85 kcal/g-at. The sign of V_1 is positive indicating an ordering tendency, and its magnitude is compatible with the temperature range of stability of the $CrNi_2$ phase. The energy parameters (h_0, h_1, s_0, and s_1) reported in Table 4.5 have been obtained by reproducing the experimental enthalpy and entropy of formation of the A1 phase [54]. A comparison between the experimental and fitted thermodynamic potentials is given in Fig.(4.5).

The lattice stability parameters of Cr in the FCC structure, have been obtained by fitting the A1 boundary describing the A1-A2 two phase equilibrium. The resulting values , 0.93 kcal/g-at. for $H_{Cr}^{bcc->fcc}$ and -0.1 cal/g-at. for $S_{Cr}^{bcc->fcc}$, differ from the values of 2.5 kcal/g-at and -0.15 cal/g-at/K given by Kaufman in Ref.[2].

Table 4.5

Energy parameters caracterizing the Ni-Cr system. H_{Ni} and S_{Ni} refer to the fcc structure; they are taken from ref.[37] for the liquid phase and from ref.[2] for the bcc structure. The lattice stability parameters of Cr refer to the bcc structure; for the liquid phase, they are taken from ref.[37], whereas for the fcc structure, they have been evaluated in order to obtain a good overall agreement with experimental results. Energies are expressed in kcal/g-at.

PHASE	V_1	V_2	h_0	h_1	s_0	s_1	s_2	H_{Ni}	S_{Ni}	H_{Cr}	S_{Cr}
					<----10^3---->				10^3		10^3
A1	0.86	----	1.79	-2.70	1.09	-1.4	0.3	0.00	0.00	0.93	-.10
A2	-.25	-.25	2.34	-0.55	1.50	0.0	0.0	1.33	0.25	0.00	0.00
Liq.	----	----	1.17	-0.34	1.00	0.0	0.0	4.18	2.42	4.05	1.90

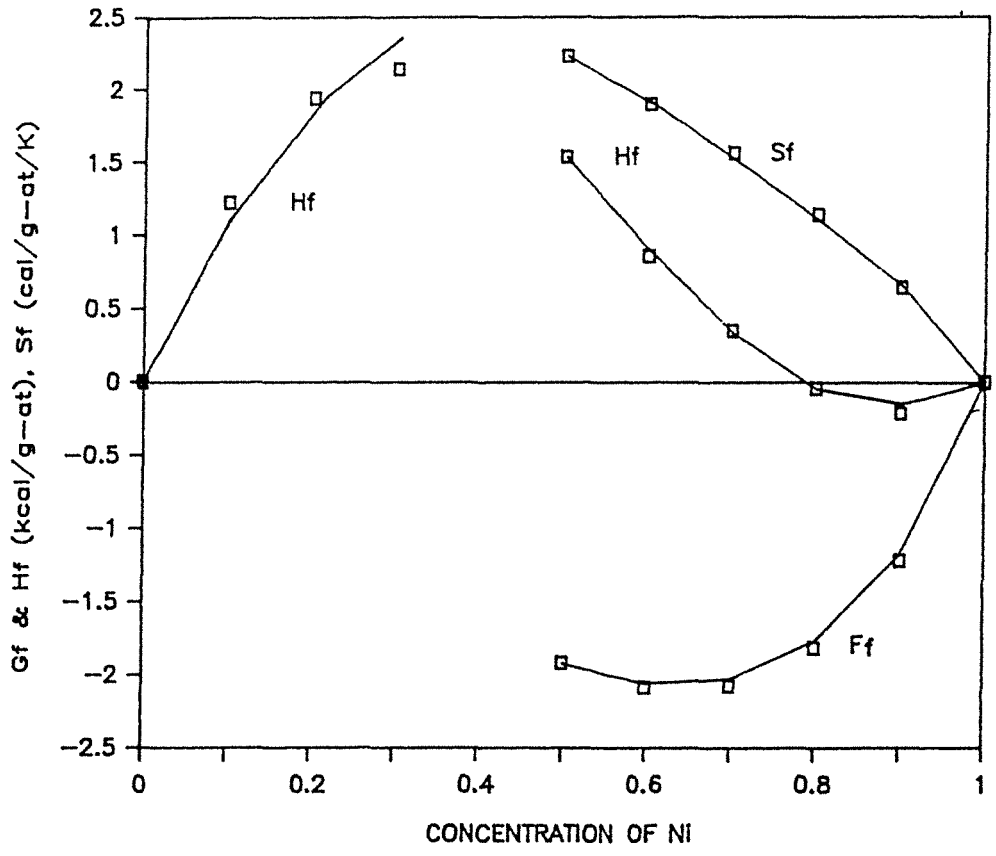

Fig. 4.5 : Comparison between the experimental (□) [54] and the fitted (full line) thermodynamic potentials of the Cr-Ni system at 1550 K.

4.4.3 BCC Solid Solution

Due to a lack of information, we have taken V_1 and V_2 to be equal. A value of -0.25 kcal for V_1 (and V_2) gives a very good overall agreement between the experimental and the calculated A2-boundary describing the A2-A1 equilibrium. Note that the value of V_1 is negative and indicates a clustering tendency. The values of h_0, h_1, and s_0 (see Table 4.5) have been calculated by reproducing the equilibrium concentration of the A2 phase (x_{Ni}=0.37) with the A1 phase (x_{Ni}= 0.50) at the eutectic temperature (1618 K), as well as the enthalpy of formation of the A2 phase (1940 ± 150 cal/g-at, x_{Ni}=0.2) at 1550 K [54].

4.4.4 Liquid Phase

The energy parameters of the liquid phase (h_0,h_1, and s_0) have been estimated by reproducing the equilibrium concentration of the liquid phase (x_{Ni} = 0.26) with the A1 phase (x_{Ni}=0.5) at the eutectic concentration (1618 K), and the slope of the liquidus in the concentration range {x_{Ni}=0-0.45}.

4.4.5 Calculated Cr-Ni Phase Diagram

The parameters describing the different contributions to the free energy of the A1, A2, and liquid phases are summarized in Table 4.5. They have been used to calculate the Cr-Ni phase diagram which is compared in Fig.(4.6) with the experimental data [56,58,60,64-65]. A

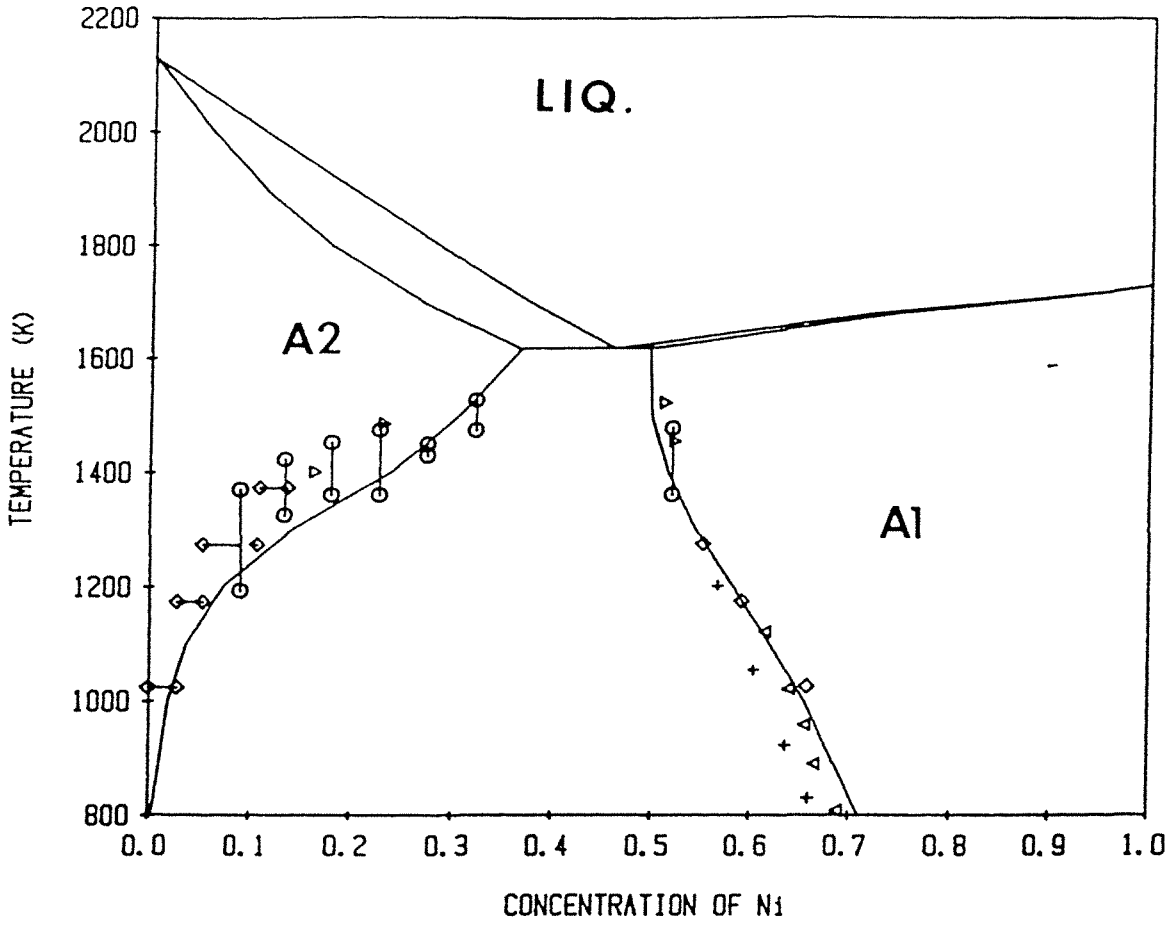

Fig. 4.6 : Calculated Cr-Ni phase diagram. Available experimental temperature-concentration data points are indicated by symbols: ◁ [56], + [58], ▷ [61], ○ [65], and ◇ [64].

very good agreement is obtained between the calculated and experimental phase diagrams. This agreement indicates that the experimental temperature-concentration data points given in Fig.(4.6) are consistent with the experimental thermodynamic data plotted in Fig.(4.5).

As seen from the parameters listed in Table 4.5, the vibrational entropy of formation for Cr-Ni alloys is quite important. In fact, we were unable to reproduce the experimental data (phase diagram and thermodynamic data) without taking into account ΔS_{vib}. The same conclusion has been reached for the Al-Li system which is investigated in the next section. In the case of the Al-Li system, we also illustrate the importance of SRO for the description of metastable order-disorder equilibria.

4.5 Al-Li System [66]

4.5.1 Introduction

Saboungi and Hsu [67] have recently proposed a thermodynamic description of the Al-Li system based on a numerical method developed by Kaufman and Nesor [1]. In their description, however, ordered phases are systematically considered as stoichiometric compounds. This approximation is not valid for the AlLi phase (β) which is stable over a wide range of concentration (45-55 at% Li) [68]. This discrepancy is removed in the thermodynamic description of McAlister [68] who used a Wagner-Schottky free energy function for the β phase. The free energy formalism for the other phases in both models is otherwise similar. Both models, although successful in the overall description of equilibrium phase diagrams, provide little insight into the different contributions to the free energies. In particular, these methods fail to describe stable and metastable order-disorder equilibria.

A comprehensive review of the thermodynamic data and equilibrium temperature-concentration phase diagram for Al-Li alloys can be found in Ref.[68] and Ref.[69]. The different stable phases appearing in the updated phase diagram of Ref.[68] are the liquid phase, the fcc Al-rich solid solution (α), the bcc Li-rich solid solution, the ordered AlLi phase (β), which has a NaTl-type structure, the Al_2Li_3 phase (γ) based on a rhombohedral structure and reported to have a very narrow range of solubility [70], and the Al_4Li_9 phase (δ) based on a monoclinic structure below 548 K and reported by Myles et al. to

transform to a different, yet undetermined, structure (δ') above 548 K [71].

The metastable Al_3Li (α') phase has a Cu_3Au structure and plays a significant role in Al-Li alloys because of its strengthening ability, a feature that the stable AlLi phase does not have. Consequently, the location of the metastable two-phase boundary in the temperature-concentration phase diagram has been investigated extensively and is well documented between room temperature and 620 K [72-76]. In this range of temperature, the concentration difference between the α and α' phases in metastable equilibria has been found to be quite large and has led to some controversy concerning the location of the metastable α-α' two-phase boundaries above 620 K [77]. Using our free energy model, we have investigated in detail the metastable equilibrium between the α solid solution and the ordered α' phase. Remarkably, our model also predicts a second level of metastable equilibrium within the concentration range where the metastable α-α' two-phase region is observed; namely, it is predicted that alloys with a composition of about 10 at% Li and quenched below 400 K show a tendency to segregate. This tendency will be discussed in the light of available experimental results.

The Al_2Li_3 (γ) and the Al_4Li_9 (δ) phases, experimentally found to be stable in a very narrow concentration range, are treated as stoichiometric compounds. On the other hand, the fcc Al-rich solid solution (α), the AlLi phase (β) and the metastable Al_3Li (α') phase are treated using the tetrahedron approximation of the CVM. Within

this approximation, the ordering energies of the α and Al_3Li phases are calculated using first nearest neighbor pair interactions whereas the ordering energy of the AlLi phase is calculated using first and second nearest neighbor pair interactions.

A summary of all parameters used in the description of the Al-Li system is given in Table 4.6. In the following sections, we indicate, for each phase, the selected set of experimental results used in order to obtain the free energy parameters of Table 4.6.

4.5.2 Liquid Phase

The free energy of the liquid phase has been investigated by Hicter et al. using the Knudsen method [79] and by Yatsenko and Saltykova using an electrochemical method [80]; their results are in good agreement. In addition, Yatsenko and Saltykova give the temperature dependence of the free energy. The expansion coefficients (h_0,h_1, s_0, and s_1) have been obtained by fitting the experimental enthalpy of formation and excess entropy given in Ref.[80] at 1023 K. A comparison between experimental and fitted data is given in Fig.(4.7). Note that effective pair interactions are not required for the liquid phase, for which SRO is neglected.

Table 4.6

Energy parameters caracterizing the Al-Li system.

PHASE	E_{rand} (kcal/g-at.)			ΔS_{vib} (cal/g-at. K)		E_{ord} (kcal/g-at)	
	h_0	h_1	h_2	s_0	s_1	V_1	V_2
FCC (Al)	-1.64	-0.25	-0.27	-1.2	0.0	0.83	----
Al_3Li	-1.64	-0.25	-0.27	-1.2	0.0	0.83	----
AlLi	-3.83	-0.10	0.00	-2.5	0.0	0.76	0.76
LIQ	-2.70	-1.24	0.00	-1.5	-0.5	----	----

COMPOUNDS

	A_g (kcal/g-at.) (reference structure: Liquid)	B_g (cal/g-at K) (reference structure: Liquid)
Al_2Li_3	-7.41	5.62
Al_4Li_9	-8.53	8.90

LATTICE STABILITY PARAMETERS
(from Ref.[67])

STRUCTURE	ALUMINUM		LITHIUM	
	H_{Al} (kcal/g-at.)	S_{Al} (cal/g-at./K)	H_{Li} (kcal/g-at.)	S_{Li} (cal/g-at./K)
	(reference structure: Liquid)			
FCC	-2.560	-2.750	-0.427	-1.710
BCC	-0.150	-1.600	-0.717	-1.580
LIQ	0.000	0.000	0.000	0.000

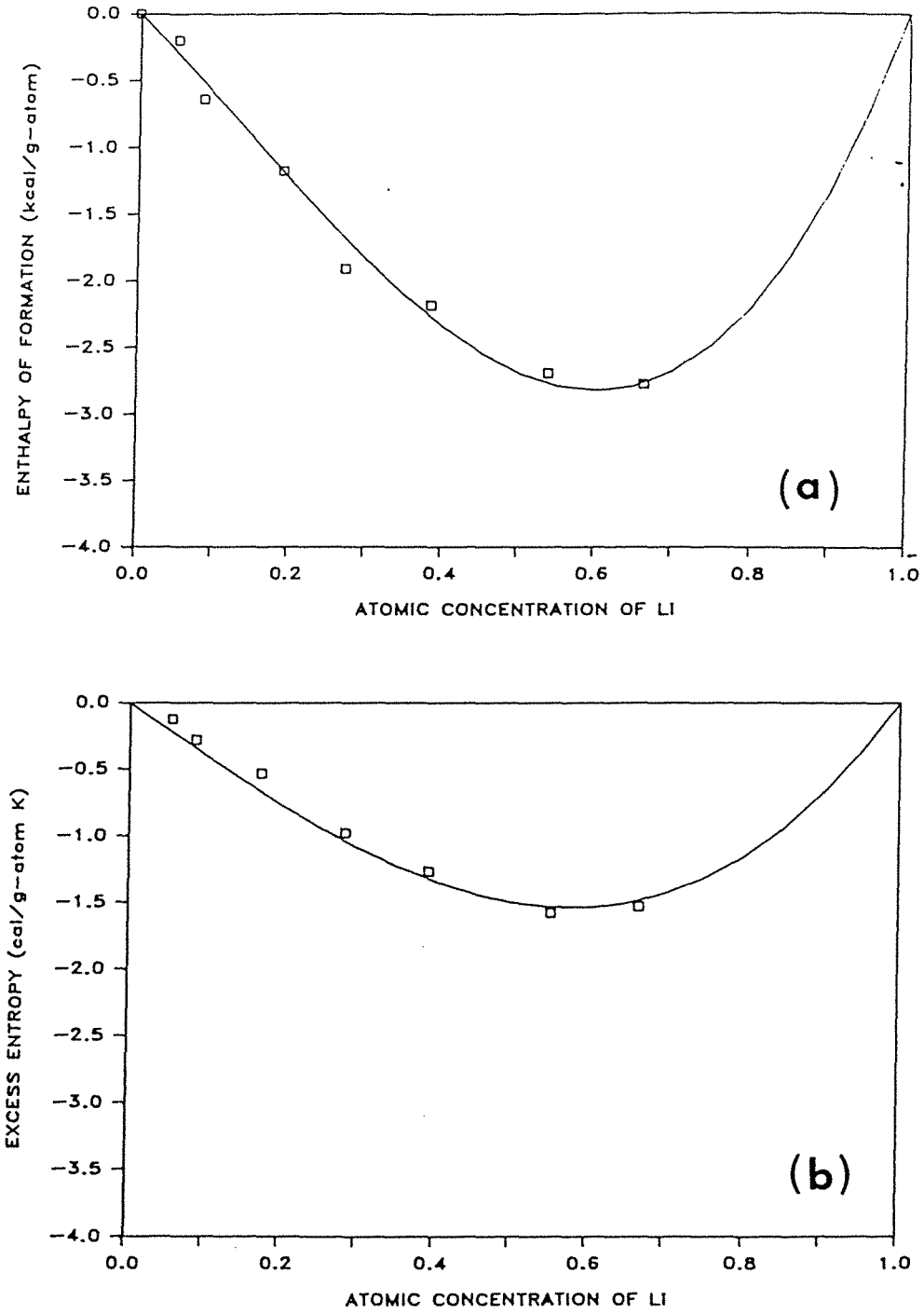

Fig. 4.7 : Comparison between the experimental (□) [80] and the fitted (full line) enthalpy of formation (a) and excess entropy (b) for the liquid Al-Li phase at 1023 K.

4.5.3 AlLi Phase (β)

The AlLi phase has a B32 structure (NaTl type). According to a ground state analysis based on first and second nearest neighbor pair interactions, the following inequalities must be verified for this phase to be stable at 0 K [81]:

$$(-3/2) < (V_1/V_2) < (3/2) \quad \{ \text{ with } V_2 > 0 \} \tag{57}$$

Equation (57) represents the only available information concerning the relative magnitude of V_1 and V_2. In our analysis we have set [$V_1 = V_2$]. The value of V_1 (and V_2) has been determined by noticing that the equilibrium solubility limits of the AlLi phase are controlled by the magnitude of V_1 (and V_2). Good agreement with the experimental liquid-β two-phase boundaries is obtained using a value of 0.76 kcal/g-at for V_1 and V_2. The resulting calculated solubility limits are 44 at% Li at 869 K, and 55 at% Li at 793 K; they compare well with the experimental value of, respectively, 45 at% and 55 at% reported in Ref.[68]. With the value of pair interaction used, the calculated AlLi phase remains ordered up to its melting point as found experimentally [71,82].

The coefficients s_0 and h_0 for the β phase, defined in Eq.(14-15), are obtained by fitting the experimental entropy of formation (-2.54 cal/g.at/K) reported in Ref.[83] at the 50/50 concentration, and the equilibrium congruent point between the liquid phase and the AlLi phase (β) estimated at 973 K (see Fig.(4.8)).

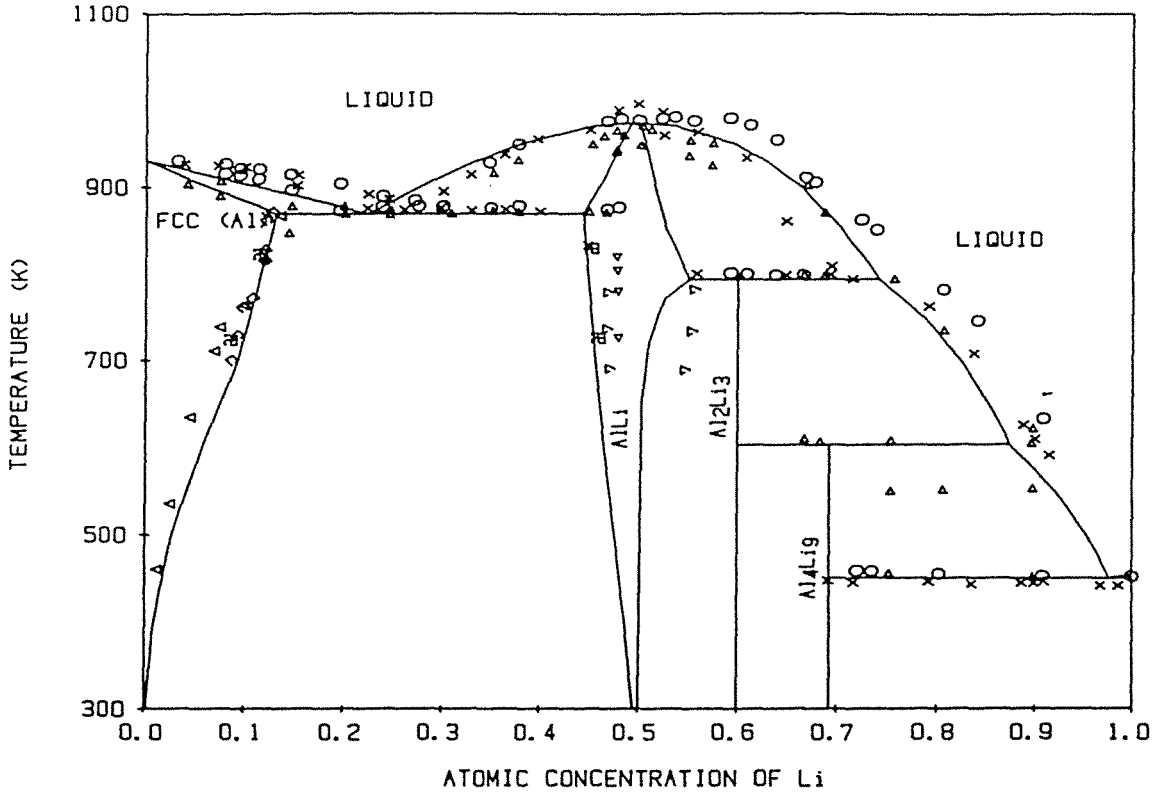

Fig. 4.8 : Comparison of the calculated phase diagram for the Al-Li system with experimental equilibrium concentrations compiled in Ref.[68].

4.5.4 α and α' Phases

Since the α and α' phases are both based on an fcc structure, we have assumed that the energy parameters in these two phases are equal. Note that we have used the same assumption to study the Al-$L1_2$ equilibrium in the Ni-Al system, and have obtained a good agreement between calculated and experimental data (see section 4.3.1).

The effective pair interaction V_1 for the Al-Li fcc-based structure was calculated by reproducing the order-disorder congruent temperature T_o (800 K) evaluated by Tamura et al. [85] for the α' phase. This value of T_o is also suggested by the differential thermal analysis results of Ref.[76]. From equation (64), a value of 0.825 kcal/g-at. is obtained for V_1. The coefficients h_0, h_1, h_2 for the fcc structure are obtained by reproducing the eutectic concentration of the α phase (13.3 at% Li) at 869 K as well as the experimental α' solvus concentration (7.6 at% Li) measured by Williams and Edington at 508 K [73]. The coefficient s_0 has been evaluated by reproducing the concentration of the α phase (1.5 at% Li) resulting from the α-β equilibrium at 463 K measured by Jones and Das [86].

4.5.5 Stoichiometric Compounds

The energy parameters of Al_2Li_3 (γ) and Al_4Li_9 (δ) are shown in Table 4.6. These parameters have been determined by reproducing the two peritectic temperatures (603 K, 793 K), and the eutectic temperature (450 K) given in Ref.[68]. Due to a lack of experimental

data, the phase transformation (δ -> δ') reported by Myles et al. [71] has not been considered in the present thermodynamic analysis. Moreover, the thermodynamic description and equilibrium phase diagram would not change drastically if one were to take this transformation into account.

4.5.6 Results for Stable Equilibria

Using the energy parameters of Table 4.6, the entire equilibrium phase diagram has been calculated and it is compared in Fig.(4.8) with the experimental points taken from Ref.[68]. As can be seen, a very good overall agreement has been obtained between experimental and calculated equilibrium concentrations. In particular, the calculated α solvus line compares very well with the different experimental concentrations shown in Fig.(4.8).

Regarding liquid-solid equilibrium, our model predicts a eutectic concentration for the liquid phase (22.4 at% Li) very close to the calculated value (24.3 at%) of McAlister [68]. The experimental data obtained for the liquidus temperature by several investigators (see Fig.(4.8) and Ref.[68]) are consistent between 25 and 50 at% Li. Furthermore, they compare well with the calculated liquidus temperatures. Beyond 50 at% Li, however, discrepancies are found in the experimentally determined liquidus temperatures. The calculated liquidus in this region agrees well with the experimental data reported by Myles et al. [71].

As seen in Fig.(4.8), the predicted concentration of Li in the AlLi (β) phase in equilibrium with the Al_2Li_3 phase (γ) is somewhat less than reported experimentally by Wen et al. [70]. The same result was obtained by McAlister in his calculation [68]. Further experimental investigation on the locus of the β-γ boundaries and on the values of free energy for the γ phase would be useful to confirm or deny the calculated results.

In the next sections we investigate metastable equilibria between phases based on an fcc structure. It is therefore of primary importance to check the accuracy of the free energies for fcc-based phases. As mentioned before, the calculated and experimental stable α-solvus lines are in good agreement. In Fig.(4.9) we compare the free energy of the α phase estimated by Wen [87] using electrochemical measurements at 696 K, with the free energies predicted by the present model at the same temperature. The calculated free energies for the α phase used by McAlister [68] and those used by Saboungi and Hsu [67] are also plotted in the same figure.

The activities of Lithium in the α-β two-phase region, have been determined by several investigators [70,83-84] at different temperatures, and have been found to be very consistent [84]. A comparison of the experimental data with values obtained from the present thermodynamic description is given in Fig.(4.10). As can be seen, the temperature dependence of the Lithium activities is reproduced well by the model. In addition, we compare in Tables

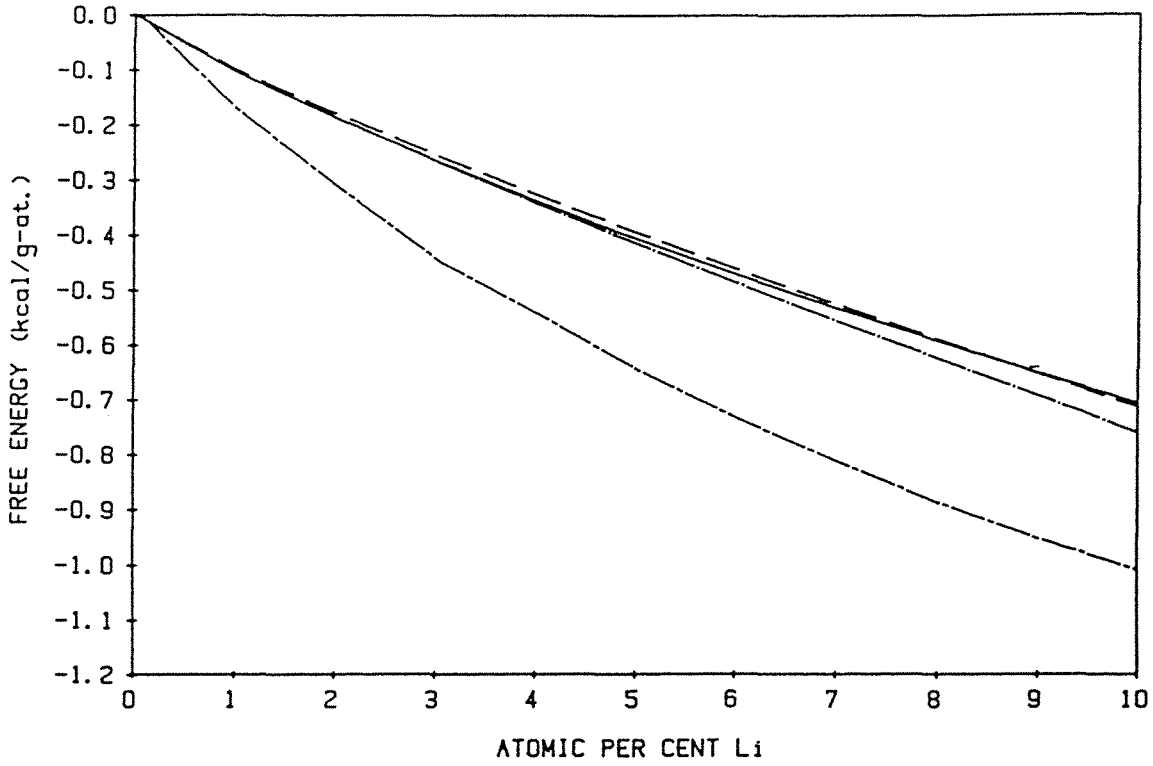

Fig. 4.9 : Comparison of the free energy of the α phase reported by Wen et al. [87] (— - —)), McAlister [68] (————), and Saboungi and Hsu [67] (- - - -), with the free energy predicted in the present work (— • —).

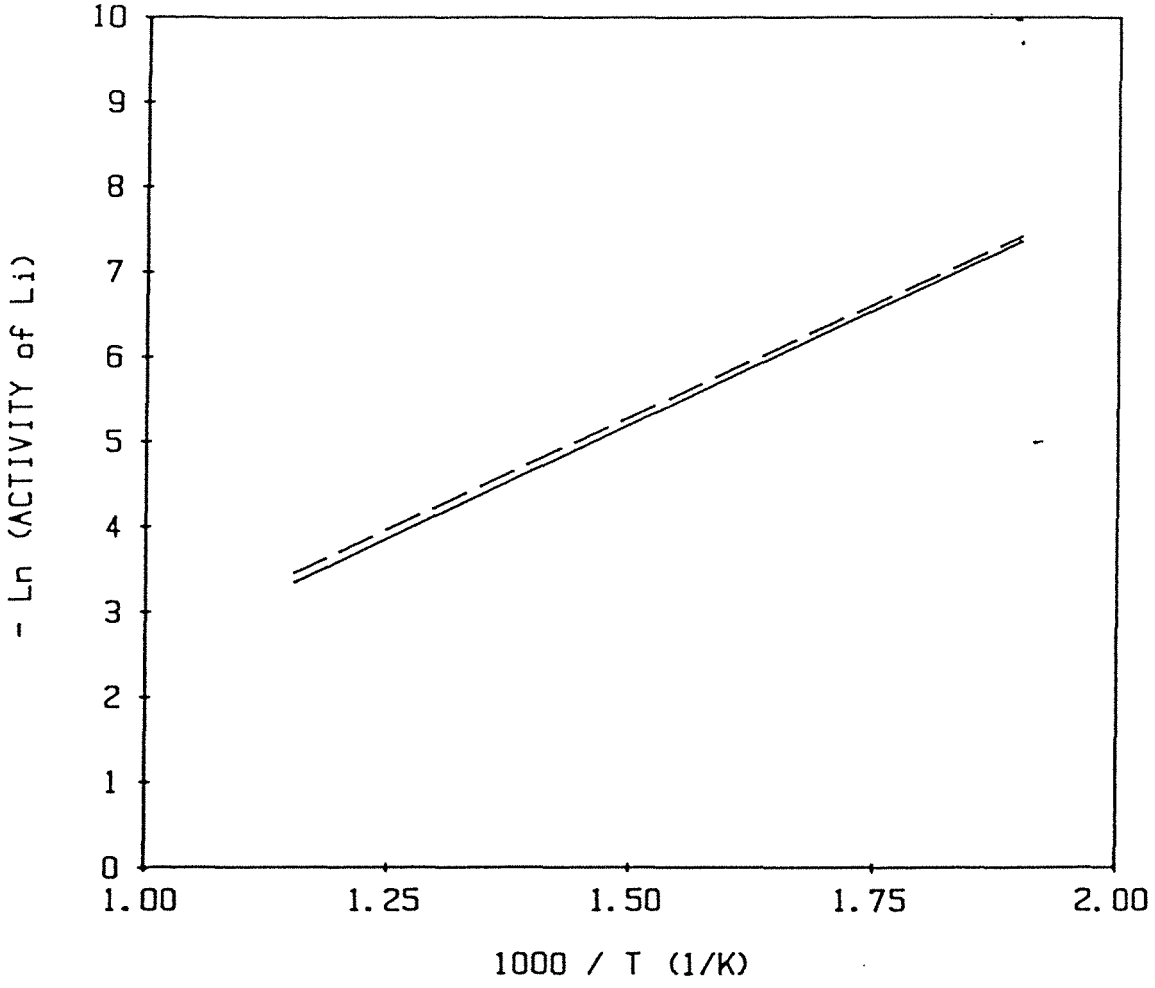

Fig. 4.10 : Calculated (full line) and experimental [84] (broken line) activity of Lithium in the α-β two-phase boundary as a function of temperature. The experimental results are given by the equation [84]: $\ln(a_{Li}) = 2.662 - 5302 / T$.

4.7-4.8 the calculated and experimental thermodynamic potentials [83,70] of the β phase at different temperatures. The experimental and calculated results agree within 100 cal/g-at. (3 %).

A very satisfactory agreement has been obtained between the calculated and experimental thermodynamic data and equilibrium concentrations. This agreement indicates that the present model is quite adequate to describe the thermodynamic properties of the Li-Al system and, at the same time, that the free energy parameters of Table 4.6 are accurate. This is of particular importance in order to predict with confidence metastable equilibria for which the available experimental data are less numerous and less accurate.

4.5.7 Metastable α'-α Order-Disorder Reaction.

As mentioned in section 4.5.1, the character of the metastable Al-rich solid solution (α) - Al_3Li (α') system has generated some controversy in the literature [77]. The large concentration difference between the α and α' phases found experimentally between room temperature and 620 K, has led some investigators to propose the existence of a eutectoid reaction in this region. Thus, in order to clarify the topology of the phase diagram, we have used the energy parameters of Table 4.6 to investigate the metastable equilibrium between the α and α' phases.

We recall from previous sections that the energy parameters of the α and α' phases have been assumed to be the same and that the

Table 4.7

Calculated and experimental enthalpies and entropies of formation of the AlLi phase (β) at the equiatomic concentration.

ENTHALPY OF FORMATION (kcal/g-at.)		ENTROPY OF FORMATION (cal/g-at. K)	
Experimental	Present work	Experimental	Present Work
-5.17 [70]	-5.16	-2.46 [70]	-2.54
-5.2 [83]		-2.54 [83]	

Table 4.8

Calculated and experimental free energies of the AlLi phase (β) at different temperatures.

TEMPERATURE (K)	FREE ENERGY (kcal/g-at.)	
	experimental	present work
573	-3.74 [83]	-3.70
623	-3.62 [83]	-3.57
653	-3.55 [83]	-3.49
688	-3.49 [70]	-3.39

experimental α' solvus concentration (7.6 at% Li) at 508 K [73] has been used to evaluate these parameters. This particular equilibrium concentration has been retained among others because it agrees very well with the α' solvus concentration determined by Noble and Thomson at 527 K [72].

The effective pair interaction V_1 plays a key role in the modelling of the metastable (α -> α') ordering reaction. Although the calculated α-α' two-phase boundary depends on the values of the random energy coefficients and on the value of the effective pair interaction (V_1), the enthalpy of the ordering reaction (α -> α') at a fixed concentration depends only on the value of the effective pair interaction. The value of V_1 calculated from the critical temperature given in Ref.[85] has been therefore tested by comparing the calculated ordering enthalpy (0.43 kcal/g-at.) of the α phase (with 25 at.% Li) at 473 K with the estimated ordering enthalpy (0.44 kcal/g-at.) of Nozato and Nakai based on Differential Thermal Analysis [76]. The agreement is quite satisfactory considering the approximations involved in the evaluation of Ref.[76].

The calculated metastable α-α' two-phase boundaries are shown in Fig.(4.11). Due to their metastable character, they fall inside the α-β two-phase region. Good agreement is obtained above 500 K between the calculated and experimental [72,73] α-α' solvus concentrations; below 500 K however, the calculated α-α' two-phase region is wider than estimated by Ceresara et al. [75] using low-angle X-ray scattering measurements. At present it remains unclear whether the

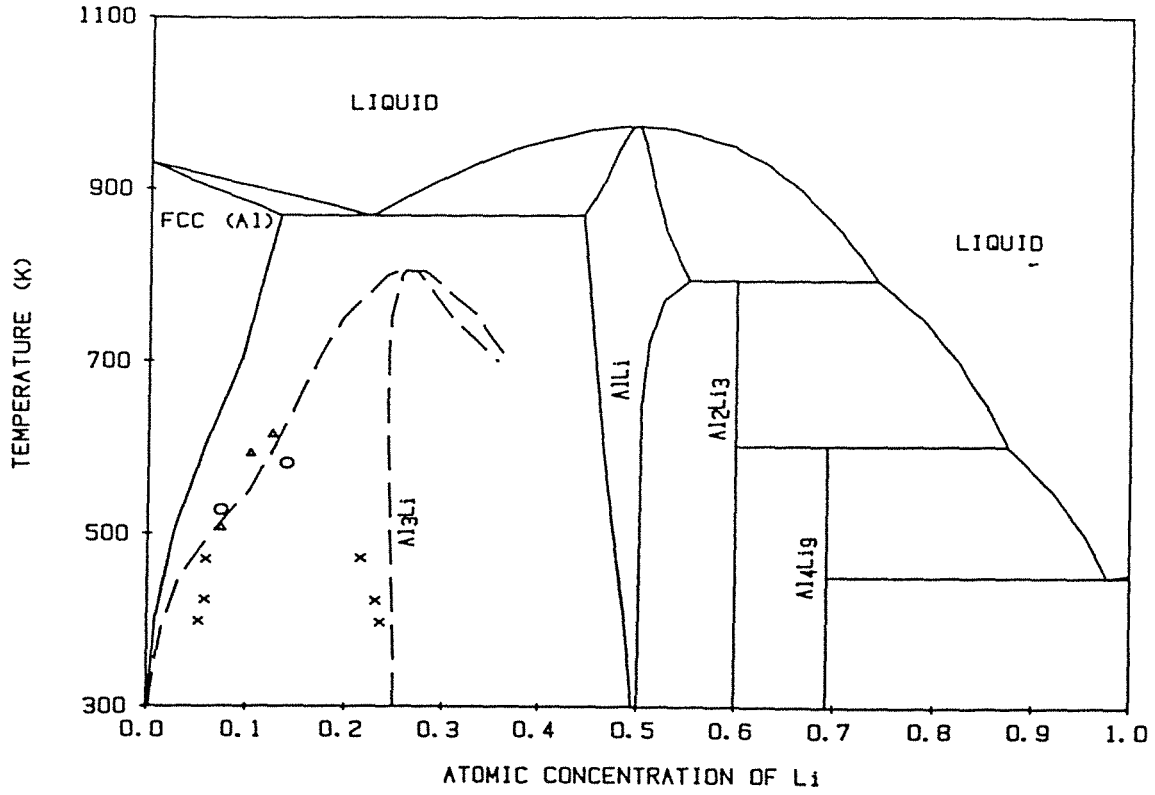

Fig. 4.11 : Calculated equilibrium Al-Li phase diagram (full line) and calculated metastable α-α' two-phase boundary (broken line). Triangles and circles are experimental data for α' solvus concentrations determined by transmission electron microscopy and reported, respectively, by Noble and Thomson [72], and by Williams and Edington [73]. Crosses are the experimental α-α' two-phase region limits determined by Ceresara et al. [75] using low-angle X-ray diffraction.

discrepancies are due to deficiencies in the model or to errors in the interpretation and analysis of the low-angle X-ray scattering measurements. The behavior of the two phase-region is explained within our thermodynamic description by the tendency of the α solid solution to segregate below 400 K. This extra level of metastability is the subject of the next subsection.

4.5.8 Metastable Miscibility Gap Within The α Phase.

Our model predicts the existence of a metastable miscibility gap below 400 K for Al-Li fcc solutions containing small amounts of Lithium. The computed miscibility gap is shown in Fig.(4.12). This segregation tendency is metastable relative to the α-β and α-α' equilibria. Consequently the miscibility gap falls inside the α-α' two-phase region. This result indicates that Al-Li alloys with small concentrations of Lithium and quenched sufficiently fast, may be expected to segregate and form characteristic Guinier-Preston zones. To the author's best knowledge, such a microstructure has not yet been observed. However, an endothermic reaction occurring in the same range of temperature and concentration has been reported by several investigators using differential thermal analysis [76,88-89].

Balmuth has attributed this reaction to the retrogression of fine Al_3Li precipitates [88]. Conversely Nozato and Nakai have interpreted the endothermic reaction to be due to a clustering reaction [76]. Our calculation supports the latter interpretation. Using differential scanning calorimetry, Papazian, Sigli, and Sanchez [89] have plotted

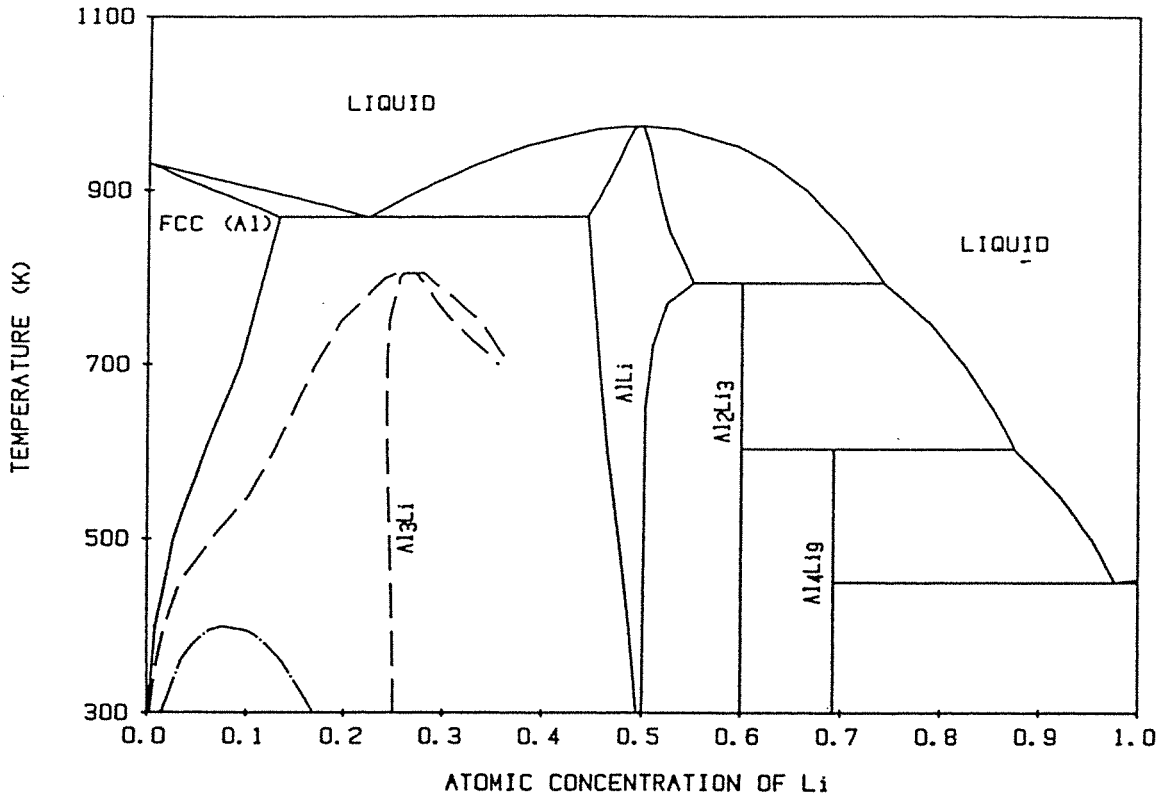

Fig. 4.12 : Calculated stable Al-Li phase diagram (————), metastable α-α' two-phase boundary (first level of metastability) (- - - -), and metastable miscibility gap α1 + α2 within the FCC solid solution α (second level of metastability) (— • —).

the observed dissolution peak temperatures as a function of the lithium content of the alloy. As can be seen in Fig.(4.13), the observed peak temperatures agree well with the miscibility gap predicted in the present analysis [89].

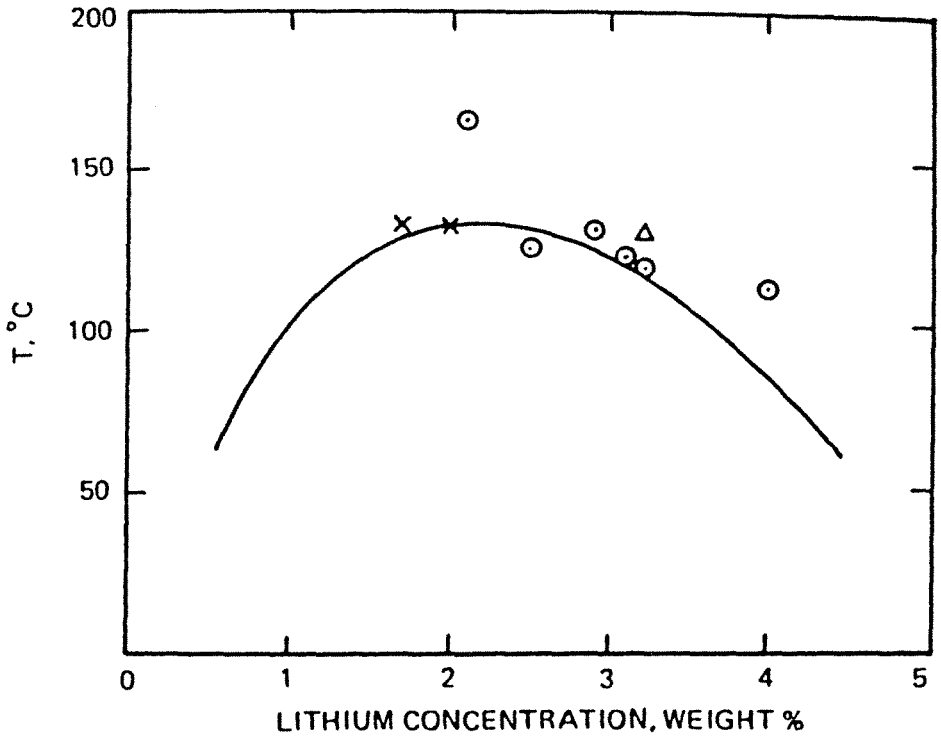

Fig. 4.13 : Comparison between the calculated metastable miscibility gap ($\alpha_1 + \alpha_2$) and the dissolution peak temperatures observed in various Al-Li alloys (⊙ [89], x [76], Δ [88]).

4.6 Conclusions of the Phenomenological Approach

A phenomenological model which allows the calculation of thermodynamic potentials and phase diagrams is a very valuable tool to extrapolate the available experimental data and to have a global thermodynamic picture of a given system. In the first part of this thesis, we have presented a phenomenological model that describes the free energy function in terms of physically meaningful contributions. Emphasis is put on the description of SRO in binary alloys by means of the cluster variation method. The contributions to the free energy are the lattice stability energies of the pure elements, the random alloy enthalpy of formation, the ordering energy, the configurational entropy, and the vibrational entropy of formation. It must be emphasized here that this thesis work represents the first application of the CVM to the thermodynamic investigation of real alloys.

The model has been applied successfully to analyze the Ni-Al, the Ni-Cr, and the more complex Al-Li system. It can be noticed that a relatively small number of selected experimental data is needed as input in the calculations. In the case of the Al-Li system, for example, 11 points in the phase diagram and three thermodynamic potentials have been used to determine the 19 energy parameters entering the model. We were then able to calculate the equilibrium Al-Li phase diagram and to investigate the metastable equilibrium between the Al-rich fcc solid solution and the Al_3Li. More remarkably, our model predicts a segregation tendency in the Al-Li system which seems to be confirmed by experiments [89].

A promising extension of this thesis work is to apply the free energy formalism to multicomponent alloys. The approach would consist in analyzing, first, all the possible binary alloys following the procedure described in this thesis. From the analysis, one can extract the energy parameters needed for the description of the multicomponent alloy. Such calculations would be of particular interest to the metallurgical field because very little is known experimentally about the thermodynamics and phase diagrams of multicomponent alloys.

5. A MICROSCOPIC THEORY FOR THE ENTHALPY OF FORMATION OF TRANSITION METAL ALLOYS.

5.1 Introduction

As demonstrated in previous chapters, the prediction of a phase diagram is a difficult task involving the calculation of all the contributions to the free energy, namely the free energy of the pure elements, the random alloy enthalpy of formation, the ordering energy, the configurational entropy, and finally, the vibrational entropy of formation. We will not attempt in this thesis to calculate all these terms from first-principles. Rather, we would like to focus our attention on the modeling of the enthalpy of formation, and test the feasibility of making quantitative predictions about the enthalpy of formation of transition metal alloys within the tight binding formalism.

The transition metals have been chosen for this analysis because their cohesive energy is dominated by the outer shell d-electrons [36,93] which are characterized by localized orbitals. These localized orbitals, in turn, provide an adequate basis for a tight-binding description of the alloy Hamiltonian [36,90-95]. An extension of the model including s-, p-, and f-electrons would allow, however, the calculation of ΔH_f for alloys of non-transition metals.

In what follows, we present a microscopic theory based on a tight binding Hamiltonian for the calculation of ΔH_f. In particular we

describe:

-1) The model tight-binding Hamiltonian used to fit the band structures of pure metals.

-2) The recursion method used to compute the density of states (or more precisely the Green function) of the pure elements.

-3) The Coherent Potential Approximation used to determine the energy of formation of random transition metal alloys.

-4) and finally, The General Perturbation Method used to calculate the effective pair interactions.

Following a description of the microscopic theory we present, in section 6, the results obtained for some transition metal alloys.

5.2 Tight-Binding Approximation For Pure Metals

In the one-electron approximation, the Hamiltonian can be written as:

$$H_{1e} = - \tilde{h}^2/(2m)\ \nabla^2 + V \qquad (58)$$

where m is the mass of the electron, $\tilde{h}$ is the Planck's constant, and V is the self-consistent Hartree-Fock potential that includes the ionic Coulomb potential and the potential arising from the Coulomb electron-electron interaction. In the tight-binding approximation, V is written as a sum of atomic potentials V_i centered at each lattice site i,

$$V = \sum_i V_i \tag{59}$$

and the eigenvectors of the Hamiltonian, $|\psi_n\rangle$, are written as a linear combination of atomic orbitals (LCAO) $|\phi_{k\lambda}\rangle$ centered at site k:

$$|\psi_n\rangle = \sum_{k,\lambda} a_{k\lambda} |\phi_{k\lambda}\rangle \tag{60}$$

where λ distinguishes between orbitals centered at the same site k.

In order to calculate the enthalpy of formation of transition metal alloys, we neglect the contribution of the core electrons (frozen core approximation) and consider only the valence electrons, here the electrons belonging to the (n-1)d shell and the (n)s shell. In a tight binding picture, these valence electrons give rise to a narrow d-band crossed by a wide s-band. In this study, we neglect the hybridization between these two bands and consider only the d-electrons in the calculation of ΔH_f. This approximation has been shown to explain, at least qualitatively, the physical properties of transition metal alloys [36,90-95].

Accordingly, we consider in Eq.(60) 5 atomic d-orbitals per lattice site (λ = 1, 2, 3, 4, 5). In addition these orbitals are chosen such that they verify the orthogonality relationship:

$$\langle \phi_{j\lambda} | \phi_{k\mu} \rangle = \delta_{\lambda\mu} \delta_{jk} \tag{61}$$

We recall here that, unlike s-orbitals, d-orbitals are not spherically symmetric and possess different symmetries depending on the value of the orbital quantum number m_l associated with them:

$m_l=0$ has the symmetry of $3z^2-r^2$ ($\lambda = 1$)

$m_l=\pm1$ has the symmetry of xy, yz ($\lambda = 2, 3$)

$m_l=\pm2$ has the symmetry of x^2-y^2, xy ($\lambda = 4, 5$)

In this basis of atomic orbitals, the Hamiltonian is written as:

$$H_{1-e} = \sum_{i,\lambda} \varepsilon^{o}_{i\lambda} \, |\phi_{i\lambda}\rangle\langle\phi_{i\lambda}| + \sum_{j,\mu,i,\lambda} \beta_{j\mu,i\lambda} \, |\phi_{j\mu}\rangle\langle\phi_{i\lambda}| \qquad (62)$$

where

$$\varepsilon^{o}_{i\lambda} = \langle\phi_{i\lambda} \mid \{ (-\tilde{h}^2/2m) \nabla^2+V \} \mid \phi_{i\lambda} \rangle \qquad (63)$$

$$\beta_{j\mu,i\lambda} = \sum_{k} \langle \phi_{j\mu} \mid V_k \mid \phi_{i\lambda} \rangle \qquad (64)$$

For a **pure metal**, $\varepsilon^{o}_{i\lambda}$ is the same for all sites and is just orbital dependent. If, in addition, we neglect the orbital dependence of $\varepsilon^{o}_{i\lambda}$, then the unique on-site energy ε^{o} is the **center of gravity** of the d-band. Concerning the hopping integrals, the three center integrals of the type $\langle\phi_{i\lambda}| V_k |\phi_{j\mu}\rangle$ are much smaller than the two center integrals $\langle\phi_{j\mu}| V_j |\phi_{i\lambda}\rangle$ and are neglected. In general, for the FCC lattice, only first nearest neighbor hopping integrals are kept in the summation of Eq.(62) (i.e. i and j are first nearest neighbor sites), whereas for the BCC lattice both first and second nearest neighbor hopping integrals are used.

Still, for a given transition metal, the number of hopping integrals to be evaluated seems to remain very large. However, Slater and Koster have shown [96] that the two center integrals, involving

sites i and j, can be expressed as a function of the direction cosines of $(\vec{r}_i - \vec{r}_j)$, and three independent integrals $dd\sigma(d_{ij})$, $dd\pi(d_{ij})$ and $dd\delta(d_{ij})$, where d_{ij} is the distance between sites i and j. This result is obtained by first considering the hopping integrals $\beta^0_{i\lambda,j\mu}$ for sites i and j sitting along the z axis. In a basis given by five orbitals having d symmetry, the matrix $\beta^0_{i\lambda,j\mu}$ is then diagonal:

$$\beta^0_{i\ 3z^2-r^2,\ j\ 3z^2-r^2} = dd\sigma(d_{ij}) \tag{65}$$

$$\beta^0_{i\ xz\ ,\ j\ xz} = dd\pi(d_{ij}) \tag{66}$$

$$\beta^0_{i\ yz\ ,\ j\ yz} = dd\pi(d_{ij}) \tag{67}$$

$$\beta^0_{i\ xy\ ,\ j\ xy^2} = dd\delta(d_{ij}) \tag{68}$$

$$\beta^0_{i\ x^2-y^2\ ,\ j\ x^2-y^2} = dd\delta(d_{ij}) \tag{69}$$

and the following inequalities hold true:

$$dd\sigma(d_{ij}) \leqq 0 \tag{70}$$

$$dd\pi(d_{ij}) \geqq 0 \tag{71}$$

$$dd\delta(d_{ij}) \leqq 0 \tag{72}$$

For an arbitrary bond direction (i-j), the expression for $\beta_{i\lambda,j\mu}$ is obtained by applying a rotational operation that brings the axis oz on the direction (i-j).

The contribution (E_T) of the d-electrons to the total energy of a pure metal is obtained by adding to the one electron energy E_{1-e}, the Coulomb ion-ion energy ($E_{ion-ion}$), and subtracting the intra- and inter-atomic electron-electron energies (E^{intra}_{e-e} and E^{enter}_{e-e}) that are counted twice in E_{1-e}:

$$E_T = E_{1-e} - E^{intra}_{e-e} - E^{inter}_{e-e} + E_{ion-ion} \tag{73}$$

The one-electron total energy (E_{1-e}) is simply given by integrating up to the Fermi energy E_f the density of states of the d-band ($\rho^o(E)$) multiplied by the energy E:

$$E_{1-e} = \int_{-\infty}^{E_f} \rho^o(E)\, E\, dE \tag{74}$$

If we assume that all the d-orbitals on a given site are equally occupied with no spin ordering, the intra-atomic electron-electron energy (per atom) can be approximated by [26,28,31]:

$$E_{e-e}^{intra} = (1/2)\, u\, n^{o\,2} \tag{75}$$

with

$$u = (9\,U - 4\,J)/10 \tag{76}$$

In Eq.(75-76), n^o is the number of d-electrons per atom, whereas U and J are the direct and exchange integrals defined as:

$$\langle \phi_{i\lambda}(\vec{r}_1)\, \phi_{i\mu}(\vec{r}_2) |\, \{(1/2)\, e^2/|\vec{r}_1-\vec{r}_2|\}\, | \phi_{i\lambda}(\vec{r}_1)\, \phi_{i\mu}(\vec{r}_2)\rangle = U \tag{77}$$

$$\langle \phi_{i\lambda}(\vec{r}_1)\, \phi_{i\mu}(\vec{r}_2) |\, \{(1/2)\, e^2/|\vec{r}_1-\vec{r}_2|\}\, | \phi_{i\lambda}(\vec{r}_2)\, \phi_{i\mu}(\vec{r}_1)\rangle = U+J\,(1-\delta_{\lambda\mu}) \tag{78}$$

where e is the charge of the electron, and where $\vec{r}_1$ and $\vec{r}_2$ refer to the coordinates of electrons "1" and "2".

To evaluate the inter-site electron-electron interaction we assume that d-electrons are spherically distributed around the atoms and neglect quadrupolar effects. The following expression is then obtained [29]:

$$E_{e-e}^{inter} = [e^2/(2\varepsilon^* N)] \sum_{i,j} (-n_i^o)(-n_j^o)/d_{ij} \qquad (79)$$

where ε^* is the dielectric constant of the medium, N is the total number of lattice sites, and n_i^o is the number of d-electrons on site i.

The Coulomb ion-ion interaction is given by a similar expression:

$$E_{ion-ion}^{inter} = [e^2/(2\varepsilon^* N)] \sum_{i,j} z_i z_j/d_{ij} \qquad (80)$$

where z_i is the charge of an ion on site i. In the case of a pure metal, we have $\{z_i = n_i^o = n^o\}$, and Eq.(73) reduces to:

$$E_T = E_{1-e} - (1/2)\, u\, (n^o)^2 \qquad (81)$$

A value of u equal to 3 eV (per electron) (see for example Ref.[97]) is taken for all transition elements.

5.3 Density of states of The pure Metals : The Recursion Method

5.3.1 Density of States, Local Density of States and Green's Function

The concept of local density of states was introduced by Friedel [98] in order to describe the electronic structure of non-periodic solids such as disordered alloys. If $\{E_n\}$ is the set of eigenvalues of the one-electron Hamiltonian, the local density of states on site i and for the orbital λ can be written as:

$$\rho_{i\lambda}(E) = \sum_n \delta(E-E_n)\, a^*_{i\lambda}(E_n)\, a_{i\lambda}(E_n) \qquad (82)$$

where $a_{i\lambda}$ is defined by Eq.(60), $a^*_{i\lambda}$ is the complex conjugate of $a_{i\lambda}$, and where $\delta(E-E_n)$ is a delta function centered at E_n. The local density of states (per orbital) on site i is then given by:

$$\rho_i(E) = (1/5) \sum_\lambda \rho_{i\lambda}(E) \qquad (83)$$

and the total density of states (per orbital and per point) is the average over the N lattice sites:

$$\rho(E) = (1/5N) \sum_i \rho_i(E) \qquad (84)$$

Note that, in the case of a pure metal, the local density of states, $\rho_i(E)$, is the same for all sites. In order to calculate the density of states, it is convenient to rewrite Eq.(82-84) in terms of the Green's function G(z) [99] defined as:

$$G(z) = (z - H)^{-1} \tag{85}$$

where z is a complex number and H is the Hamiltonian of the system. It can be shown that $\langle\psi|G(z)|\psi\rangle$ is an Herglotz function, i.e. $\mathrm{Im}\{\langle\psi|G(z)|\psi\rangle\} < 0$ when $\mathrm{Im}(z)>0$, and $\mathrm{Im}\{\langle\psi|G(z)|\psi\rangle\} > 0$ when $\mathrm{Im}(z)<0$. If $\{\Psi_n\}$ is the set of eigenvectors corresponding to the set of eigenvalues $\{E_n\}$, the Green's function can be expressed using the equation:

$$G(z) = \sum_n \{1/(z-E_n)\} \; |\Psi_n\rangle\langle\Psi_n| \tag{86}$$

or

$$\langle\phi_{k\lambda}|\, G(z)\, |\phi_{k\lambda}\rangle = \sum_n \{1/(z-E_n)\}\, a^*_{k\lambda}(E_n)\, a_{k\lambda}(E_n) \tag{87}$$

Using the definition of the delta function, namely,

$\{\delta(E-E_n) = -(1/\pi) \lim_{\eta->0^+} \mathrm{Im}\{ 1/(E+i\eta-E_n) \} \}$, the following identity is obtained:

$$(-1/\pi) \lim_{\eta->0^+} \mathrm{Im}\langle\phi_{k\lambda}|\, G(E+i\eta)\, |\phi_{k\lambda}\rangle = \sum_n \delta(E-E_n)\, a^*_{k\lambda}(E_n)\, a_{k\lambda}(E_n)$$

or

$$\rho_{k\lambda}(E) = (-1/\pi) \lim_{\eta->0^+} \mathrm{Im}\langle\phi_{k\lambda}|\, G(E+i\eta)\, |\phi_{k\lambda}\rangle \tag{89}$$

In order to determine the local density of states $\rho_{k\lambda}$ of a pure metal, we have used Eq.(89) and the recursion method for the calculation of the Green's function. The recursion method has been chosen over a reciprocal space integration, because of its wide potential applications in material science. Indeed, the recursion method applies naturally to non periodic systems such as non crystalline solids, surfaces, impurities [100] ...., whereas k-space calculations require a periodic lattice.

5.3.2 The Recursion Method

The recursion method [36,100-105] consists in constructing from the LCAO orthogonal basis $\{|\phi_{i\lambda}\rangle\}$, a new **orthogonal** basis $\{|\zeta_k\rangle$, k =1, 2, ... } where the tight binding Hamiltonian matrix, (H), is tridiagonal:

$$(H) = \begin{vmatrix} a_1 & b_1 & 0 & 0 & \\ b_1 & a_2 & b_2 & 0 & \\ 0 & b_2 & a_3 & b_3 & \\ 0 & 0 & b_3 & a_4 & \\ & & & & \ddots \end{vmatrix} \qquad (90)$$

If $|\zeta_1\rangle$ is made equal to $\phi_{i\lambda}$, it can be shown [36,100-105], that the Green's function of this Hamiltonian is given by the continued fraction:

$$\langle\phi_{i\lambda}|G(z)|\phi_{i\lambda}\rangle = \cfrac{1}{z - a_1 - \cfrac{b_1^2}{z - a_2 - \cfrac{b_2^2}{z - a_3 - \ldots}}} \qquad (91)$$

In order to apply Eq.(91), it is necessary to calculate the series $\{a_n\}$ and $\{b_n\}$. In what follows we present an efficient method, referred to as the recursion method, that allows the calculation of the coefficients $\{a_n\}$ and $\{b_n\}$.

The first step of the recursion method consists in choosing an initial

vector $|\zeta_1\rangle$. The local density of states at site 1 having the character λ ($\rho_{1\lambda}(E)$) is obtained by making $|\zeta_1\rangle$ equal $|\phi_{1\lambda}\rangle$. The value of a_1 is then given by:

$$a_1 = \langle\zeta_1| H |\zeta_1\rangle = \langle\phi_{1\lambda}| H |\phi_{1\lambda}\rangle \quad (92)$$

$|\zeta_2\rangle$ is obtained in two steps. A vector $|\zeta_2'\rangle$ is constructed such that it is orthogonal to $|\zeta_1\rangle$, and then normalized:

$$|\zeta_2'\rangle = H|\zeta_1\rangle - a_1 |\zeta_1\rangle \quad (93)$$

$$|\zeta_2\rangle = |\zeta_2'\rangle / \{\langle\zeta_2'|\zeta_2'\rangle^{1/2}\} \quad (94)$$

Finally the off-diagonal element of H, $b_1=\langle\zeta_2|H|\zeta_1\rangle$, is given by:

$$b_1^2 = \langle\zeta_2'| H |\zeta_1\rangle \quad (95)$$

$$= \langle\zeta_2' |\zeta_2'\rangle \quad (96)$$

At the level n of the recursion method we know, from previous steps, the values of $\{a_1, a_2, \ldots a_{n-1}\}$, $\{b_1, b_2, \ldots b_{n-1}\}$ and the vectors $(|\zeta_{n-1}\rangle, |\zeta_n\rangle)$. The matrix elements, a_n and b_n, and the vector $|\zeta_{n+1}\rangle$ are calculated using:

$$a_n = \langle\zeta_n| H |\zeta_n\rangle \quad (97)$$

$$|\zeta_{n+1}'\rangle = H|\zeta_n\rangle - b_{n-1} |\zeta_{n-1}\rangle - a_n |\zeta_n\rangle \quad (98)$$

$$|\zeta_{n+1}\rangle = |\zeta_{n+1}'\rangle / \{\langle\zeta_{n+1}'|\zeta_{n+1}'\rangle^{1/2}\} \quad (99)$$

$$b_n^2 = \langle\zeta_{n+1}'| H |\zeta_n\rangle \quad (100)$$

$$= \langle\zeta_{n+1}'|\zeta_{n+1}'\rangle \quad (101)$$

The new vectors $|\zeta_i\rangle$ are characterized by their coordinates in the LCAO basis $|\phi_{i\lambda}\rangle$, i.e. by a matrix $(c_{i\lambda})$ where i refers to the different lattice sites and λ refers to the 5 d-orbitals on each site. The number 1 is attributed to the site on which the orbital $|\zeta_1\rangle=|\phi_{1\lambda}\rangle$ is centered. To optimize the usage of computer memory, one can notice

that $|\zeta_{n+1}\rangle$ has coordinates $(c_{i\lambda})$ equal to zero when the corresponding site i cannot be reached from site 1 by less than n nearest-neighbor jumps in the case of an FCC lattice, and by less than n nearest-neighbor or next nearest-neighbor jumps in the case of a BCC lattice. At the level n of the recursion, it is convenient to define the cluster that includes all the points that can be reached, from site 1, by less than n near-neighbor jumps for the FCC structure, and by less than n near-neighbor or next nearest neighbor jumps for a BCC structure.

Considering the rapid growth of the cluster size with the number of levels and the limited amount of memory allocated in a computer, the continued fraction expansion must be truncated at a relatively low level N (usually 5 to 10). The corresponding density of states is then made of N delta functions [36,102]. In addition, it can be shown that **a level N of the recursion guarantees that the 2N+1 first moments of the density of states are reproduced exactly** [36,100-104]. We recall here that the n^{th} moment (μ_n) of the density of states is defined by:

$$\mu_n = \int E^n \rho(E)\, dE \qquad (102)$$

5.3.3 Termination of The Continued Fraction Expansion

As mentioned in the previous sub-section, the density of states of a continued fraction truncated at level N is made of N delta functions. It is however possible to obtain a better description of the density of states by terminating the truncated continued fraction with a complex function $\sum(z)$ which approximates the higher level

contribution to the green function.

$$\langle \phi_{i\lambda} | G(z) | \phi_{i\lambda} \rangle = \cfrac{1}{z - a_1 - \cfrac{b_1^2}{z - a_2 - \cdots - \cfrac{b_{N-1}^2}{z - a_N - \sum(z)}}} \qquad (103)$$

where the exact form of the termination $\sum(z)$ is given by:

$$\sum(z) = \cfrac{b_N^2}{z - a_{N+1} - \cfrac{b_{N+1}^2}{z - a_{N+2} - \cdots}} \qquad (104)$$

In the absence of band gaps, the coefficients $\{a_i\}$ and $\{b_i\}$ have been shown to converge toward limits [105], i.e. $\{\lim_{n\to\infty} a_n = a_\infty\}$ and $\{\lim_{n\to\infty} b_n = b_\infty\}$. If these limits have been reached at the level N of the recursion then $a_\infty = a_N$ and $b_\infty = b_{N-1}$, and the termination $\sum(z)$ verifies the identity:

$$\sum(z) = \frac{b_\infty^2}{z - a_\infty - \sum(z)} \qquad (105)$$

By solving this second order equation and retaining the root for which $\mathrm{Im}\{G(z)\}$ is negative when $\mathrm{Im}(z)$ is positive leads to the equation:

$$\sum(z) = (1/2)\left\{ z - a_\infty - \left[(z - a_\infty)^2 - 4\, b_\infty^2 \right]^{1/2} \right\} \qquad (106)$$

Note that $\{(-1/\pi) \lim_{\eta\to 0^+} \mathrm{Im}\, \sum(E+i\eta)\}$ describes a semi-elliptical density of states centered at a_∞ and of band width $4\, b_\infty$. As a result, truncating the continued fraction at level N and terminating it by Eq.(106) is equivalent to embedding the cluster of level N in an effective medium characterized by a semi-elliptical density of states.

When the coefficients a_n and b_n have not converged at level N, some approximation must be made about the values of a_∞ and b_∞. For arbitrary values of a_∞ and b_∞, the termination $\sum(z)$ is a real number outside the interval $I=[a_\infty-2b_\infty, a_\infty+2b_\infty]$, and so is the continued fraction except at some isolated energies corresponding to spurious delta functions in the density of states. Inside the interval I, $\sum(z)$ has an imaginary part corresponding to a band of allowed energies. Accordingly, if b_∞ is underestimated, spurious delta functions are obtained in the density of states between the real band limits and the interval I. If b_∞ is overestimated then an artificially large band width is obtained. However, the additional tail introduced in the density of states has a very small spectral weight. A good compromise for the determination of a_∞ and b_∞ has been proposed by Beer and Pettifor [106], and consists in finding a_∞ and b_∞ such that density of states corresponding to the terminated continued fraction has one delta function at the band edges $E=a_\infty\pm 2b_\infty$, and no delta function outside the band. At the band edges, $\sum(a_\infty \pm 2\, b_\infty)$ is equal to $\pm\, b_\infty$ and the terminated continued fraction at level N is given by:

$$\langle\phi_{i\lambda}|G(a_\infty+z)|\phi_{i\lambda}\rangle = \cfrac{1}{z-(a_1-a_\infty) - \cfrac{b_1^{\,2}}{z-(a_2-a_\infty) - \cdots - \cfrac{2b_{N-1}^{\,2}}{z-2(a_N-a_\infty)}}} \qquad (107)$$

where $z=2b_\infty$. The truncated continued fraction given in Eq.(107) describes the Hamiltonian:

$$\begin{vmatrix} (a_1-a_\infty) & b_1 & & & & \\ b_1 & (a_2-a_\infty) & b_2 & & & \\ & b_2 & \ddots & \ddots & & \\ & & \ddots & \ddots & b_{N-1} & \\ & & & b_{N-1} & (a_N-a_\infty) & \end{vmatrix}$$

For a given a_∞, the density of states of this Hamiltonian is made of N delta functions which are located at the eigenvalues $\{\lambda_1, \lambda_2, \ldots \lambda_N\}$ of the Hamiltonian. In order to get a delta function at both band edges and no delta function outside the band, the value of a_∞ is varied until $|\text{Max}(\{\lambda_i\})| = |\text{ min}(\{\lambda_i\})|$. Then $\{2b_\infty\}$ is made equal to $|\text{Max}(\{\lambda_i\})|$ or $|\text{ Min}(\{\lambda_i\})|$.

In this thesis we have applied the recursion method to pure transition metals in the FCC or BCC structures (the density of states of the HCP structure is taken to be equal to that of the FCC structure, see section 5.4.2). The continued fraction is terminated at the fifth level (11 exact moments in the density of states) and the method of Beer and Pettifor is used to calculate a_∞ and b_∞.

5.3.4 Off-diagonal elements of the Green's function

As we shall see in section 5.7, the values of the off diagonal elements of the Green's function must be determined in order to calculate effective pair interactions in the alloy (see Eq.(138) of section 5.7).

The off diagonal element of the green function $G_{i\lambda,j\mu}=\langle\phi_{i\lambda}|G(z)\ |\phi_{j\mu}\rangle$ can be calculated by using the recursion method three times in order to obtain the values of $\langle\phi_{i\lambda}+\phi_{j\mu}|G(z)|\phi_{i\lambda}+\phi_{j\mu}\rangle$, $G_{i\lambda,i\lambda}$, and $G_{j\mu,j\mu}$. The following expression is then used:

$$2\ G_{i\lambda,j\mu} = \langle\phi_{i\lambda}+\phi_{j\mu}|\ G(z)\ |\phi_{i\lambda}+\phi_{j\mu}\rangle - (G_{i\lambda,i\lambda} + G_{j\mu,j\mu}) \qquad (108)$$

5.4 Choice of Tight Binding Parameters for Pure Metals

The values of the on-site energy ε^0, and of the Slater-Koster parameters ddl (l = σ, π, δ) are needed as input for the calculation of the density of states, whereas the number of d electrons n^0 is needed as input for the determination of the pure metal Fermi energy.

5.4.1 On-site Energy ε^0 And Number of d-Electrons n^0

In general, it is difficult to determine the on-site energy of a pure metal from band structure calculations, since in such calculations, the zero of energy is not well defined and may vary from one element to another. This problem is usually circumvented by approximating the on-site energy of the d-band (ε^0) with the d-energy level of a **free atom.** It can be argued however that the electronic configuration of the atom in a metal is different from that of the free atom which is $s^2\ d^{Z-2}$ or, for some elements, $s^1\ d^{Z-1}$ (see for example Ref.[107]). In fact, detailed band structure calculations have shown that the configuration of the atom in the metal is close to $s^{1.3}\ d^{Z-1.3}$ [108], where Z is the total number of valence electrons. Following these results, we have used a number of d-electrons (n^0) equal to (Z-1.3) for all transition metals. To evaluate ε^0 , we have taken the d-energy level of a free atom in the configuration $s^1\ d^{Z-1}$ calculated by Robbins [109] (see Table 5.1 and Fig.(5.1)) and we have applied the following configuration correction (see section 5.6.1):

$$\varepsilon^0 = \varepsilon^{\square} - u\ 0.3 \qquad (109)$$

Table 5.1

Input parameters for the microscopic theory : d-band width Wd (in eV) [111], and the d-energy level of the free atom in the configuration $(s^1 d^{Z-1})$ ($\varepsilon^\square$) (in eV) [109]. The value of the number of d electrons (n°) as well as the corresponding Fermi energy (Ef) of the pure metal in the stable structure are also given for each atom. For all elements, a value of u=3 eV is used.

	Sc	Ti	V	Cr	Mn	Fe	Co	Ni	Cu
	HCP	HCP	BCC	BCC		BCC	HCP	FCC	FCC
n°	1.7	2.7	3.7	4.7		6.7	7.7	8.7	9.7
$\varepsilon^\square$	-1.51	-2.10	-2.63	-3.14		-4.07	-4.51	-4.93	-5.34
Wd	5.13	6.08	6.77	6.56		4.82	4.35	3.78	2.80
Ef	-2.78	-3.24	-3.40	-2.88		-3.30	-3.54	-3.83	-4.39

	Y	Zr	Nb	Mo	Tc	Ru	Rh	Pd	Ag
	HCP	HCP	BCC	BCC	HCP	HCP	HCP	FCC	FCC
n°	1.7	2.7	3.7	4.7	5.7	6.7	7.7	8.7	9.7
$\varepsilon^\square$	-1.77	-2.50	-3.22	-3.95	-4.68	-5.42	-6.17	-6.92	-7.68
Wd	6.59	8.37	9.72	9.98	9.42	8.44	6.89	5.40	3.63
Ef	-3.40	-4.08	-4.35	-3.55	-3.91	-4.06	-4.53	-5.33	-6.47

		Hf	Ta	W	Re	Os	Ir	Pt	Au
		HCP	BCC	BCC	HCP	HCP	FCC	FCC	FCC
n°		2.7	3.7	4.7	5.7	6.7	7.7	8.7	9.7
$\varepsilon^\square$		-2.18	-2.86	-3.56	-4.26	-4.98	-5.70	-6.44	-7.18
Wd		9.56	11.12	11.44	11.02	10.31	8.71	7.00	5.28
Ef		-3.97	-4.16	-3.10	-3.34	-3.34	-3.65	-4.36	-5.41

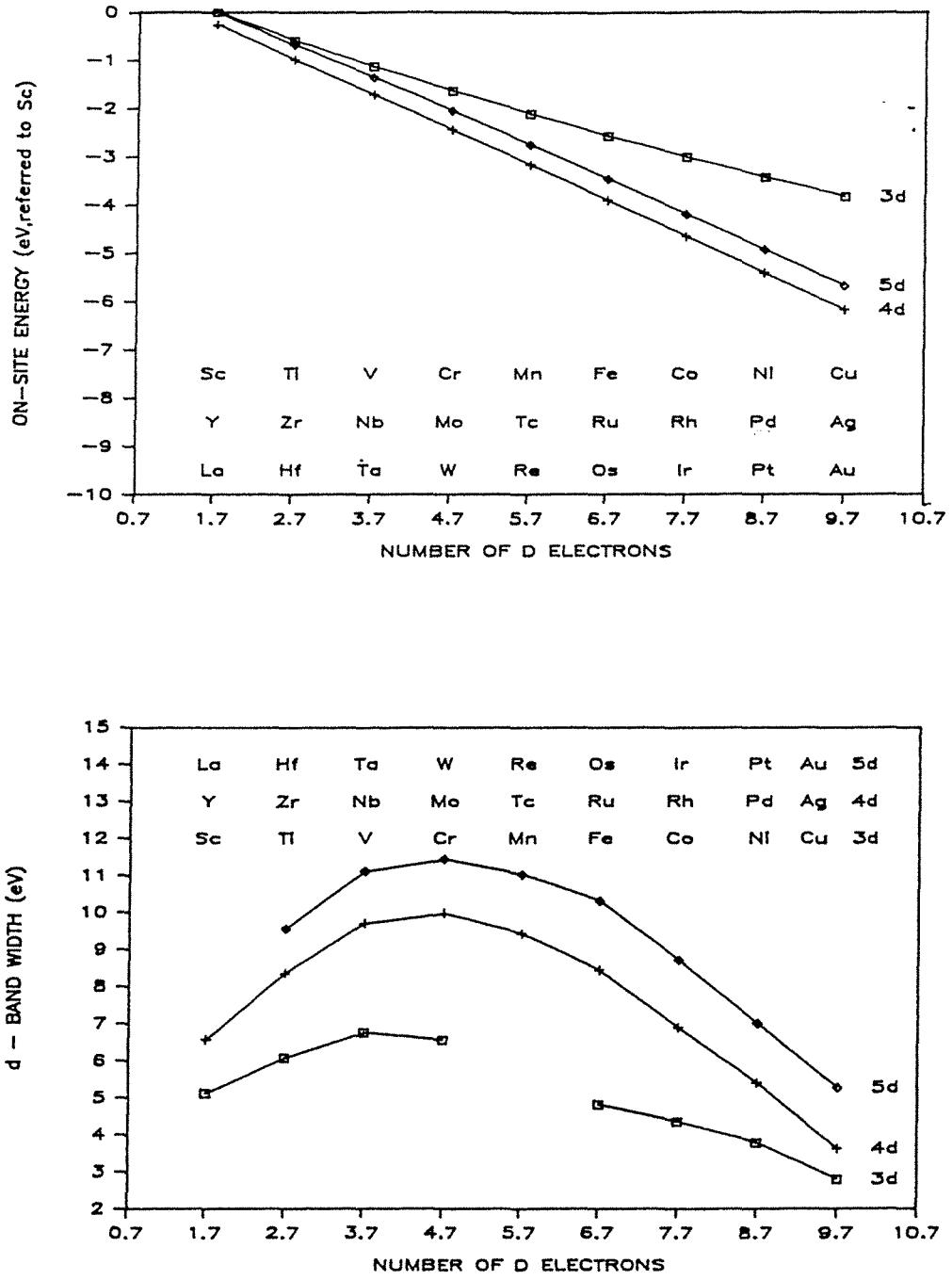

Fig. 5.1 : Input parameters for the microscopic theory: d-energy level of the free atoms in the configuration $(s^1 d^{Z-1})$ $(\varepsilon^{\square})$ [109], and d-band widths (Wd) [111] of the pure transition metals in their stable structures at 0 K.

The atomic energies, $\varepsilon^{\square}$, were calculated [109] for relativistic atoms in the configuration $s^1 d^{Z-1}$, with all d orbitals equally occupied, and no spin polarization. Exchange and correlations were included using the local-density functional calculated by Ceperley and Alder [110]. A value of u equal to 3 eV is chosen for all elements.

5.4.2 Slater-Koster Parameters

As shown by Harrison [111], the general form of the Slater-Koster parameters $dd\sigma(d_{ij})$, $dd\pi(d_{ij})$ and $dd\delta(d_{ij})$ can be derived from the Muffin Tin Orbital theory. The following expressions are obtained:

$$ddl(d_{ij}) = \eta_{ddl}\ \tilde{h}^2/m\ \ (r_d^3/d_{ij}^5) \qquad (110)$$

where the constants η_{ddl} ($l = \sigma, \pi, \delta$) are the same for all transition metals, and where the length r_d is characteristic of the pure element. This equation has the advantage of reducing the number of parameters characterizing the hopping integrals to only one parameter (r_d) and to provide a law of variation with distance for the hopping integrals.

The inter-atomic distances d_{ij} between different sites are taken to be the equilibrium ones at room temperature. The temperature dependence of the inter-atomic distance is neglected in this analysis. The approximation in question has not noticeable effect in our final results since we are interested in calculating the alloy enthalpy of formation, i.e. the difference between the total energy of the alloy and the total energies of the pure elements weighted by their concentrations. It must be emphasized, however, that the effect of

thermal expansion on total energies is not negligible, although it virtually cancels out in the calculation of the alloy enthalpy of formation.

In order to obtain the values of the constants η_{ddm}, Harrison has fitted the band structure of BCC chromium calculated by Mattheiss [112]. To do so, the on-site energy ϵ^0 of the Hamiltonian was assumed independent of the symmetry of the d-orbitals. In addition, first and second nearest neighbor hopping integrals were included in the Hamiltonian of BCC Chromium and were used together with Eq.(110) to fit the special points lying at the center of the Brillouin zone ($k=2\pi/a$ (000)) and at the edge of the Brillouin zone ($k=2\pi/a$ (100)). In this fitting procedure, the value of $dd\delta(d_{ij})$ is always very small in magnitude [36,111] and was taken equal to zero. The constants η_{ddm} proposed by Harrison to fit the band structure of BCC chromium are:

$$\eta_{dd\sigma} = -16.2 \tag{111}$$

$$\eta_{dd\pi} = 8.75 \tag{112}$$

$$\eta_{dd\delta} = 0 \tag{113}$$

These values are assumed to be the same for all elements and structures. Harrison has obtained the values of r_d [111] by reproducing the band widths predicted by Andersen and Jepsen [113] which are presented in Table 5.1 as well as in Fig.(5.1).

In the BCC structure the d-band width is given by [111]:

$$W_d = 115.04\ (\tilde{h}^2/m)\ (r_d^3/d^5) \tag{114}$$

whereas for the FCC structure W_d is given by:

$$W_d = 132.20\ (\tilde{h}^2/m)\ (r_d^3/d^5) \qquad (115)$$

Assuming only first nearest neighbor hopping integrals in the Hamiltonian, it can be shown that the first three moments of the density of states of an HCP structure are respectively equal to the first three moments of an FCC structure [36]. Therefore, in order to simplify the calculations we will neglect the difference between higher moments for the density of states in the HCP and FCC structures.

5.5 Choice of Tight Binding Parameters for Alloys

In a binary alloy, a given lattice site can be occupied by either an A or a B atom and the on-site energy will equal, respectively, ε_A or ε_B. This type of disorder is referred to as **diagonal disorder.** Another type of disorder is also present in the alloy and is called **off-diagonal disorder,** corresponding to the fact that the hopping integrals can now be of different types, i.e. $\beta_{A\lambda,A\mu}$, $\beta_{A\lambda,B\mu}$ or $\beta_{B\lambda,B\mu}$.

5.5.1 On-Site Energy ε_i

When alloying the pure metals A and B, a certain amount of charge transfer takes place between atom A and B. If the Fermi energy of metal A is lower than the Fermi energy of metal B, charge transfer occurs from B to A. We define here the charge transfer on atom i (Δn_i) as the difference between the numbers of d-electrons on atom "i" in the alloy (n_i) and in the pure metal "i" (n_i^o):

$$\Delta n_i = n_i - n_i^o \tag{116}$$

Any charge transfer changes the self-consistent site potentials $V_i(r)$. In general, a change in the site potentials $\Delta V_i(r)$ implies a change in the on-site energies (ε_i^o, i= A,B) **and** a change in the hopping integrals (see Eqs.(63-64)). For simplicity, we will assume that **charge transfer affects only the on-site energies.**

For a random alloy, the on-site energy is affected by charge

transfer through the intra-atomic electron-electron interactions only [29]. However, when SRO is present in the alloy, the on-site energy ε_i should also be affected by the inter-atomic electron-electron interactions. This second effect on ε_i has also been neglected in the present study. The change of the on-site energy (ε_i) due to a charge transfer (Δn_i) is then given by [31]:

$$\varepsilon_i = \varepsilon_i^o + u\ \Delta n_i \tag{117}$$

The new on-sites energies will, in turn, define a new charge transfer which will change ε_A and ε_B ... The process must be iterated until the Hartree-Fock electronic self-consistency is obtained. Note that the charge transfers on A and B are not independent and are related by the equation:

$$x_A\ \Delta n_A + x_B\ \Delta n_B = 0 \tag{118}$$

5.5.2 Slater-Koster Parameters

In general, the inter-atomic distance between two "i" (i = A,B) atoms in the alloy is a function of their local environment. We have assumed here that, **on the average**, the inter-atomic distance between two "i" atoms is the same in the alloy and in the pure metal "i". This approximation implies, in turn, that the Slater-Koster Parameters between two "i" atoms are the same in the alloy and in pure metal "i".

Concerning now the Slater-Koster parameters between A and B atoms, the Muffin Tin theory predicts that they should scale as the geometrical mean of those of pure A and pure B [111,113]:

$$ddl(d_{AB}) = s_{ddl} \{|ddl(d_{AA})\ ddl(d_{BB})|\}^{1/2} \quad (119)$$

where s_{ddl} is the sign of the Slater-Koster parameter given by Eq.(70-72). This equation was first assumed by Shiba and is often referred to as the Shiba's approximation [114]. This result is of particular importance because it greatly simplifies the alloy electronic structure calculation.

Indeed, we can now refer all the hopping integrals between A-A, A-B, and B-B atoms to the hopping integrals of a reference pure metal R of arbitrary band width W_R [114,115]:

$$\beta_{A\lambda,A\mu} = \chi_A\ \beta_{R\lambda,R\mu}\ \chi_A \quad (120)$$

$$\beta_{A\lambda,B\mu} = \chi_A\ \beta_{R\lambda,R\mu}\ \chi_B \quad (121)$$

$$\beta_{B\lambda,B\mu} = \chi_B\ \beta_{R\lambda,R\mu}\ \chi_B \quad (122)$$

where

$$\chi_i = \{ddl(d_{ii})/ddl(d_{RR})\}^{1/2} = (W_i/W_R)^{(1/2)} \quad (123)$$

It is then possible to define an effective Green function, $G^{\odot}_{i\lambda,j\mu}$, which is related to the actual Green function $G_{i\lambda,j\mu}$ by the relation:

$$G^{\odot}_{i\lambda,j\mu} = \chi_i\ G_{i\lambda,j\mu}\ \chi_j \quad (124)$$

The effective Green function $G^{\odot}_{i\lambda,j\mu}$ corresponds to the effective Hamiltonian:

$$H^{\odot} = \sum_{i,\lambda} \varepsilon_i^{\odot}(E)\ \ |\phi_{i\lambda}\rangle\langle\phi_{i\lambda}| + \sum_{i,\lambda,j,\mu} \beta_{R\lambda,R\mu}(d_{ij})\ \ |\phi_{i\lambda}\rangle\langle\phi_{j\mu}| \quad (125)$$

where

$$\varepsilon_i^{\odot}(E) = E + (\varepsilon_i - E)/\chi_i^{\,2} \quad (126)$$

The new effective Hamiltonian $H^{\odot}$ defined in Eq.(125) does not

include any off-diagonal disorder, i.e. the hopping integrals are that of the reference metal R. This fact greatly simplifies the application of the coherent potential approximation to the calculation of the random alloy density of states.

5.6 Random Alloy Density of States : Coherent Potential Approximation (CPA)

The fundamental difficulty in calculating the density of states of a disordered alloy is the lack of translational periodicity which prevents the use of k-space integration techniques and makes the recursion method very cumbersome to use. Indeed, if we were to use the recursion method, we would have to apply the method to a very large number of alloy configurations and average their respective density of states.

The idea of the CPA is to replace the actual random distribution of A and B atoms by a periodic system where each site is occupied by the same average atom. This system is referred to as the average CPA medium and is symbolically represented in Fig.(5.2.a). The average atom is characterized by an on-site energy σ, called the coherent potential, which is in general a complex number.

The Hamiltonian H_{CPA} of the CPA average medium is given by:

$$H_{CPA} = \sum_{i,\lambda} \sigma \quad |\phi_{i\lambda}><\phi_{i\lambda}| + \sum_{i,\lambda,j,\mu} \beta_{R\lambda,R\mu}(d_{ij}) \quad |\phi_{i\lambda}><\phi_{j\mu}| \qquad (127)$$

To this Hamiltonian corresponds a Green's function which is equal to $G^{\dagger}(z-\sigma)$, where $G^{\dagger}(z)$ is the Green's function of the pure reference metal R (with $\varepsilon_R^o=0$). $G^{\dagger}(z)$ is calculated using the recursion method presented in section 5.3.

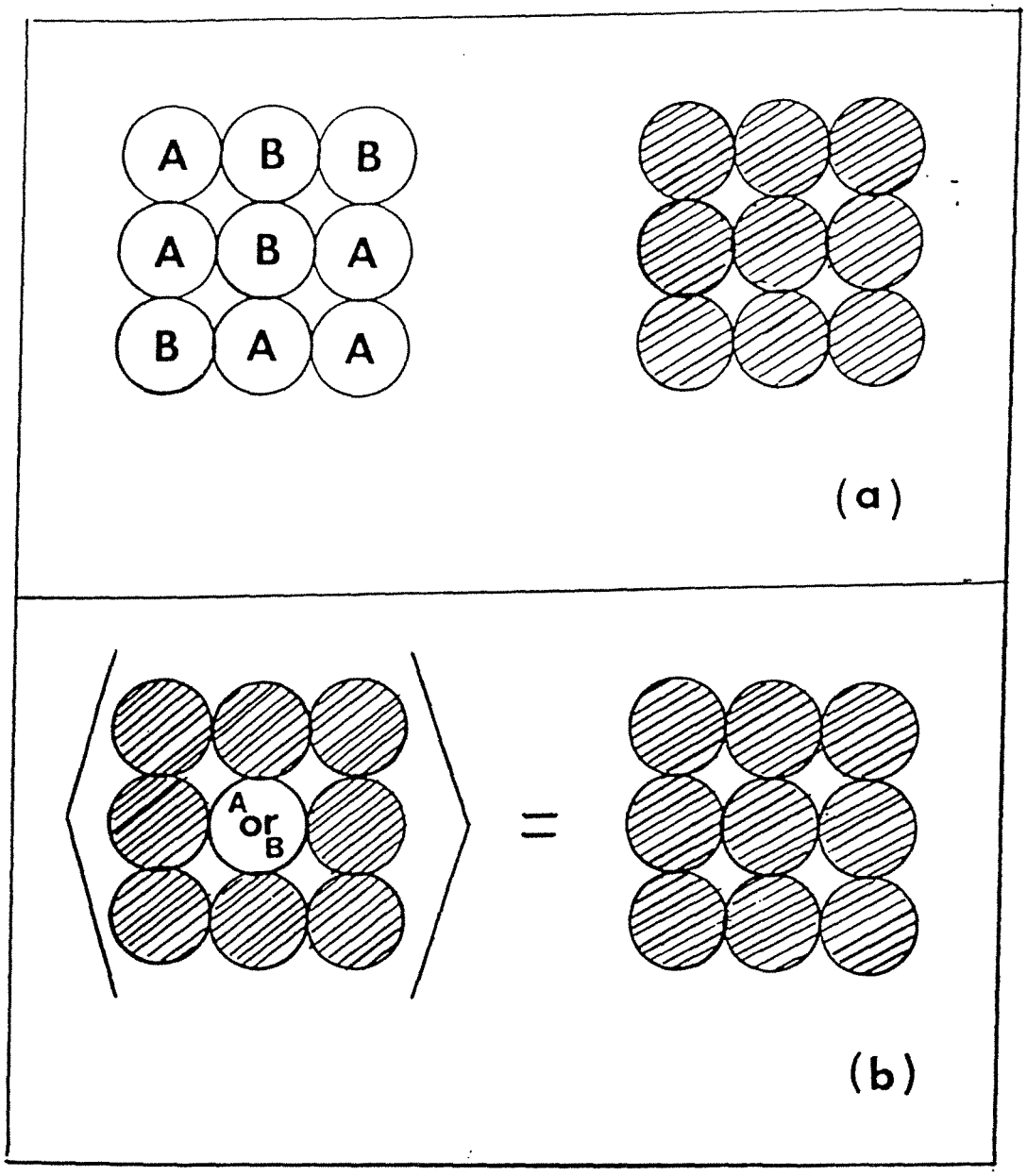

Fig. 5.2 : In the CPA, the ensemble of random alloys with all possible configurations of atoms (A, B) is represented by a periodic system with the average atom (shaded atom) at each site (Fig 5.2.a). The average atom is determined such that the scattering of an A or B atom surrounded by average atoms is, on the average, equal to zero (Fig 5.2.b). This represents the self-consistent condition of the CPA.

The coherent potential σ is obtained self-consistently, by requiring that the scattering of an "i" atom (i = A, B) placed, for example, at the origin (o) of the CPA average medium is, on the average, equal to zero (Fig.(5.2.b):

$$\langle t \rangle = c_A\, t_A + c_B\, t_B = 0 \tag{128}$$

where the scattering element t_i (i= A,B) is related to the perturbation of the on-site energy at the origin, $\Delta\varepsilon_i^{\odot} = \varepsilon_i^{\odot} - \sigma$, by the relation:

$$t_i = \Delta\varepsilon_i^{\odot} / \{\, 1 - \Delta\varepsilon_i^{\odot}\, G_{oo}^{\dagger}(E-\sigma) \,\} \tag{129}$$

and where we have used the notation:

$$G_{oo}(z) = 1/5 \sum_{\lambda} \langle \phi_{o\lambda} |\, G(z)\, | \phi_{o\lambda} \rangle \tag{130}$$

Equation (128) represents the self-consistent condition of the CPA. It is conveniently written under the form:

$$\sigma = x_1\, \varepsilon_1^{\odot} + x_2\, \varepsilon_2^{\odot} - (\varepsilon_1^{\odot} - \sigma)\, [G_{oo}^{\dagger}(E-\sigma)]\, (\varepsilon_2^{\odot} - \sigma) \tag{131}$$

and is used to find σ through an iteration procedure at each energy E. The projected Green's function on an "i" atom is then calculated using the identity:

$$G_{ii}^{\odot}(E) = [G_{oo}^{\dagger}(E-\sigma)]\, \{\, 1 + t_i\, [G_{oo}^{\dagger}(E-\sigma)] \}\, \tag{132}$$

and the actual projected Green's function is expressed as (see Eq.(124)):

$$G_{ii}(E) = G_{ii}^{\odot}(E) \,/\, \chi_i^{\,2} \tag{133}$$

The one-electron energy of the random alloy is obtained by integrating the energy multiplied by the density of states of the random alloy ($\rho(E)$). Note that $\rho(E)$ is expressed as:

$$\rho(E) = - (1/\pi) \, Im \, [x_A \, G_{AA}(E) + x_B \, G_{BB}(E)] \qquad (134)$$

The random alloy enthalpy of formation is then calculated using:

$$E_{rand} = E_{alloy} - x_A \, E_A - x_B \, E_B \qquad (135)$$

where the total energy of the alloy E_{alloy} is obtained by subtracting form the one-electron energy the intra-atomic electron-electron energy:

$$E_{alloy} = E_{1-e} - (1/2) \, u \, \{ \, x_A \, n_A^{\,2} + x_B \, n_B^{\,2} \, \} \qquad (136)$$

5.7 Effective Pair Interactions: the Generalized Perturbation Method (GPM)

The GPM has been proposed and developed by Gautier, Ducastelle, and co-workers [33-36,115] in order to calculate effective pair interactions in transition metal alloys. In this method, the EPIs are obtained by perturbing the average CPA medium by fluctuations in concentration that deviate from randomness. We recall in this sub-section the basic results of the GPM.

We will neglect in this thesis the effect of SRO on charge transfer. It can then be shown that the ordering energy per lattice point, E_{ord}, takes the form [33]:

$$E_{ord} = - 2/(\pi \, N) \;\; Im \int_{-\infty}^{E_f} dE \; Tr \sum_{p=2}^{\infty} \{ \, (G^{\dagger}(E-\sigma) \; T_d)^p \; (1/p) \, \}$$

$$+ (1/2N) \sum_{i,j} V \; (d/d_{ij}) \; \Delta n_i \; \Delta n_j \qquad (137)$$

where T_d is the diagonal part of the scattering matrix (i.e. $T_d=(t_i)$),

N is the total number of lattice points, Tr stands for the operator "trace" , d is the nearest-neighbor distance, and V is equal to $(1/4\pi\varepsilon^{*}d)$. The first term in Eq.(137) defines a cluster expansion of the ordering energy where the terms for which p equals 2 correspond to pair terms, the terms for which p equals 3 correspond to triplet terms... The second term in Eq.(137) represents an electrostatic interactions between ions screened by their respective clouds of d-electrons. The net charge on each pseudo-atom i is Δn_i.

It has been shown [34] that the contributions of triplet and larger clusters to the ordering energy may, in most cases, be neglected. Accordingly, we will keep only the pair terms (p=2) in the first part of Eq.(137). The corresponding effective pair interactions V_{ij} between sites i and j are then given by:

$$V_{ij} = -\frac{1}{(2\pi)}\,\mathrm{Im}\int_{-\infty}^{E_f} dE\ (t_A-t_B)^2 \sum_{\lambda,\mu} \{G^{\dagger}_{i\lambda,j\mu}(E+\sigma)\}^2 + V\,(d/d_{ij})\,\Delta^2/4 \qquad (138)$$

where $G^{\dagger}(z)$ is the Green function of pure R (with $\varepsilon^{o}_{R}=0$), and Δ is defined as:

$$\Delta = \Delta n_A / x_B = -\Delta n_B / x_A \qquad (139)$$

In this study, we have used the value of V (V=0.4 eV) adopted by Robbins and Falicov [116].

In the page 100, we give a flowchart of the microscopic theory that includes the input parameters of the theory (i.e. the results of calculations for the pure elements), the CPA self-consistency loop,

the electronic self-consistency loop, and finally the GPM. At the end of the process, the calculated random alloy enthalpy of formation (E_{rand}) and the EPIs (V_k) are obtained and can be input in the CVM to calculate the configurational entropy and the amount of SRO in the alloy, for a given concentration and temperature.

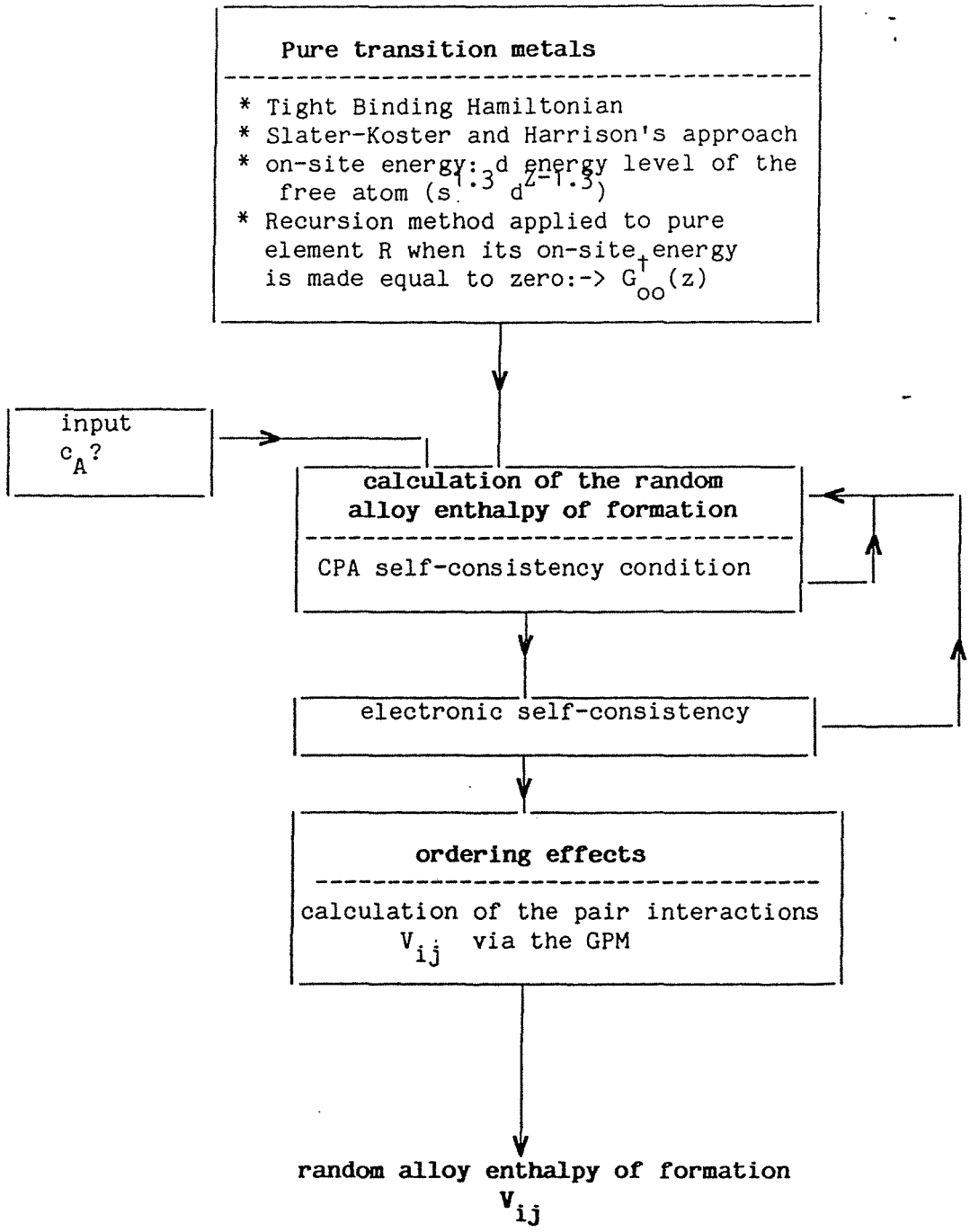
Pure transition metals
* Tight Binding Hamiltonian
* Slater-Koster and Harrison's approach
* on-site energy: d energy level of the free atom ($s^{1.3}$ $d^{Z-1.3}$)
* Recursion method applied to pure element R when its on-site energy is made equal to zero:-> $G^{\uparrow}_{oo}(z)$
input c_A?
calculation of the random alloy enthalpy of formation
CPA self-consistency condition
electronic self-consistency
ordering effects
calculation of the pair interactions V_{ij} via the GPM
random alloy enthalpy of formation V_{ij}

6.RESULTS OF THE MICROSCOPIC THEORY.

6.1 Approximations in The Model And Range of Applicability.

The model presented in section 5 includes two approximations which limit its range of applicability among the transition metal alloys. Namely, we have neglected spin polarization effects and the contributions of s- and p-electrons in the calculation of the enthalpy of alloy formation.

Since spin polarization is not included in our calculations, we will not consider alloys of Iron, Cobalt, and Manganese. For these systems, the calculations of Moruzzi and co-workers [117] have shown that the predicted lattice parameters change noticeably when spin polarization effects are taken into account. As a result, the A-A (A = Fe, Co, Mn) inter-atomic distance in a paramagnetic alloy is expected to be different from that in the (magnetic) pure metals. Consequently, the assumption made in section 5.5.2 that the average A-A inter-atomic distance is the same in the pure metal and in the alloy is not expected to be valid. Our model should provide, however, reasonable results for the other magnetic transition metals, FCC-Ni and BCC-Cr, since the calculations of Moruzzi and co-workers [117] show that the lattice parameter can be accurately predicted when spin polarization effects are neglected.

The contribution of s- and p-electrons to the enthalpy of formation is expected to be negligible for alloys with almost

half-filled d-bands since, in that case, the d-bonding contribution to the total energy is maximum [93]. We will study BCC-alloys obtained by mixing elements belonging to the VB and VIB columns in the periodic table (V, Nb, Ta, Cr, Mo, and W). At the equiatomic concentration, these alloys have an average number of d-electrons equal to 3.7, 4.2, or 4.7. We will also study the enthalpy of formation of alloys obtained by mixing the hexagonal metals, Ti, Zr, and Hf with the FCC metals, Ni, Pd, and Pt. At the equiatomic concentration, the number of d-electrons of these alloys is equal to 5.7. Note that, as mentioned in section 5.4.2, the density of states of the HCP structure will be approximated by that of the FCC structure with the same nearest neighbor distance.

6.2 Results For BCC Alloys [118]

6.2.1 Random Alloys

The enthalpies of formation predicted for the selected BCC-alloys are summarized in Fig.(6.1). The results are given for random equiatomic alloys and are compared with available high temperature measurements made in the disordered BCC-solid solution [119-123]. As can be seen, a very good agreement between theory and experiment [119-121] is obtained for the Cr-Mo, Mo-Nb, and Mo-Ta alloys. Discrepancies are obtained for the Cr-V and Ta-W systems. Note however that the experimental data reported in Ref.[122] for the Cr-V system are very inaccurate and have an estimated experimental error which is four times larger than the experimental data themselves. Concerning

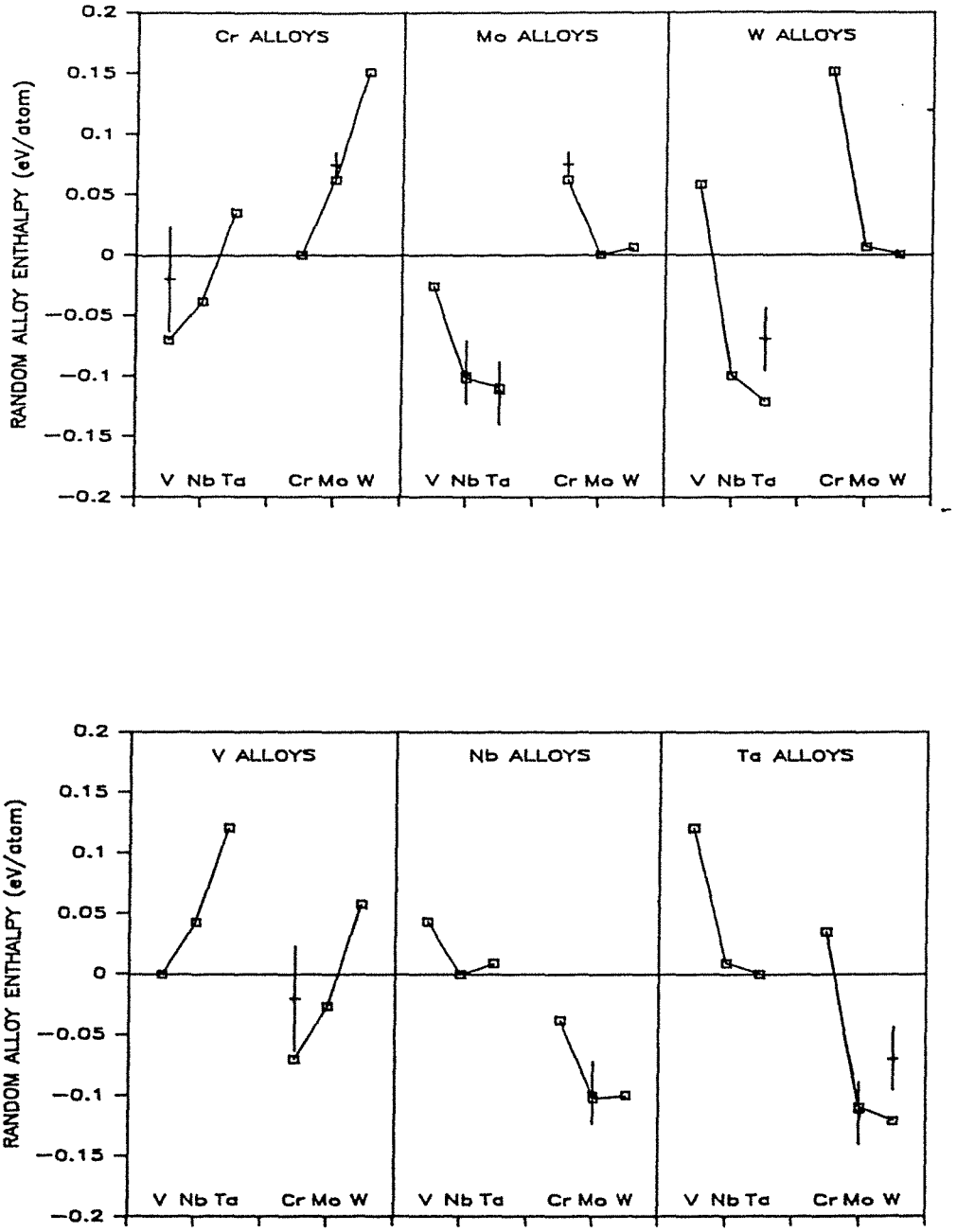

Fig. 6.1 : Random alloy enthalpies of formation calculated for the equiatomic BCC binary alloys. The binary alloys considered are obtained by mixing Cr, Mo, W, V, Nb and Ta (□). Available experimental data are indicated by crosses with error bars.

the Ta-W system, our result is about twice as large as the only available measurement [123].

In our model, the enthalpy of formation of a random alloy (AB) depends on three parameters characterizing the pure elements: the diagonal disorder ($\Delta\varepsilon=\varepsilon_A^o-\varepsilon_B^o$), the off-diagonal disorder ($\Delta W=W_A-W_B$), and the difference in the number of d electrons between A and B ($\Delta n=n_A^o-n_B^o$). Note that the two other input parameters, the effective intra-atomic Coulomb integral (u) and the inter-atomic potential (V), are fixed and are equal to 3 eV and 0.4 eV respectively. The diagonal disorder and the difference in the number of d-electrons represent negative contributions to the enthalpy of formation, whereas the off-diagonal disorder represents a positive contribution to the enthalpy of formation.

Off-diagonal disorder and the self-consistent effect of charge transfer have often been assumed to contribute negligibly to the enthalpy of formation. Our results indicate, however, that both effects are as important as that of diagonal disorder. To illustrate this point, the enthalpy of formation of the random Cr-Mo alloy has been calculated at the equiatomic concentration neglecting electronic self-consistency and off-diagonal disorder effects. A value of -0.137 eV was then obtained for E_{rand}. The negative sign of E_{rand} indicates an ordering tendency in the Cr-Mo system which is contrary to experiment [119]. By including electronic self-consistency in the calculation but still neglecting off-diagonal disorder effects, we obtained a value of E_{rand} equal to 0.016 eV. In this case, the sign is

consistent with experiment but the calculation is in poor quantitative agreement with the experimental measurement of 0.075±0.010 eV reported in Ref.[119]. Finally if both effects are taken into account, a value for E_{rand} of 0.062 eV is obtained and is in fair agreement with experiment.

The effect of off-diagonal disorder can be clearly seen in Fig.(6.1) in the case of Chromium alloyed with Molybdenum or Tungsten. The positive value obtained for the enthalpy of formation is explained by the dominant effect of ΔW (see Table 5.1). The increase in E_{rand} from Cr-Mo to Cr-W is due to an increase in off-diagonal disorder (and a small decrease in diagonal disorder). The Δn effect can be seen by considering, for example, the Cr-Nb system for which there is nearly no diagonal disorder and a noticeable off-diagonal disorder. The negative sign obtained for E_{rand} is explained by the fact that the difference in the number of d-electrons (Δn) offsets the positive contribution arising from the difference in band-width (ΔW). With reference to Fig.(6.1), we can distinguish a family of alloys for which $\Delta n=0$, and a family of alloys for which $\Delta n=\pm 1$ (alloys in a family are connected by a solid line in Fig.(6.1)). As expected, we see from the figure that the enthalpies of formation for alloys with $\Delta n=\pm 1$ are systematically lower than for alloys with $\Delta n=0$.

There have been some attempts in the literature [90-92] to use the tight-binding model in order to fit directly experimental enthalpies of formation. This procedure is to be distinguished from the one used in this thesis where the input parameters of the model are the results

of pure element ab-initio calculations. For example, Colinet, Pasturel, and Hicter (CPH) [91] have used a tight-binding Hamiltonian to calculate the enthalpy of formation of random transition metal alloys by reproducing only the first two moments of the density of states. These authors took into account intra-atomic electron-electron interactions using a value of the effective Coulomb integral u equal to 6 eV. The input parameters of their model (i.e. on-site energies and band widths) were obtained by fitting available experimental enthalpies of formation. The band widths obtained by their fitting procedure are compared in Fig.(6.2) with Andersen's and Jepsen's predictions which are used in the present work. The striking discrepancies which are observed between CPH's and Andersen's band widths cast some doubts about the overall physical meaning of the fitting procedure developed by CPH.

Watson and Bennett (WB) [90,92] have used a square-band model to calculate the enthalpy of transition metal alloys at the equiatomic concentration. They have estimated d on-site energies from first principle calculation [90] and have obtained d-band fillings and d-band widths by fitting a large set of experimental enthalpies of formation. The fitted band-width of BW are in general agreement with Andersen's and Jepsen's predictions (see Fig.(6.3)). Nevertheless, significant discrepancies remain.

In Table 6.1, we compare our results with the data obtained by CPH [91] and BW (BW1 [90] & BW2 [92]). As can be seen CPH and BW fail to reproduce the segregation tendency observed experimentally in the

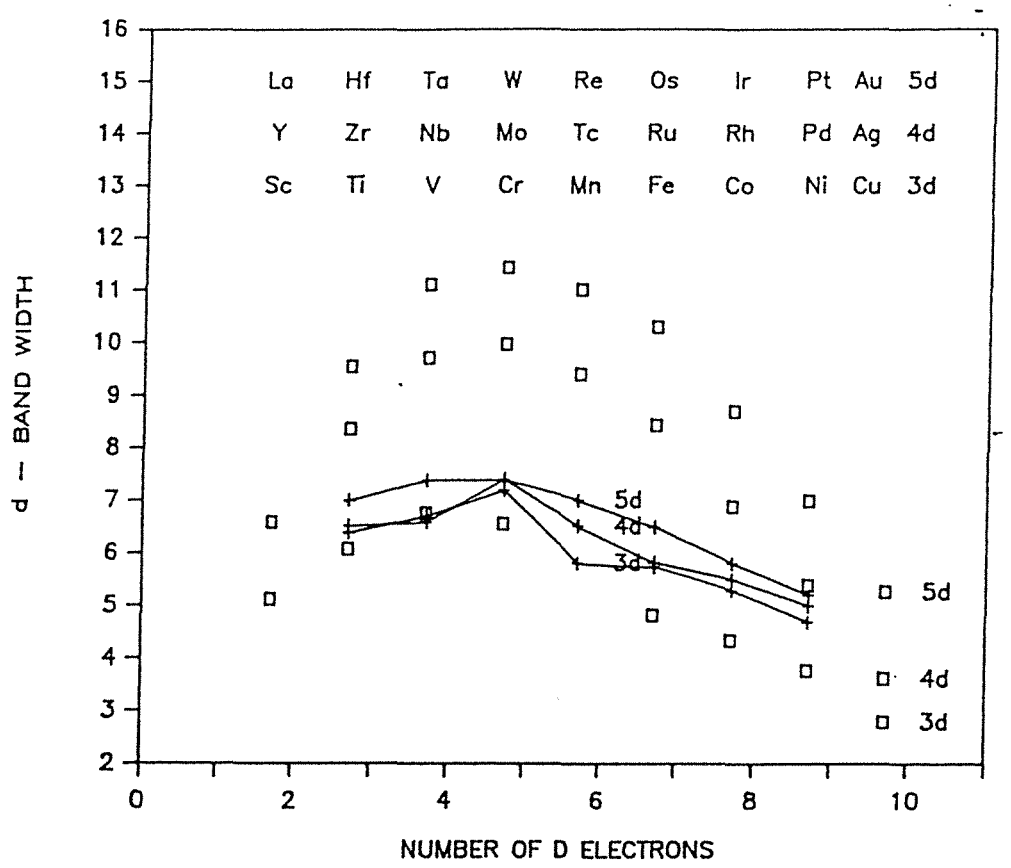

Fig. 6.2 : Comparison of the fitted d-band widths of Colinet and co-workers [91] (+) with the d-band widths predicted by Andersen and Jepsen [113] (□). Andersen's and Jepsen's values are used as input parameters in the present work.

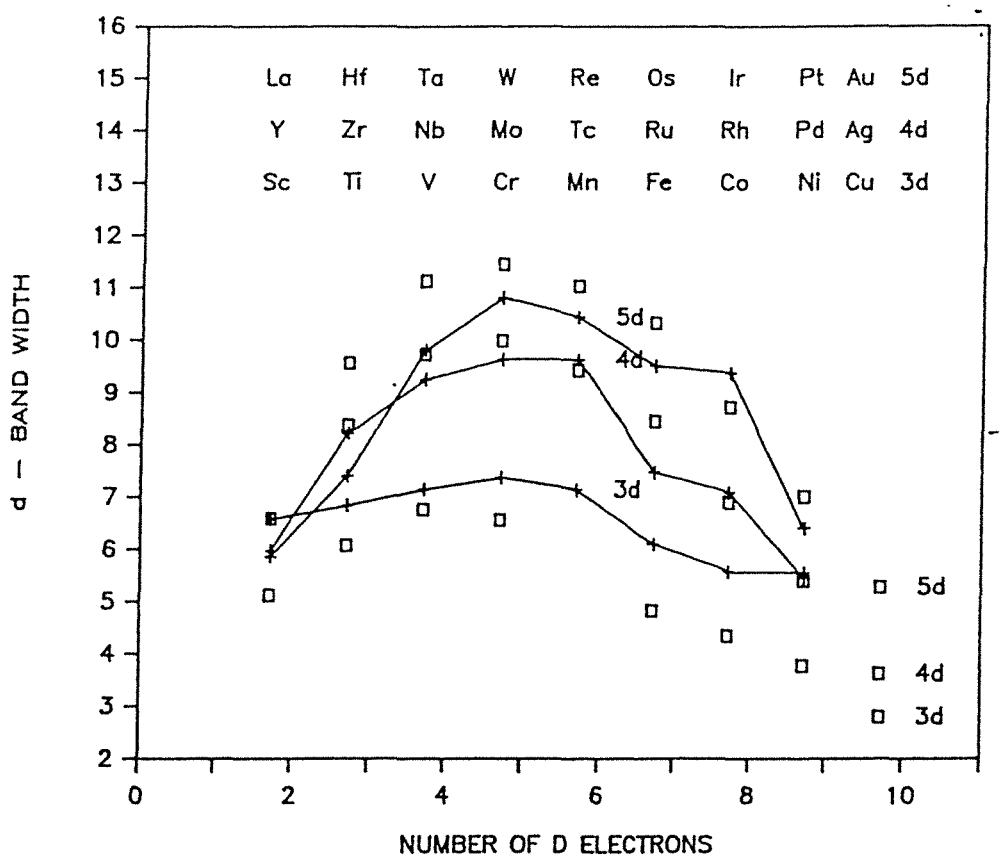

Fig. 6.3 : Comparison of the fitted d-band widths of Watson and Bennett [92] (+) with the d-band widths predicted by Andersen and Jepsen [113] (□). Andersen's and Jepsen's values are used as input parameters in the present work.

Table 6.1

Comparison of the present work's results, with the results of BW [90,92] and CPH [91], and with the experimental results. The comparison is made for those bcc alloys which have an experimental enthalpy of formation or phase diagram information. All enthalpies are given in eV at the equiatomic concentration.

ALLOY	EXPERIMENTAL ENTHALPY	PHASE DIAGRAM INFORMATION	PRESENT WORK Erand	BW1 [90]	BW2 [92]	CPH [91]
Cr-Mo	+0.075 [119]	Miscibility Gap below 1200 K [119]	+0.062	-0.014	0.006	0.0
Cr-W	--------	Miscibility Gap below 1950 K [124]	+0.151	0.001	-0.02	0.0
Mo-Nb	-0.097 [120]	Solid Solution above 1200 K	-0.102	-0.023	-0.03	-0.031
Mo-Ta	-0.110 [121]	Solid solution above 1200 K	-0.110	-0.027	-0.05	+0.010
Ta-W	-0.069 [123]	Solid solution above 1200 K	-0.121	-0.026	-0.09	+0.021
Cr-V	-0.02 ? [122]	Solid solution above 1200 K	-0.070	-0.020	-0.01	+0.010

Cr-Mo and the Cr-W alloys. Concerning the ordering systems (Mo-Nb, Mo-Ta, Ta-W), our calculated enthalpies agree better with the experimental data than the results of BW or CPH.

The observed discrepancies in the results of BW or CPH are explained by several flaws in their fitting procedure. In particular, they have neglected the ordering energy and proceeded to fit the experimental enthalpy of ordered phases with a random alloy enthalpy. They have also tried to reproduce experimental data which have large uncertainties. This explains the differences that can be seen in Table 6.1 between the results of BW1 [90] and BW2 [92]. In Ref.[92], Bennett and Watson have updated some of the experimental results used to calculate the input parameters of the model. The modification in the input parameters changes, in turn, the calculated enthalpies of formation. We can see in Table 6.1 that BW2 agrees slightly better with the experiment than BW1 does. Finally, BW and CPH have attempted to fit experimental measurements outside the range of applicability of the model: Fe-, Co-, or Mn-alloys, or alloys with a nearly empty or a nearly full band.

6.2.2 Ordered phases and Short Range Order

We present in Fig.(6.4) through Fig.(6.18) the calculated enthalpies of formation for the random alloy (E_{rand}) together with the first and second nearest neighbor pair interactions (V_1 and V_2). It should be noted that the effective pair interactions (EPI) are almost concentration independent, due to the fact that Δn is small for this

set of alloys. At a given temperature and concentration, the random alloy enthalpy of formation and the EPIs can be input to the CVM in order to calculate the configurational entropy and the amount of SRO in the alloy. Furthermore, if we neglect the vibrational entropy of formation, we can use the configurational entropy given by the CVM and calculate phase diagrams for the systems under consideration. We will discuss here the set of alloys for which experimental enthalpies of formation are available (i.e. Cr-Mo, Cr-V, Mo-Nb, Mo-Ta, Ta-W). The experimental data were obtained at high temperatures (above 1200 K) in the BCC solid solution. At these temperatures, our calculation indicates that the SRO contribution (i.e. the ordering energy) to the enthalpy of formation is approximately one tenth of E_{rand}. As explains below, the ordering energy becomes more significant at lower temperatures.

The first nearest neighbor pair interaction (V_1) is negative for the Cr-Mo system indicating a clustering tendency, whereas the sign of V_1 for Mo-Nb, Mo-Ta, Cr-V, and Ta-W is positive indicating an ordering tendency. In fact, our model predicts the presence of a miscibility gap for Cr-Mo below 1310 K. This result is in fair agreement with the experimental results of Kubaschewski and Chart indicating the presence of a miscibility gap below 1200K. For the W-Ta, Ta-Mo, Mo-Nb, and Cr-V we predict the existence of a CsCl (B_2) ordered phase below 920 K, 1040 K, 800 K, and 590K respectively. These results are consistent with the complete solubility found in these alloys above 1200 K. To the author's best knowledge, however, no experimental evidence is currently available concerning the existence of a low temperature B_2

phase.

Williams, Gelatt, and Moruzzi [125] have used the local density approximation together with a Muffin-Tin Hamiltonian in order to predict the enthalpy of formation of the MoNb compound in the CsCl structure. Our result (-146meV), obtained by adding E_{rand} (-102meV) and E_{ord} (-44meV), is in remarkable agreement with their calculation (-152meV). Our analysis however enables us to describe the disordered phase and to calculate a disordering temperature (800 K) for the compound MoNb in the CsCl structure. Note that the ordering energy of MoNb (CsCl) represents an important contribution to the total enthalpy of formation (about one third). This observation emphasizes once more the important role played by SRO in the enthalpy of alloy formation.

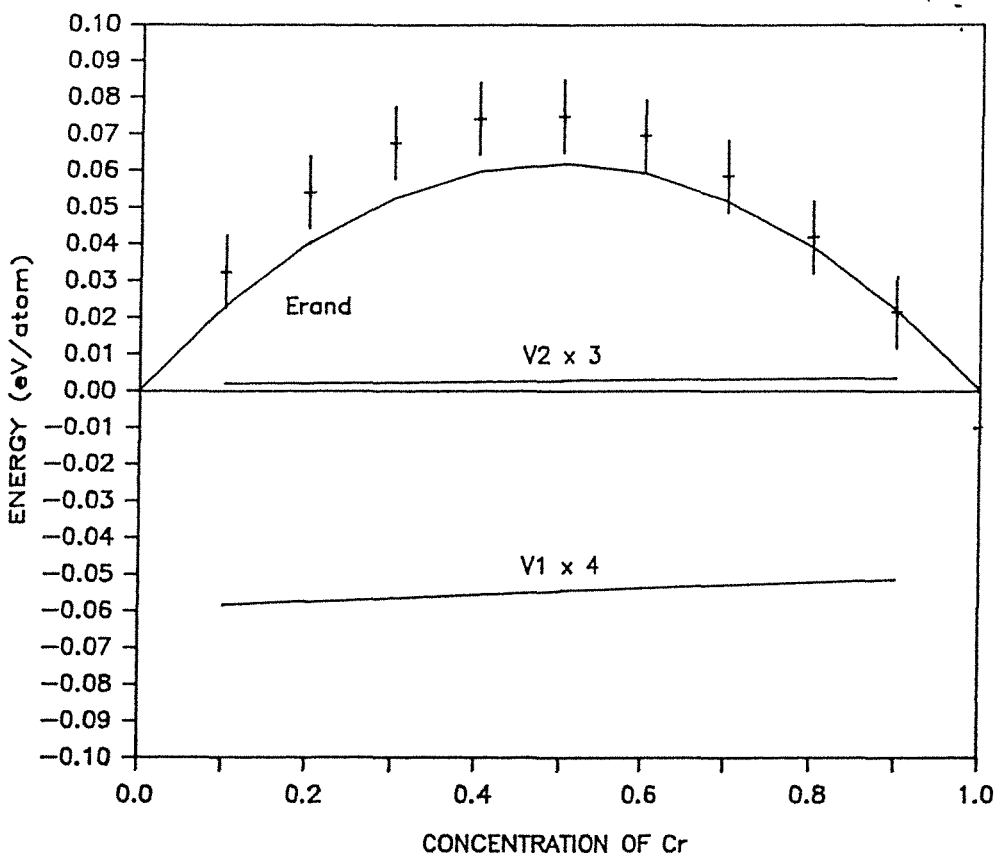

Fig. 6.4 : BCC Cr-Mo system. The calculated enthalpy of formation for the random alloy (E_{rand}) is shown in full line together with the first and second nearest neighbor effective pair interactions (V_1, V_2). The experimental enthalpy of formation measured at 1471 K [119] is indicated by crosses with error bars.

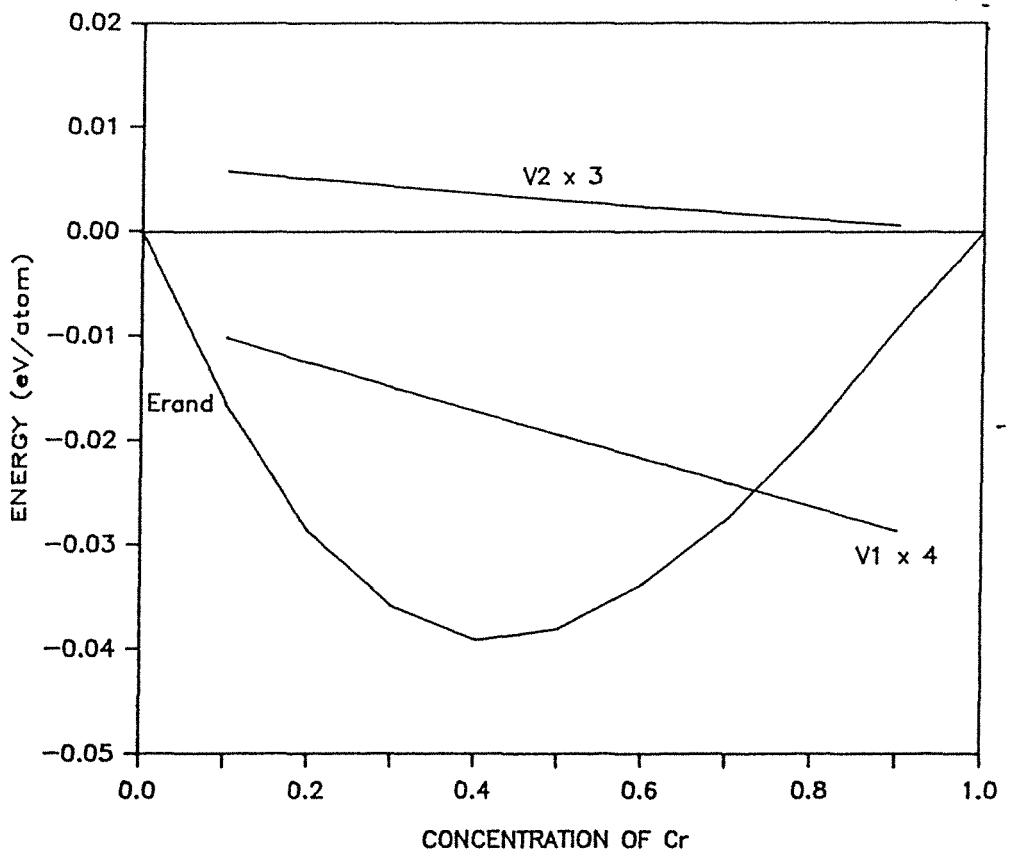

Fig. 6.5 : BCC Cr-Nb system. The calculated enthalpy of formation for the random alloy (E_{rand}) is shown in full line together with the first and second nearest neighbor effective pair interactions (V_1, V_2).

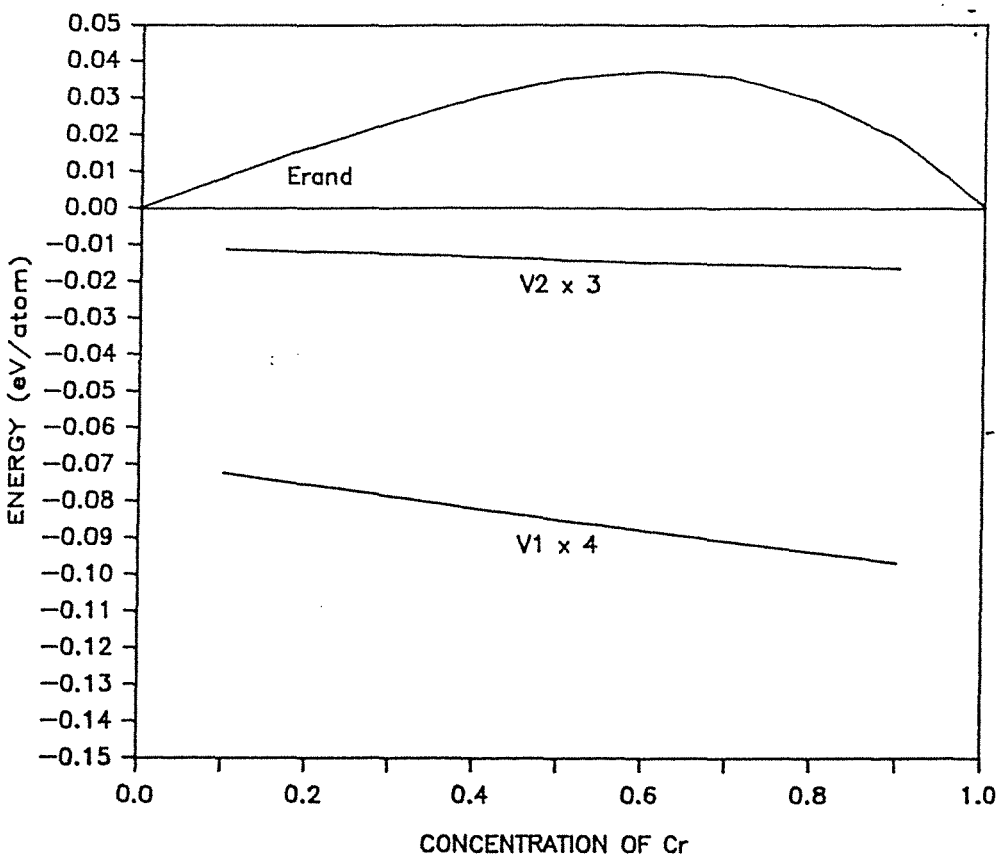

Fig. 6.6 : BCC Cr-Ta system. The calculated enthalpy of formation for the random alloy (E_{rand}) is shown in full line together with the first and second nearest neighbor effective pair interactions (V_1, V_2).

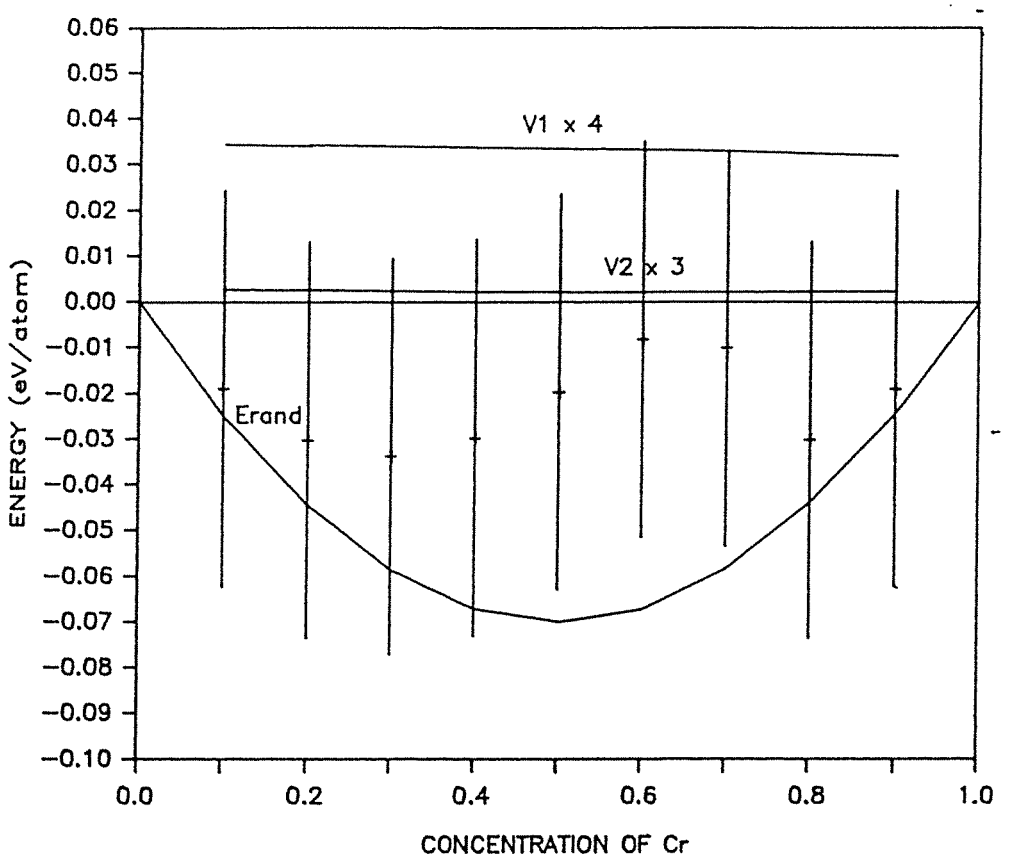

Fig. 6.7 : BCC Cr-V system. The calculated enthalpy of formation for the random alloy (E_{rand}) is shown in full line together with the first and second nearest neighbor effective pair interactions (V_1, V_2). The experimental enthalpy of formation measured at 1550 K [122] is indicated by crosses with error bars.

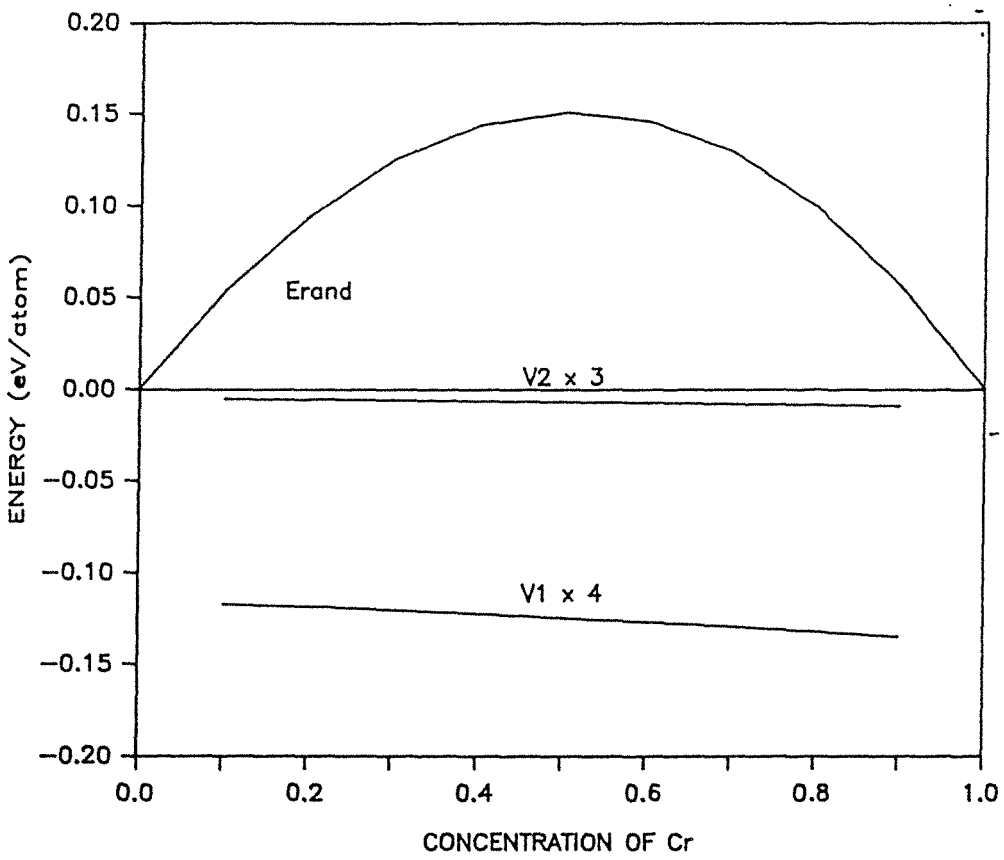

Fig. 6.8 : BCC Cr-W system. The calculated enthalpy of formation for the random alloy (E_{rand}) is shown in full line together with the first and second nearest neighbor effective pair interactions (V_1, V_2).

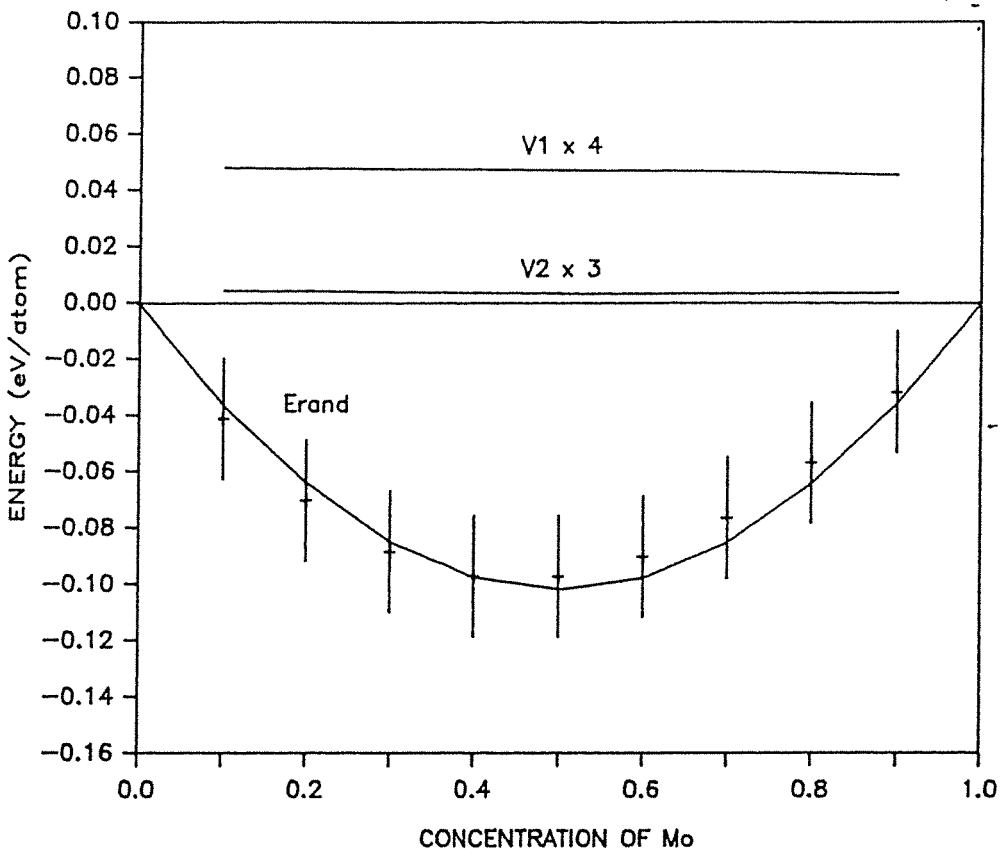

Fig. 6.9 : BCC Mo-Nb system. The calculated enthalpy of formation for the random alloy (E_{rand}) is shown in full line together with the first and second nearest neighbor effective pair interactions (V_1, V_2). The experimental enthalpy of formation measured at 1200 K [120] is indicated by crosses with error bars.

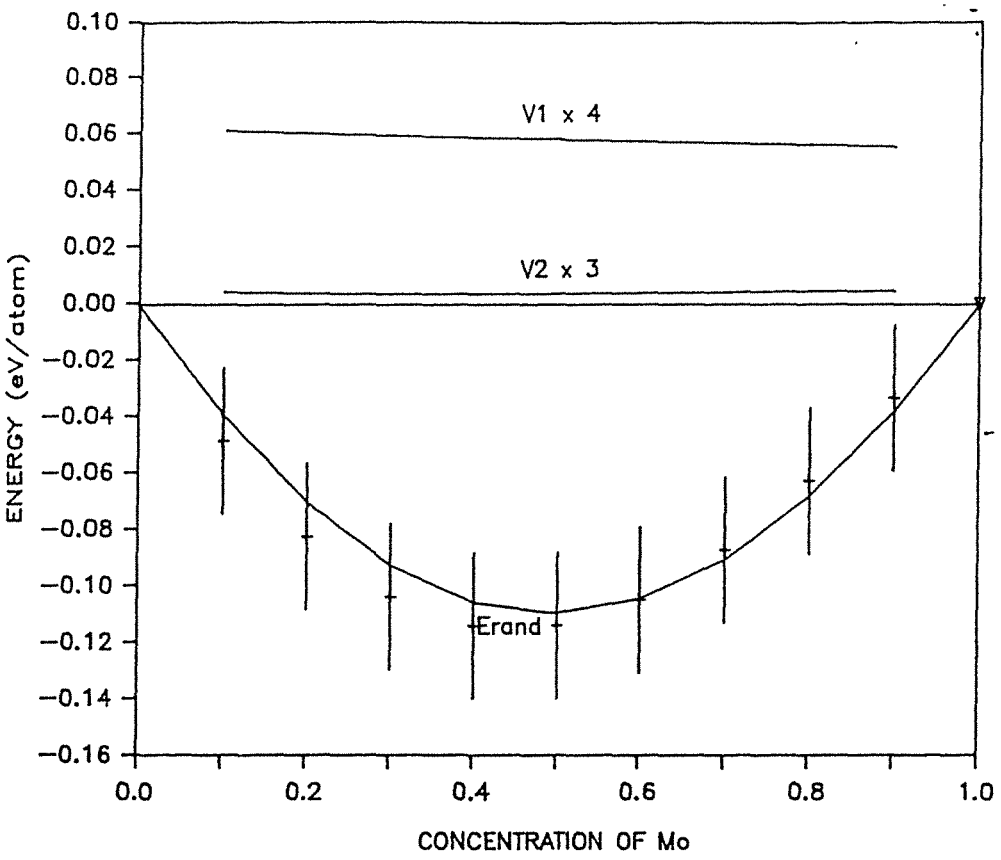

Fig. 6.10 : BCC Mo-Ta system. The calculated enthalpy of formation for the random alloy (E_{rand}) is shown in full line together with the first and second nearest neighbor effective pair interactions (V_1, V_2). The experimental enthalpy of formation measured at 1200 K [121] is indicated by crosses with error bars.

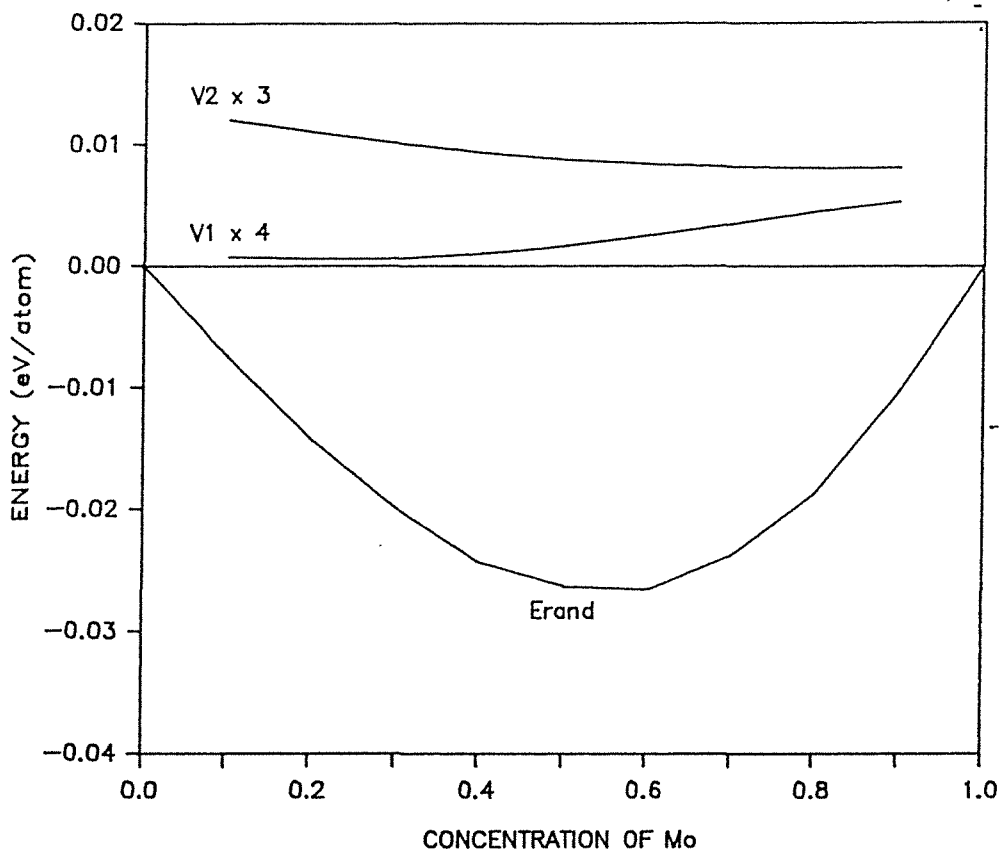

Fig. 6.11 : BCC Mo-V system. The calculated enthalpy of formation for the random alloy (E_{rand}) is shown in full line together with the first and second nearest neighbor effective pair interactions (V_1, V_2).

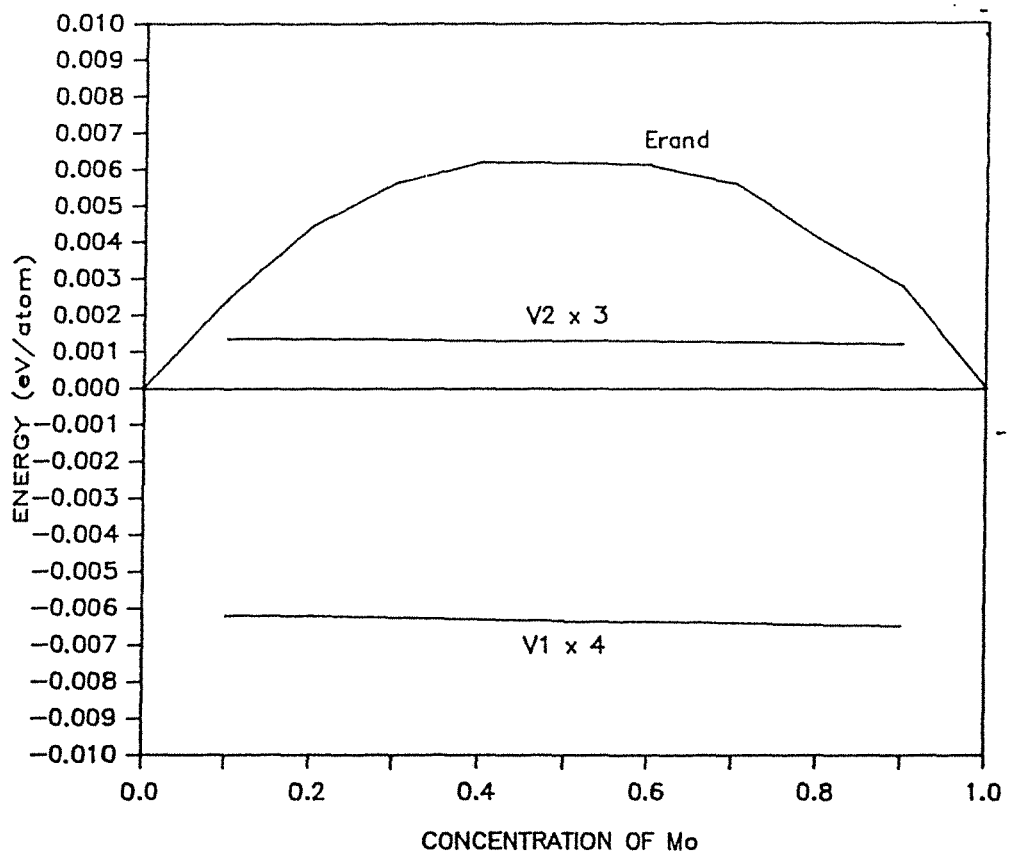

Fig. 6.12 : BCC Mo-W system. The calculated enthalpy of formation for the random alloy (E_{rand}) is shown in full line together with the first and second nearest neighbor effective pair interactions (V_1, V_2).

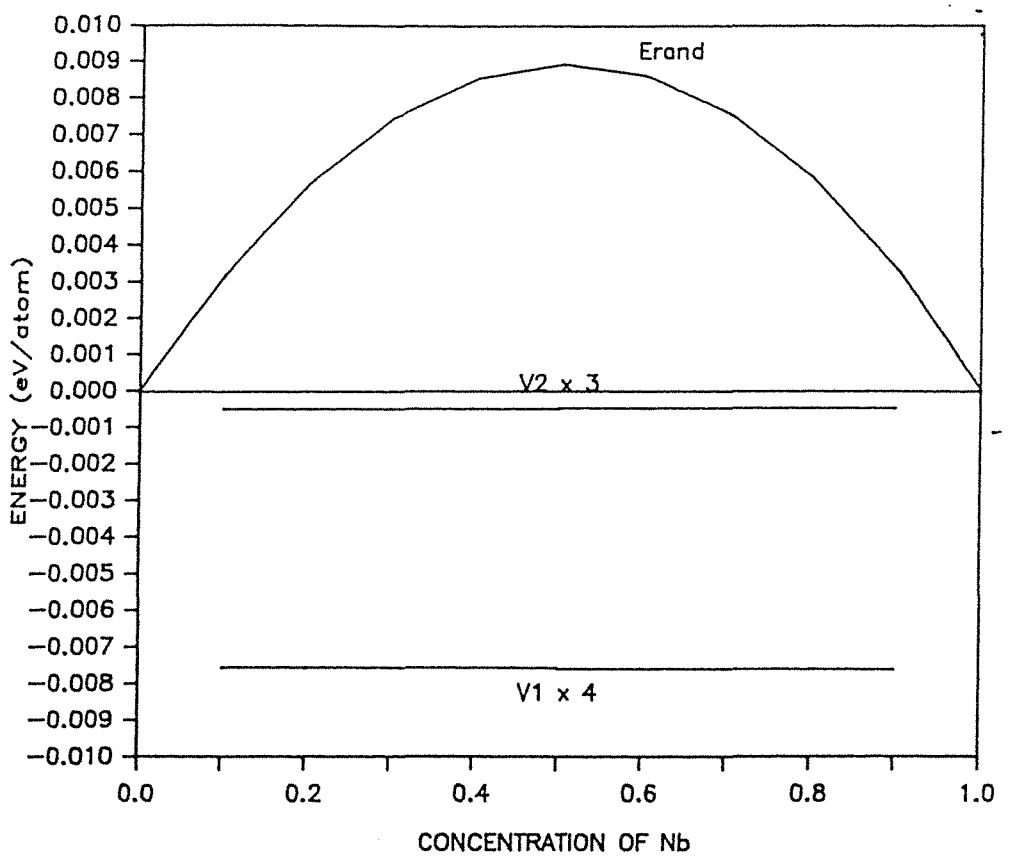

Fig. 6.13 : BCC Nb-Ta system. The calculated enthalpy of formation for the random alloy (E_{rand}) is shown in full line together with the first and second nearest neighbor effective pair interactions (V_1, V_2).

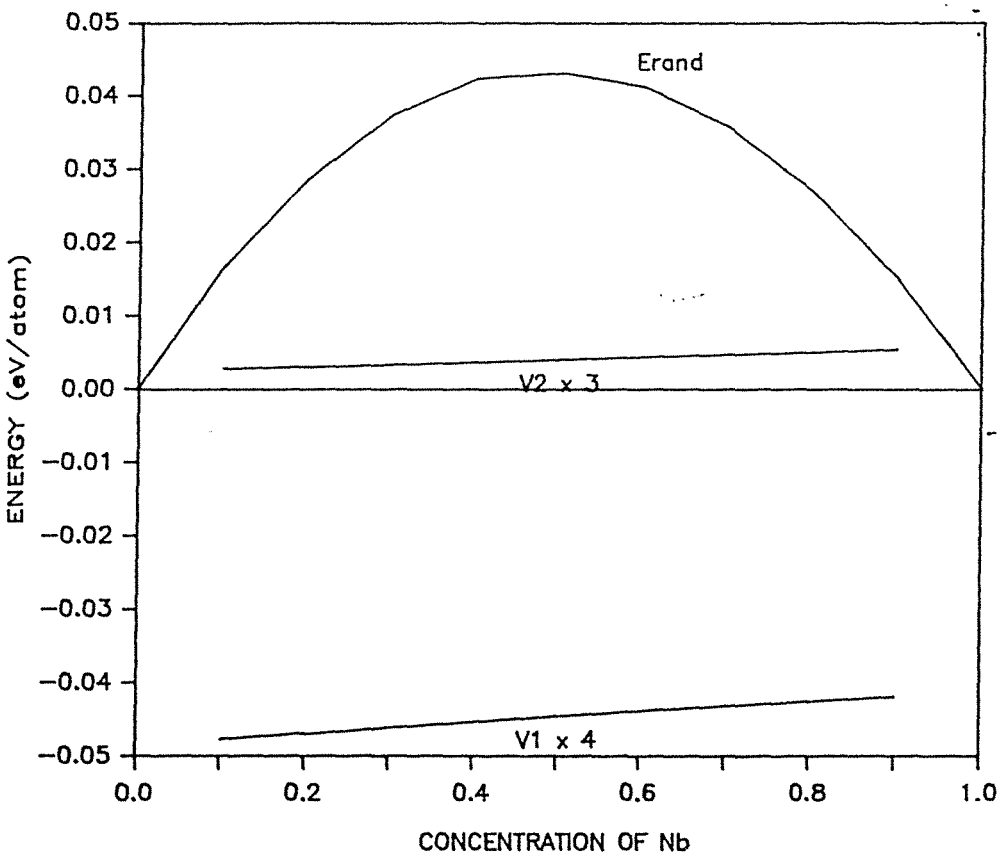

Fig. 6.14 : BCC Nb-V system. The calculated enthalpy of formation for the random alloy (E_{rand}) is shown in full line together with the first and second nearest neighbor effective pair interactions (V_1, V_2).

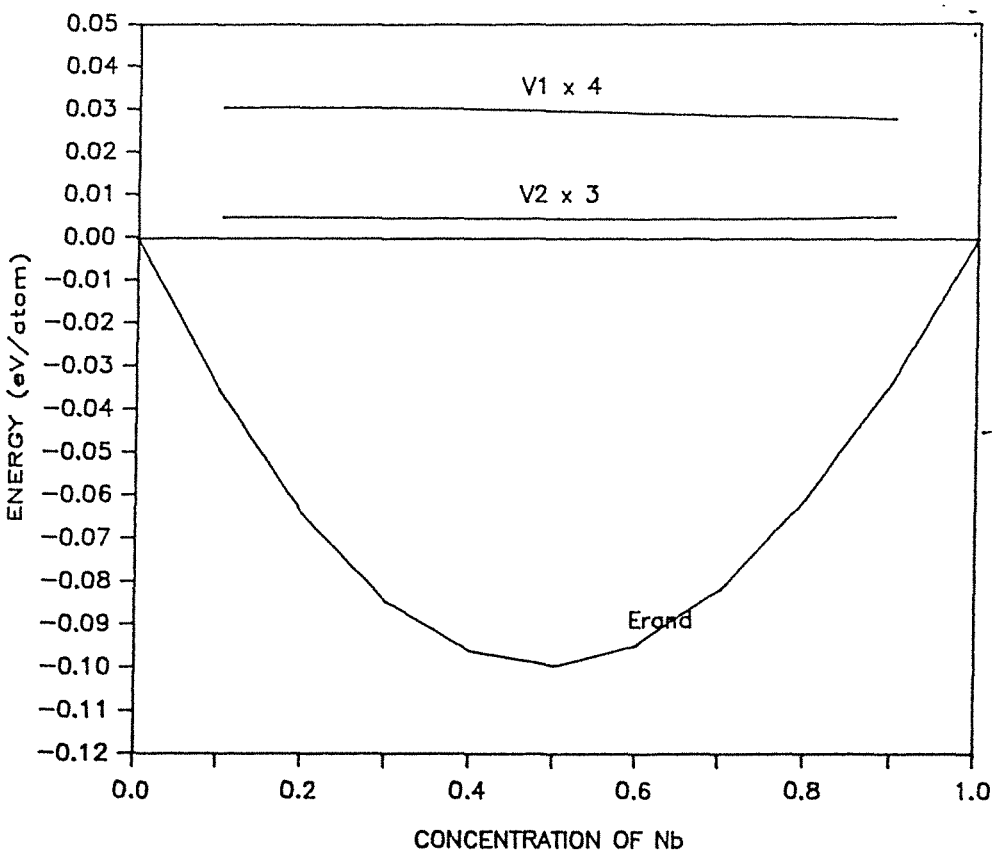

Fig. 6.15 : BCC Nb-W system. The calculated enthalpy of formation for the random alloy (E_{rand}) is shown in full line together with the first and second nearest neighbor effective pair interactions (V_1, V_2).

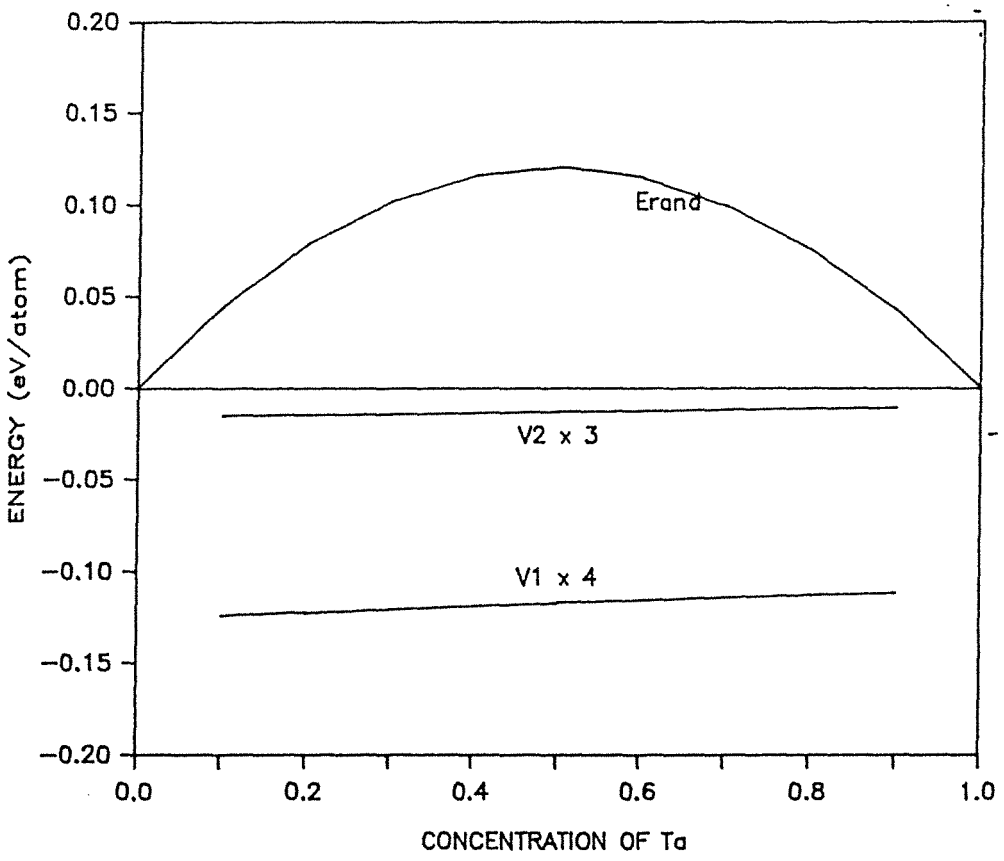

Fig. 6.16 : BCC Ta-V system. The calculated enthalpy of formation for the random alloy (E_{rand}) is shown in full line together with the first and second nearest neighbor effective pair interactions (V_1, V_2).

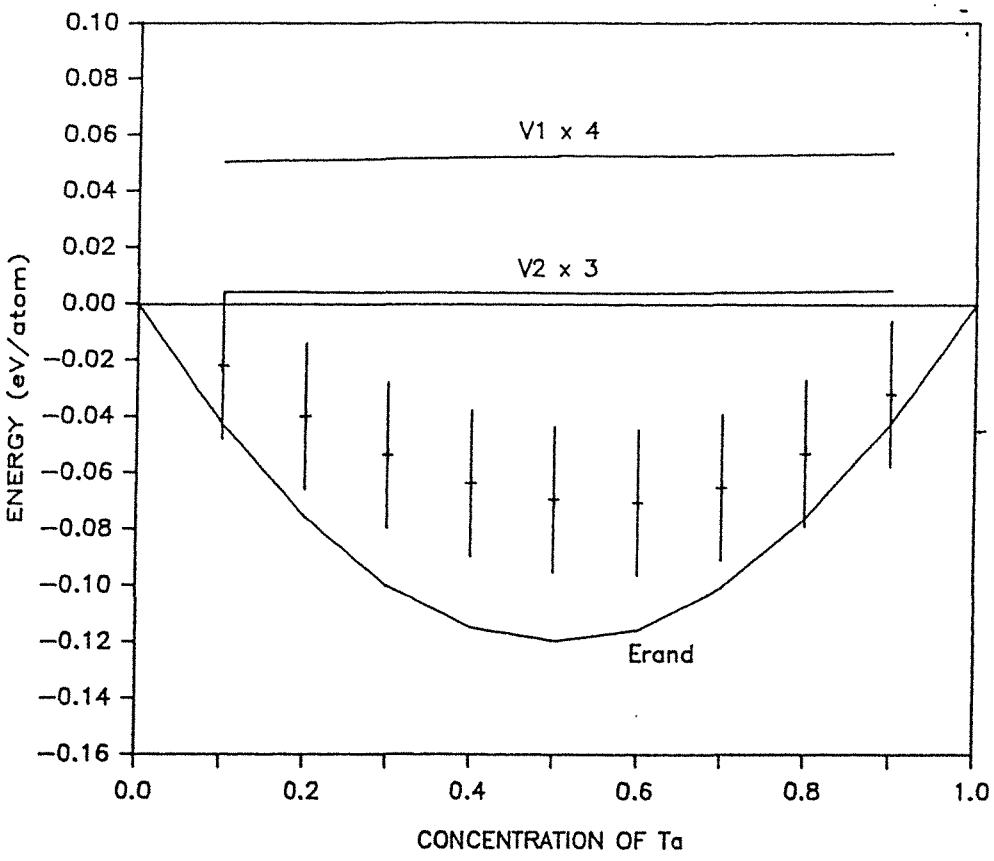

Fig. 6.17 : BCC Ta-W system. The calculated enthalpy of formation for the random alloy (E_{rand}) is shown in full line together with the first and second nearest neighbor effective pair interactions (V_1, V_2). The experimental enthalpy of formation measured at 1200 K [123] is indicated by crosses with error bars.

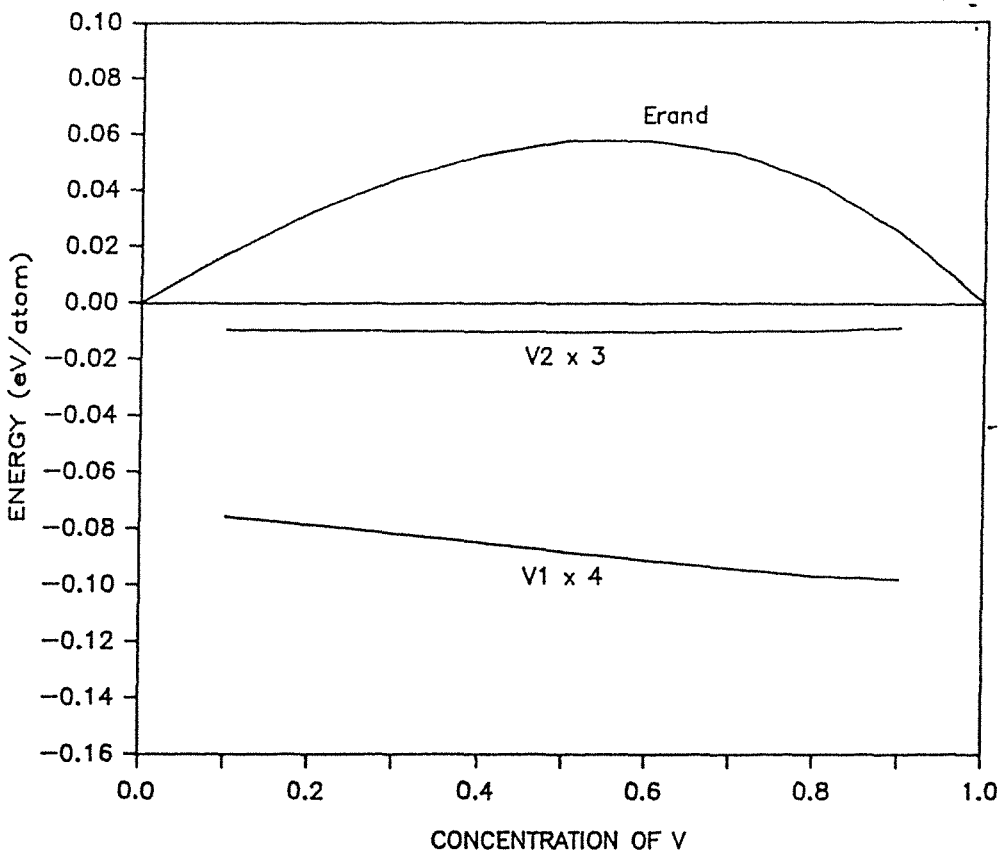

Fig. 6.18 : BCC V-W system. The calculated enthalpy of formation for the random alloy (E_{rand}) is shown in full line together with the first and second nearest neighbor effective pair interactions (V_1, V_2).

6.3 Results For The IVB-VIIIB Closed Packed (CP) Alloys

The set of closed packed (FCC OR HCP) alloys we have studied are the alloys obtained by mixing Ni, Pd, Pt (VIIIB elements), with Ti, Zr, Hf (IVB elements). We summarize in Fig.(6.19) the results obtained for the random alloys at the equiatomic concentration (squares in the plot). In the same figure, we also indicate the calculated enthalpy of formation of the perfectly ordered CuAu ($L1_0$) structure (diamonds in the plots). For a given alloy, the difference in energy between a square and a diamond represents the maximum ordering energy that can be obtained using first nearest neighbors EPIs only. Available experimental measurements of enthalpies of formation are indicated by crosses. One can notice that, for a given alloy, the scattering of the experimental data is generally larger than the ordering energy. Within this uncertainty, our results agree well with experiment. Note that the enthalpies of formation of these alloys are much more negative than that of the BCC-alloys presented in the last section. Within our model, this is well explained by the fact that the $\Delta\varepsilon$ and Δn values for the CP alloys are larger than that for the BCC alloys studied in section 6.2.

The Ni-alloys have a smaller diagonal disorder than Pt- or Pd-alloys (see Fig.(5.1)). Accordingly, the enthalpies of formation calculated for the Ni-alloys are smaller than the ones calculated for the Pt- or Pd-alloys (see Fig.(6.19)). The off-diagonal disorder effect is small but can still be seen when going from Ni-Ti, to Ni-Zr, to Ni-Hf where the increase in ΔW is manifested by an increase in the

enthalpies of formation of the random and perfectly ordered alloys.

We have plotted in Fig.(6.20) through Fig.(6.28) the enthalpies of formation of the random alloys and the first nearest neighbor pair interactions (V_1) as a function of concentration. The calculations are performed in the FCC structure. Results for the random alloy enthalpies are given in full lines. The calculated enthalpies for the ordered phases (CuAu ($L1_0$) and Cu_3Au ($L1_2$)) are indicated by triangles, whereas the available experimental results are indicated by crosses. In general, the alloys under study have complex ordered structures at low temperatures, whereas our calculations are carried out in the FCC structure. Thus, our analysis and comparison with experimental data neglect the structural energy involved in going from the FCC to the actual complex ordered structures.

The Pt-Ti system provides an interesting case for comparison with our results since an ordered $TiPt_3$ phase having the Cu_3Au structure ($L1_2$) exists experimentally [138] and its enthalpy of formation has been measured [134]. We recall here that the $L1_2$ phase is based on an FCC structure. Accordingly, no structural energy is involved, and we expect the model to describe accurately the energy of formation of the $TiPt_3$ phase. Furthermore, Ref.[134] provides a measured enthalpy of formation for the disordered FCC-solid solution (A1). Accordingly, the accuracy of the model to describe SRO-effects can be tested in the Pt-Ti alloys by comparing the calculated and experimental enthalpies of formation of the A1 and $L1_2$ phases. We have used the CVM and minimized the free energy of the A1 and $L1_2$ phases at the experimental

concentration and temperature. We report in Table 6.2 the results of the analysis and compare them with experimental data. The good agreement between calculated and experimental results indicates that ordering effects are well described by the theory, at least for the case of simple ordered phases such as the $L1_2$ structure. For the other alloys investigated here, the detailed analysis of the results is complicated by the scattering of the experimental data and the structural energy associated with the complex ordered structures observed experimentally. Nevertheless, within the scattering of the experimental measurements, our results are in good agreement with experimental data

The variation of the first nearest neighbor EPI (V_1) with concentration is qualitatively the same for all the IVB-VIIIB alloys: an increase in magnitude of V_1 as the concentration of the VIIIB element increases up to about 0.75, followed by a slight decrease in magnitude. Experimentally, the dependence of V_1 with concentration is not well known. However, the phase diagrams of these alloys [139] show that the temperatures of the congruent points between ordered phases and the liquid phase increase as the content of the VIIIB element increases. A plausible explanation for this behavior is that V_1 (or equivalently the ordering energy) increases, as the content of the VIIIB element increases. As a result, the ordered phases are much more stabilized relative to the liquid phase for high contents of the VIIIB element.

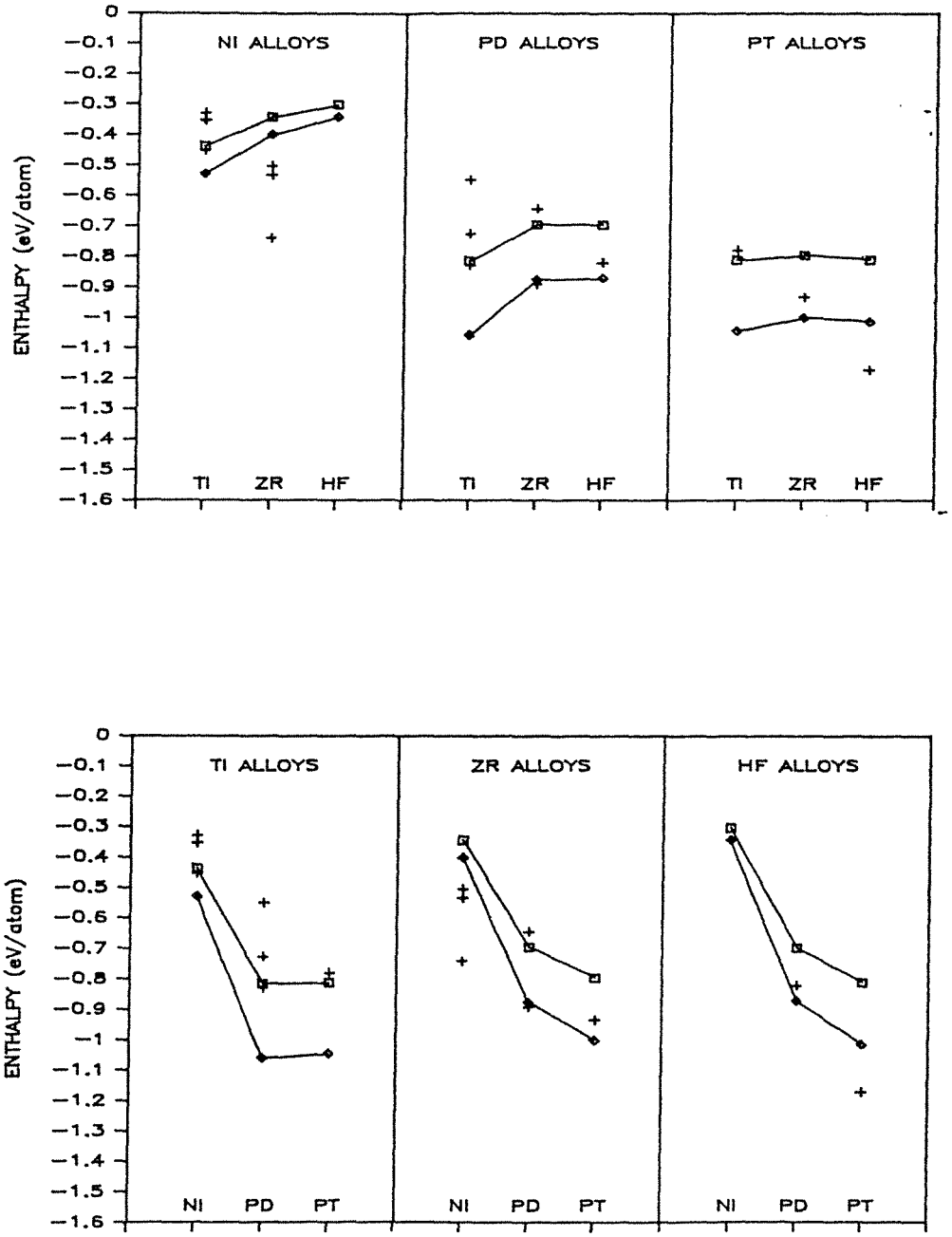

Fig. 6.19 : Enthalpies of formation calculated for the equiatomic IVB-VIIIB binary alloys. The calculations are carried out for the FCC structure. The calculated enthalpies of formation are indicated by squares for random alloys, and by diamonds for alloys in the $L1_0$ configuration. Available experimental enthalpies of formation are shown by crosses.

Table 6.2

Comparison of the calculated enthalpies of formation for the Pt_3Ti and A1 phases (X_{Pt}=0.9) with the available experimental data [134](energies in eV).

PHASE	Calculated Random Alloy Enthalpy E_{rand}	Calculated Ordering Energy E_{ord} at T=1300 K	Calculated Enthalpy of Formation at T=1300 K	Measured Enthalpy of Formation [134] (1300 K)
Pt_3Ti ($L1_2$)	-0.653	-0.245	-0.898	-0.886 ± .034
(A1) X_{Pt}=0.9	-0.318	-0.034	-0.352	-0.407 ± .034

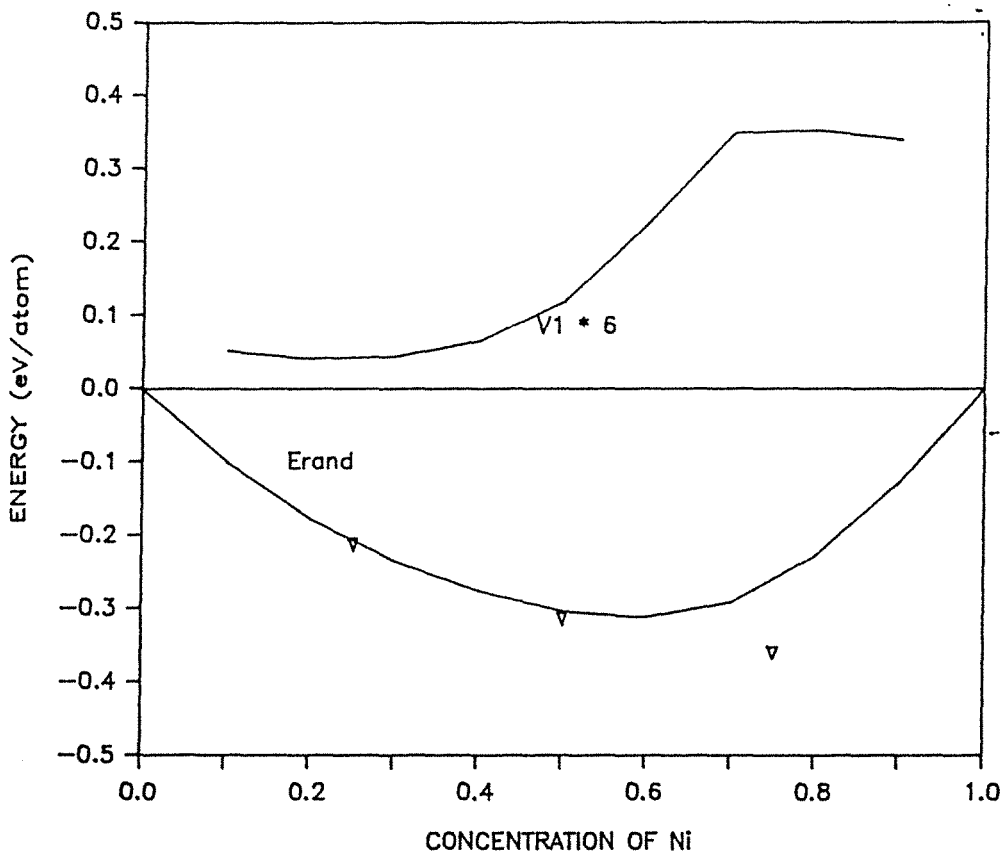

Fig. 6.20 : FCC Ni-Hf system. The calculated enthalpy of formation for the random alloy (E_{rand}) is shown in full line together with the first nearest neighbor effective pair interactions (V_1). Enthalpies of formation for alloys in the $L1_2$ or $L1_0$ configuration are indicated by triangles.

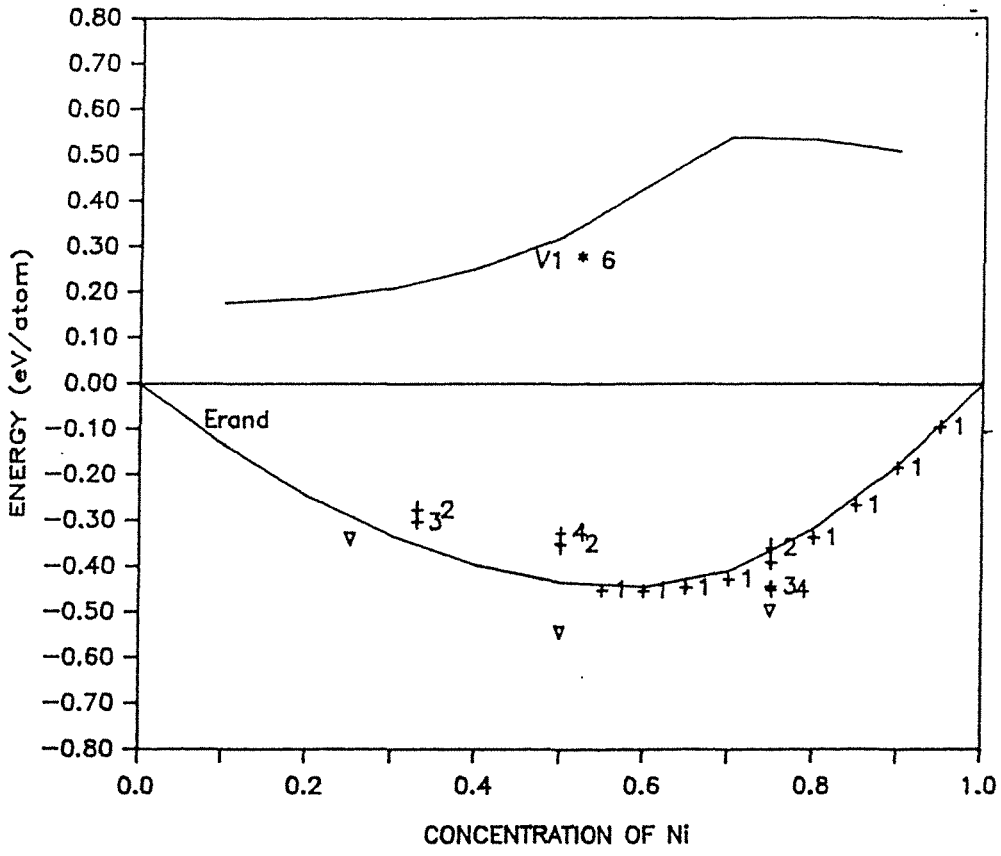

Fig. 6.21 : FCC Ni-Ti system. The calculated enthalpy of formation for the random alloy (E_{rand}) is shown in full line together with the first nearest neighbor effective pair interactions (V_1). Calculated enthalpies of formation for alloys in the $L1_2$ or $L1_0$ configuration are indicated by triangles. Available experimental data are indicated by crosses with error bars (+1 [126], +2 [53], +3 [127], and +4 [128]).

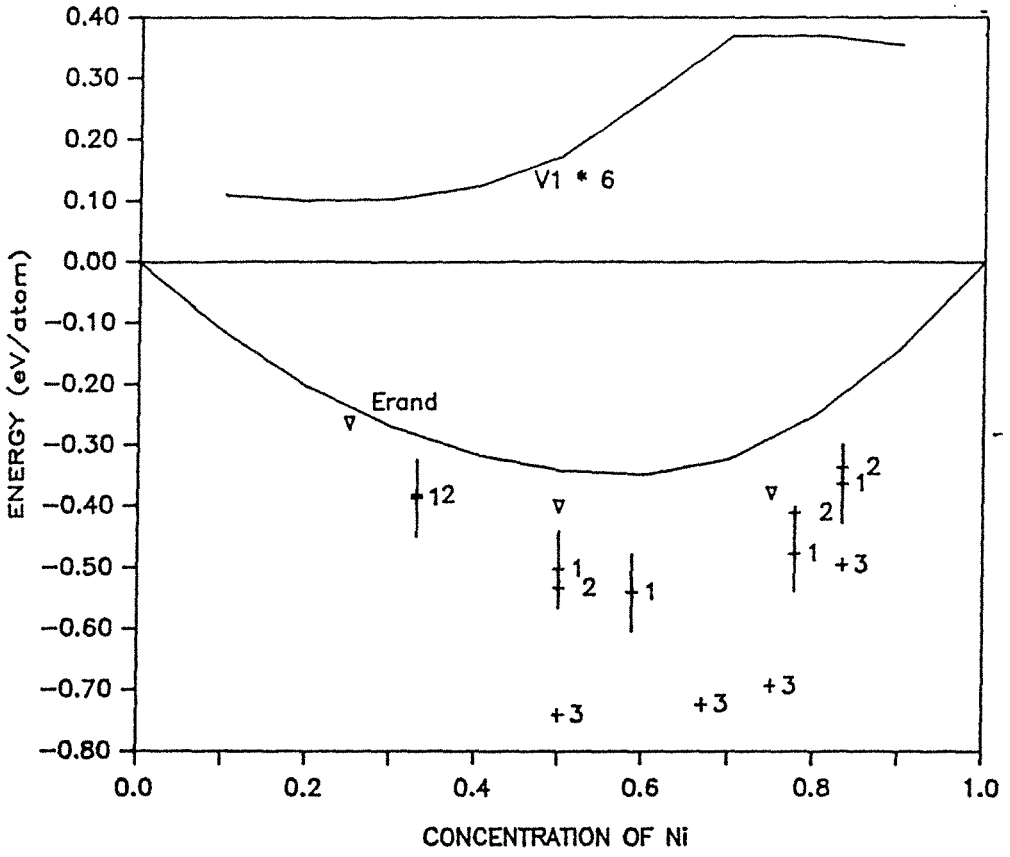

Fig. 6.22 : FCC Ni-Zr system. The calculated enthalpy of formation for the random alloy (E_{rand}) is shown in full line together with the first nearest neighbor effective pair interactions (V_1). Calculated enthalpies of formation for alloys in the $L1_2$ or $L1_0$ configuration are indicated by triangles. Available experimental data are indicated by crosses with error bars (+1 [129], +2 [127], and +3 [130].

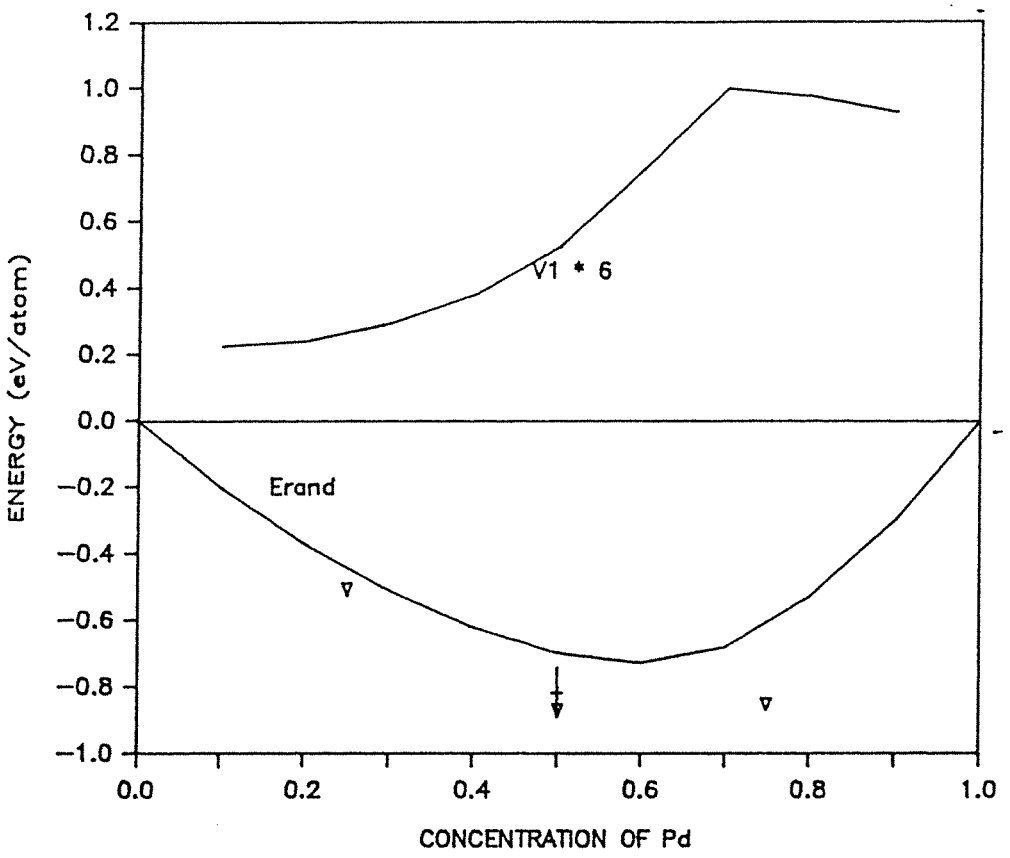

Fig. 6.23 : FCC Pd-Hf system. The calculated enthalpy of formation for the random alloy (E_{rand}) is shown in full line together with the first nearest neighbor effective pair interactions (V_1). Calculated enthalpies of formation for alloys in the $L1_2$ or $L1_0$ configuration are indicated by triangles. Available experimental data [131] are indicated by crosses with error bars.

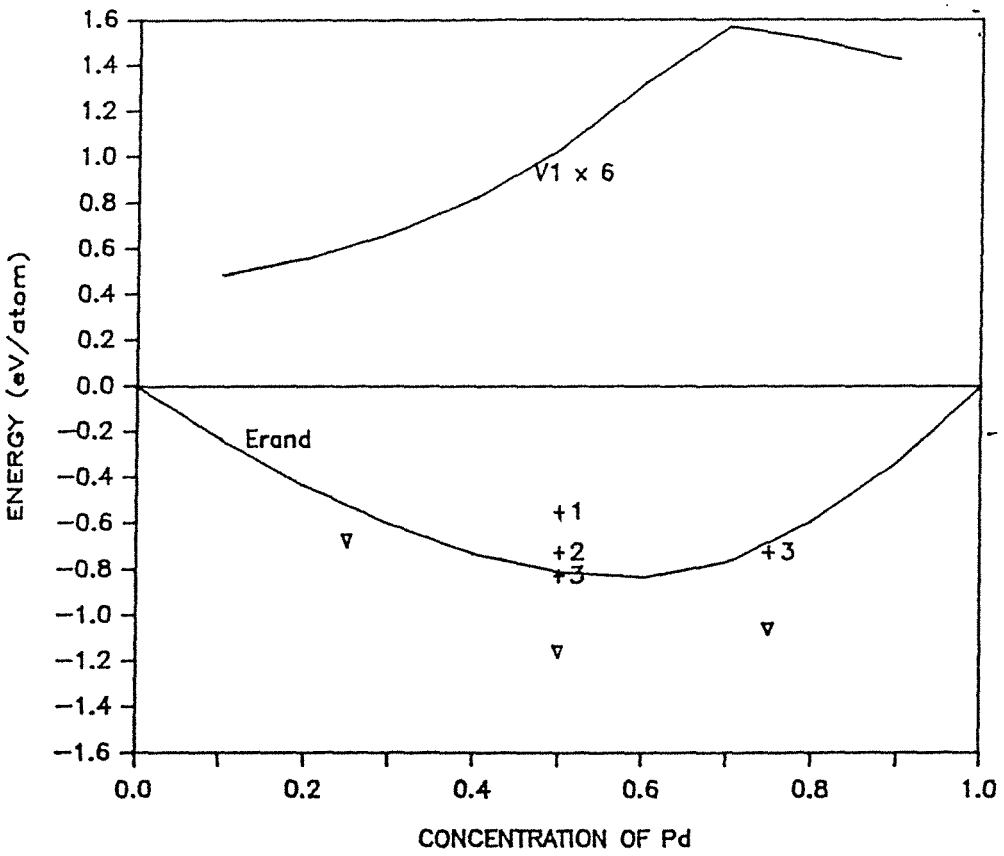

Fig. 6.24 : FCC Pd-Ti system. The calculated enthalpy of formation for the random alloy (E_{rand}) is shown in full line together with the first nearest neighbor effective pair interactions (V_1). Calculated enthalpies of formation for alloys in the $L1_2$ or $L1_0$ configuration are indicated by triangles. Available experimental data are indicated by crosses with error bars (+1 [131], +2 [132], and +3 [133]).

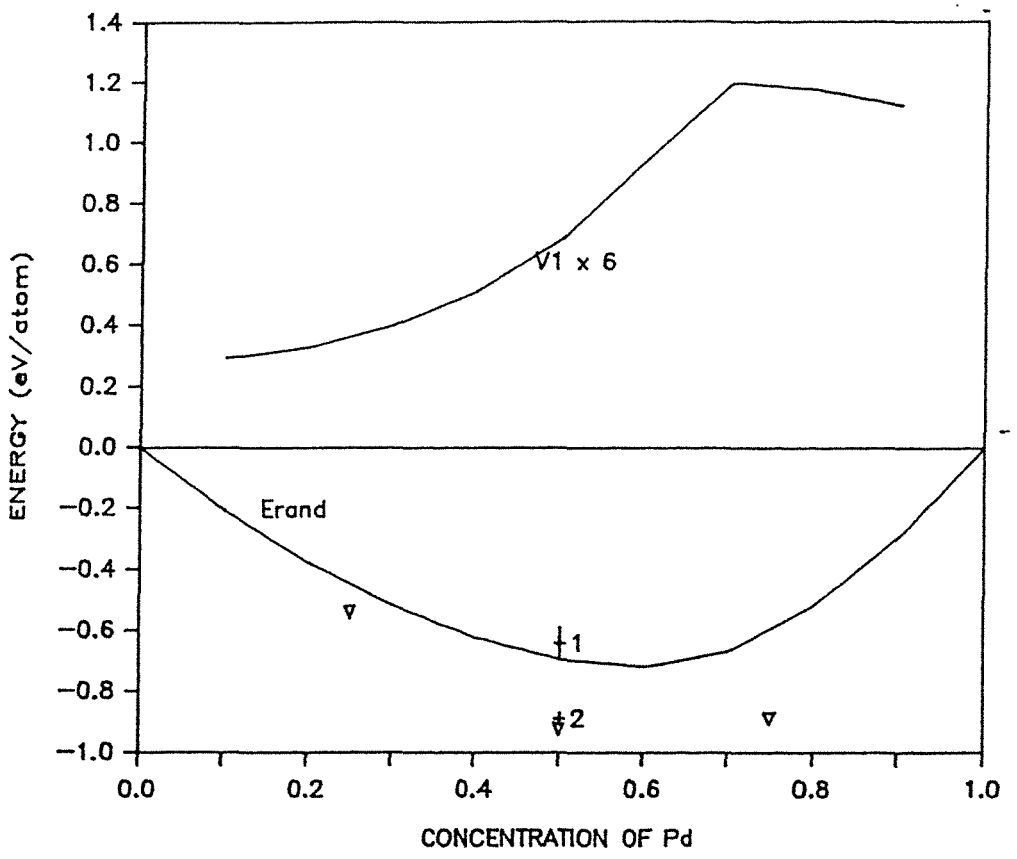

Fig. 6.25 : FCC Pd-Zr system. The calculated enthalpy of formation for the random alloy (E_{rand}) is shown in full line together with the first nearest neighbor effective pair interactions (V_1). Calculated enthalpies of formation for alloys in the $L1_2$ or $L1_0$ configuration are indicated by triangles. Available experimental data are indicated by crosses with error bars (+1 [131], and +2 [132]).

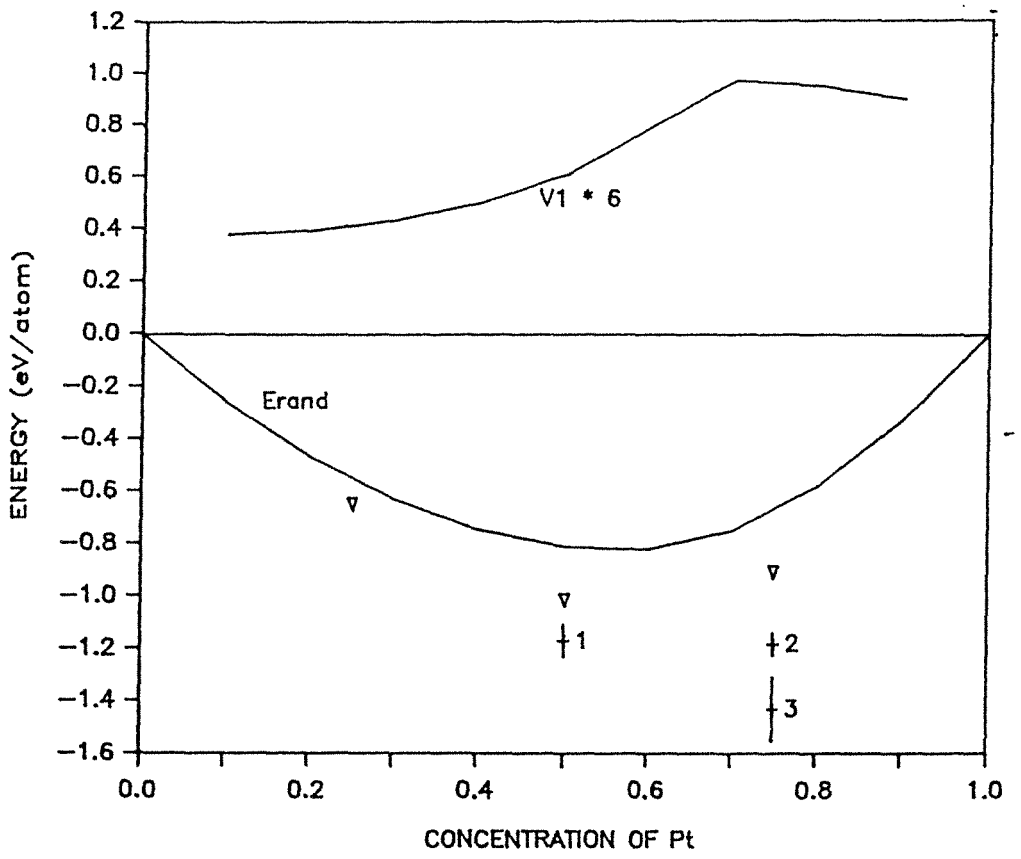

Fig. 6.26 : FCC Pt-Hf system. The calculated enthalpy of formation for the random alloy (E_{rand}) is shown in full line together with the first nearest neighbor effective pair interactions (V_1). Calculated enthalpies of formation for alloys in the $L1_2$ or $L1_0$ configuration are indicated by triangles. Available experimental data are indicated by crosses with error bars (+1 [131], +2 [135], and +3 [136]).

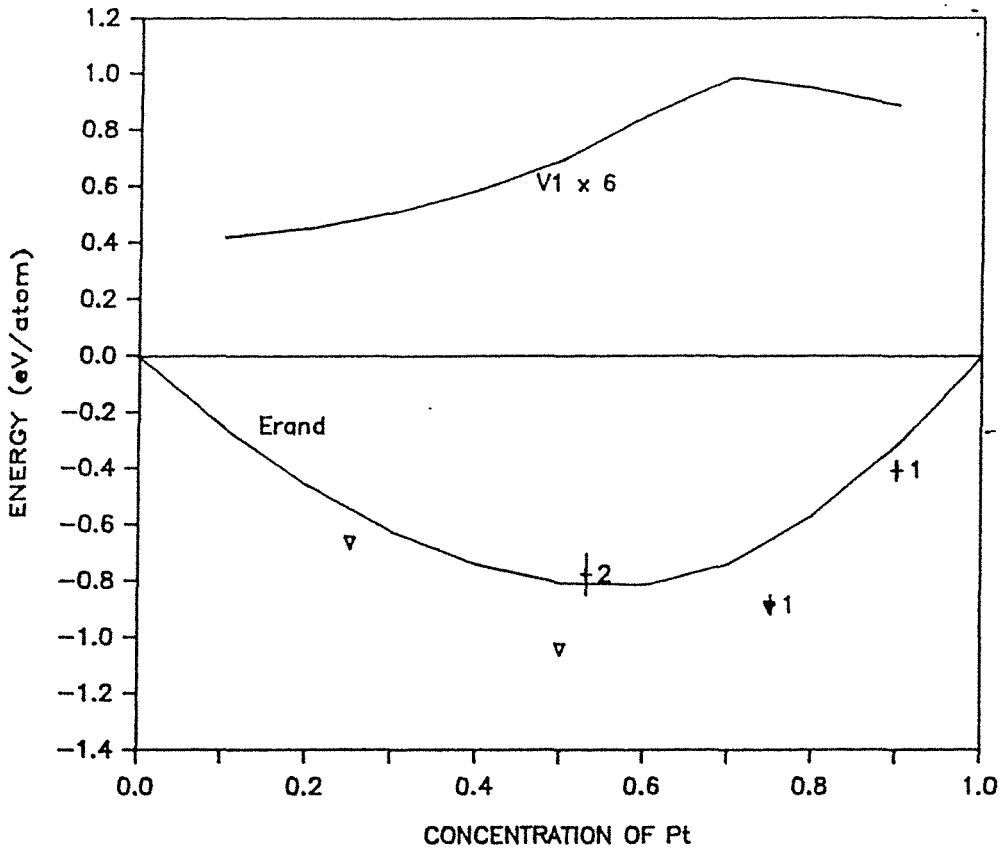

Fig. 6.27 : FCC Pt-Ti system. The calculated enthalpy of formation for the random alloy (E_{rand}) is shown in full line together with the first nearest neighbor effective pair interactions (V_1). Calculated enthalpies of formation for alloys in the $L1_2$ or $L1_0$ configuration are indicated by triangles. Available experimental data are indicated by crosses with error bars (+1 [131], and +2 [134]).

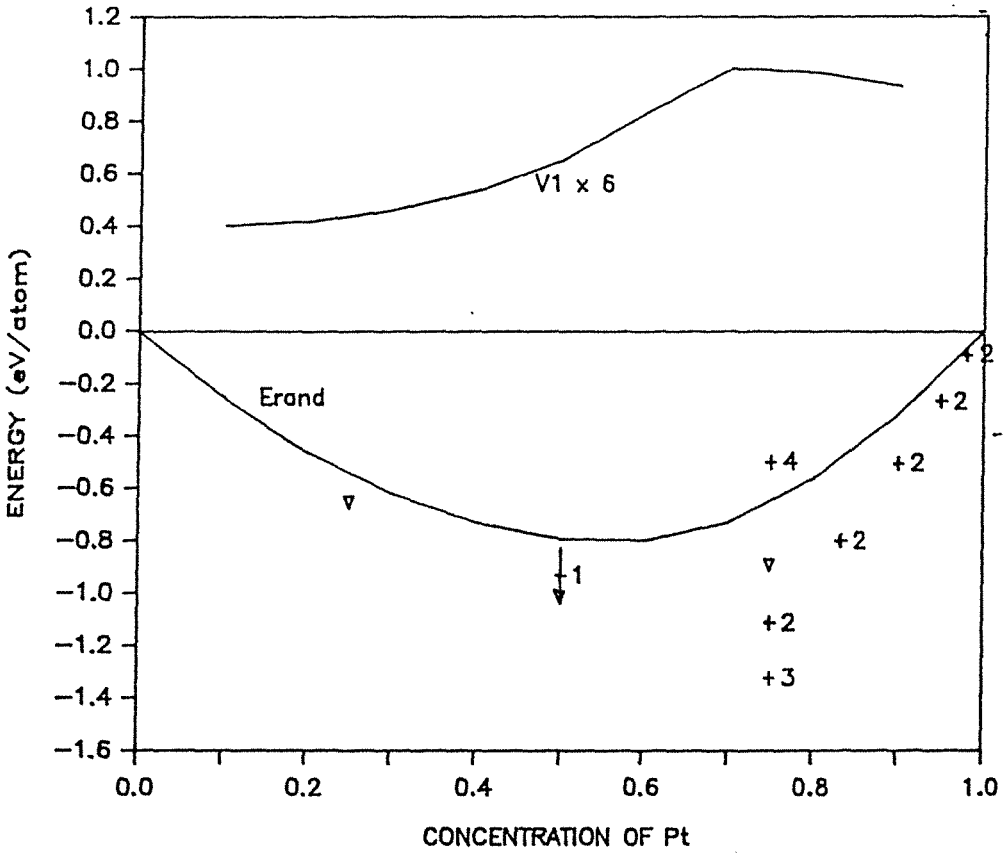

Fig. 6.28 : FCC Pt-Zr system. The calculated enthalpy of formation for the random alloy (E_{rand}) is shown in full line together with the first nearest neighbor effective pair interactions (V_1). Calculated enthalpies of formation for alloys in the $L1_2$ or $L1_0$ configuration are indicated by triangles. Available experimental data are indicated by crosses with error bars (+1 [131], +2 [135], +3 [136], and +4 [137]).

6.4 Discussion of The Microscopic Theory And Extensions Of The Thesis Work

In the second part of this thesis we have presented a microscopic theory for the calculation of the enthalpy of formation of transition metals which is based on a tight binding hamiltonian. Significant improvements over previous calculations have been implemented by combining the three following features:

i) the topological approximation of the cluster Bethe lattice method is lifted using the CPA-GPM method together with the recursion method.

ii) off-diagonal disorder is included in the tight binding Hamiltonian

iii) the effects of charge transfer in the random alloy are treated self-consistently within the Hartree-Fock approximation.

The overall accuracy achieved by our calculations follows from the fact that we have included off-diagonal disorder and treated charge transfer self-consistently in the random alloy. For example, if we were to neglect those two effects, the model would predict a negative enthalpy of formation in the Cr-Mo alloys which contradicts experimental results. Although the microscopic theory we use is not ab-initio, it only requires the results of pure element ab-initio calculations as input parameters. In this regard, the model can be considered parameter free.

We have concentrated our attention on two different classes of

alloys: the BCC-isomorphic alloys and the IVB-VIIIB alloys. Within our approach, the small values of the diagonal disorder ($\Delta\varepsilon$) and of the difference in the number of d-electrons (Δn) explain well the small enthalpies of formation observed experimentally for the BCC alloys. The off-diagonal disorder is responsible for the segregation tendency observed for some of the systems. On the other hand, the IVB-VIIIB alloys have large $\Delta\varepsilon$ and Δn values which results in very negative enthalpies of formation. The off-diagonal disorder, though not negligible, plays here a less significant role. For the two classes of alloys, the calculated enthalpies of formation show good agreement with experiment.

The value of the ordering energy (i.e. the value of the EPIs) has been tested in the case of $TiPt_3$ (Cu_3Au structure) for which the model should apply without caveats. The enthalpy of formation ($E_{rand} + E_{ord}$) as well as its SRO dependence agree well with the experimental data. We have also found remarkable agreement between the total enthalpy of formation predicted for NbMo in the CsCl structure and the result predicted by Moruzzi and co-workers for the same compound [125].

The investigated alloys are characterized by a nearly half filled d-band at the equiatomic concentration. In that case, the d-bonding effects are the strongest, and having neglected of s- and p-electrons is expected to be unimportant. One possible extension of this thesis work is to generalize the model to other alloy systems by including s- and p-electrons. The model should then be able to describe accurately the enthalpy of formation of nearly empty or nearly filled d-band

alloys. Another possible extension of this thesis work is to incorporate in the model spin polarization effects in order to describe magnetic alloys such as Fe-, Co-, or Mn-alloys. A more satisfactory description of the magnetic Ni- and Cr-alloys would also be obtained by this extension.

REFERENCES

1. L. Kaufman and H. Bernstein, Computer Calculation of Phase Diagrams, Academic Press, New York (1970).

2. L. Kaufman, CALPHAD 1, 28 (1977).

3. L. Kaufman and H. Nesor, Met. Trans. 5, 1623 (1974).

4. L. Kaufman and H. Nesor, CALPHAD 2, 337 (1978).

5. M. Hillert and L.I. Staffanson, Acta Chem. Scand. 24, 3618 (1970).

6. M. Hillert and M. Jarl, CALPHAD 2, 227 (1978).

7. B. Sundman and J. Agren, J. Phys. Chem. Solids 42, 297 (1981).

8. S. Hertzman and B. Sundman, CALPHAD 6, 67 (1982).

9. A. F. Guillermet, CALPHAD 6, 127 (1982).

10. W. Shockley, J. Chem. Phys. 6, 130 (1938).

11. D. de Fontaine and R. Kikuchi, Nat. Bur. Stand., Report No. SP-496, p. 999 (1978).

12. R. Kikuchi, Phys. Rev. 81, 988 (1951).

13. C. M. van Baal, Physica (Utrecht) 64, 571 (1973).

14. R. Kikuchi and D. de Fontaine, Nat. Bur. Stand., Report No. SP-496, p. 967 (1978).

15. J. M. Sanchez and D. de Fontaine, Phys. Rev. B17, 2926 (1978).

16. J. M. Sanchez and D. de Fontaine, Phys. Rev. B21, 216 (1980).

17. J. M. Sanchez, W. Teitler and D. de Fontaine, Phys. Rev. B26, 1456 (1982).

18. J. M. Sanchez and C. H. Lin, Phys. Rev. B30, 1448 (1984).

19. J. M. Sanchez, J. R. Barefoot, R. N. Jarrett and J. K. Tien, Acta Metall. 32, 1519 (1984).

20. C. Sigli and J. M. Sanchez, CALPHAD 8, 221 (1984); J.M. Sanchez, R.N. Jarrett, C. Sigli, and J.K. Tien, in "High Temperature Alloys: Theory and Design" (Edited by J.O. Stiegler), Met. Soc. of AIME, pp 83-101 (1984).

21. R. Kikuchi, J. M. Sanchez, D. de Fontaine, and H. Yamauchi, Acta Metall. 28, 651 (1980).

22. A. de Roody, E. W. van Royen, P. M. Bronsveld and J. Th. M. de Hosson, Acta Metall. 28, 1339 (1980).

23. J.W.D. Connolly and A.R. Williams, Phys. Rev. B27, 5169 (1983).

24. J.S. Faulkner, Progress in Materials Science, Vol. 27, PP. 1-187, Pergamon Press, London, 1982.

25. H. Winter and G.M. Stocks, Phys. Rev. B27, 882 (1982).

26. R.J. Hawkins, M.O. Robbins and J.M. Sanchez, Phys. Rev. B33, 4782 (1986).

27. R.J. Hawkins, PhD Thesis submitted to the University of Columbia at New York, 1984 (unpublished).

28. M.O. Robbins, PhD Thesis submitted to the University of California at Berkeley, 1983 (unpublished).

29. M.O Robbins and L.M. Falicov, Phys. Rev. B29, 1333 (1984).

30. M.O. Robbins and L.M. Falicov, Phys. Rev. B25, 2343 (1982)

31. F. Gautier, J. van der Rest and F. Brouers, J. Phys. F5, 1884 (1975).

32. J. van der Rest, F. Gautier and F. Brouers, J. Phys. F5, 2283 (1975).

33. G. Treglia, F. Ducastelle and F. Gautier, J. Phys. F8, 1437 (1978).

34. A. Bieber, F. Gautier , G. Treglia and F. Ducastelle, Sol. St. Comm. 39, 149 (1981).

35. F. Gautier, in "High Temperature Alloys: Theory and Design" (Edited by J.O. Stiegler), Met. Soc. of AIME, pp 163-181 (1984).

36. P. Turchi, Phd Thesis submitted in the University of Paris VI at Paris (1984).

37. R. Hultgren, P. D. Desai, D. T. Hawkins, M. Gleiser, K. K. Kelley and D. D. Wagman, Selected Values of the Thermodynamic Properties of the Elements, A. S. M., Metals Park, Ohio (1973).

38. J.M. Sanchez, F. Ducastelle and D. Gratias, Physica 128A, 334 (1984).

39. M.S. Richards and J.W. Cahn, Acta Metall. 19, 1263 (1971).

40. M. Allen and J.W. Cahn, Acta Metall. 20, 423 (1972)

41. J. Kanamori and Y. Kakehashi, J. Phys. (Paris) 38, Suppl. C7-274 (1978).

42. J.M. Sanchez and D. de Fontaine, in "Structure and Bonding in Crystals" (Edited by M. O'Keeffe and A. Navrotsky), Vol.2, p.117, Academic Press, New York (1981).

43. A. Finel, D. Gratias and R. Portier, in "L'Ordre et le Désordre dans les Matériaux", Les éditions de Physique, pp 9-76 (1984).

44. C. Booth and J.S. Rowlinson, Trans Faraday Soc. 51, 463 (1955).

45. P.J. Wojtowicz and j.g. Kirkwood, J. Chem. Phys. 33, 1299 (1960).

46. A.A.H.J. Waegmaekers and H. Bakker, in Phase Transformations in Solids" (Edited by T. Tsakalakos), MRS symp. proceedings, Vol 21, pp 343-349 (1984).

47. J.A. Barker, Proc. R. Soc. A216, 45 (1953).

48. T. Morita, J. Phys. Soc. Jpn. 12, 753, 1060 (1957).

49. D. Gratias, in "L'Ordre et le Désordre dans les Matériaux", Les Editions de Physique, pp119-133 (1984).

50. R. Kikuchi, J. Chem. Phys. 66, 3352 (1977).

51. D. de Fontaine, Solid State Physics (Edited by H. Ehrenreich, F. Seitz, and D. Turnbull), Vol 34, p. 174, Academic Press, New York (1973).

52. C. Sigli and J.M. Sanchez, Acta Metall. 33, 1097 (1985).

53. R. Hultgren, P.D. Desai, D.T. Hawkins, M. Gleiser, and K.K. Kelley, in "Selected Values of Thermodynamic Properties of Binary Alloys", p.192, Am. Soc. of Metals, Metals Park (1973).

54. R. Hultgren, P.D. Desai, D.T. Hawkins, M. Gleiser, and K.K. Kelley, in "Selected Values of Thermodynamic Properties of Binary Alloys", p.708, Am. Soc. of Metals, Metals Park (1973).

55. C.H.M. Jenkins, A.H. Bucknall, C.R. Austin, and G.A. Mellor, J. Iron Steel Inst. 136, 187 (1937).

56. H.G. Baer, Z. Metallkunde 49, 614 (1958)

57. Ju.A. Bagarjatskij and Ju.D. Tjapkin, Dokl. Akad. Nauk. SSSR 122, 806 (1958).

58. L. Karmazin, Czech. J. Phys. B28, 1175 (1978); L. Karmazin, Material Science and Engineering 54, 274 (1982).

59. D.S. Bloom and N.J. Grant, Trans. AIME 191, 1009 (1951).

60. C. Stein and N.J. Grant, Trans. AIME 203, 127 (1955).

61. N. Yukawa, M. Hida, T. Imura, M. Kawamura, and Y. Mizuno, Met. Trans. 3, 887 (1972).

62. A.T. Grigor'ev, E.M. Sokolvskaya, N.A. Nedumov, M.V. Maksimova, L.G. Sokolova, and Yeh Yu-pu, Russian J. of Inorganic Chemistry 6, 639 (1961).

63. G.V. Raynor and V.G. Rivlin, Bull. Alloy Phase Diag. 2 (1), 100 (1981).

64. A. Taylor and R.W. Floyd, J. Inst. Metals 80, 577 (1951-52).

65. W.C. Wyder and M. Hoch, Trans. AIME 227, 588 (1963).

66. C. Sigli and J.M. Sanchez, Acta Metall. 34, 1021 (1986).

67. M.L. Saboungi, C.C. Hsu, CALPHAD 1, 237 (1977).

68. A.J. McAlister, Bull. Alloy Phase Diagram 3 (2), 177 (1982).

69. R.P. Elliott and F.A. Shunk, Bull. Alloy Phase Diagrams 2 (3), 353 (1981).

70. C.J. Wen, B.A. Boukamp, R.A. Huggins and W. Weppner, J. Electrochem. Soc. 126, 2258, (1979).

71. K.M. Myles, F.C. Mrazek, J.A. Smaga and J.L. Settle, Proc. Symp. and Workshop on Adv. Battery Res. and Design: U.S. ERDA Report ANL-76-8, March (1976).

72. B. Noble and G.E. Thomson, Met. Sci. J. 5, 144 (1975).

73. D.B. Williams and J.W. Edington, Met. Sci. J. 9, 529 (1975).

74. S. Ceresara, G. Cocco, G. Fagherazzi and L. Schiffini, Philos. Mag. 35, 373 (1977).

75. S. Ceresara, G. Cocco, G. Fagherazzi, A. Giarda and L. Schiffini, La Metall. Italiana 1, 20 (1978).

76. R. Nozato, and G. Nakai, Trans. J.I.M. 18, 679 (1977).

77. F.W. Gayle and J.B. Vander Sande, Bull. Alloy Phase Diagrams 5 (1), 19 (1984).

78. A. Bieber, F. Gautier, G. Treglia and F. Ducastelle, Solid St. Commun. 39, 149 (1981).

79. J.M. Hicter, A. Vermande, I. Ansara and P. Desre, Rev. Int. Temper. Refr. 8, 197 (1971).

80. S.P. Yatsenko and E.A. Saltykova, Russ. J. Phys. Chem. 48, 1402 (1974).

81. S.M. Allen and J.W. Cahn, Acta Metall. 20, 423 (1972).

82. S. Sussman and T.O. Brun, Report SSS-79-183, 1979.

83. N.P. Yao, L.A. Heredy and R.C. Saunders, J. Electrochem. Soc. 118, 1039 (1971).

84. E. Veleckis, J. Less-Common Met. 73, 49 (1980).

85. M. Tamura, T. Mori and T. Nakamura, J. Jpn. Inst. Met. 34, 919 (1970).

86. W.R.D. Jones and P.P. Das, J. Inst. Met. 87, 338 (1959).

87. C.J. Wen, W. Weppner, B.A. Boukamp, and R.A. Huggins, Met. Trans. 11B, 131 (1980).

88. E.S. Balmuth, Scripta Met. 18, 301 (1984).

89. J.M. Papazian, C. Sigli, and J.M. Sanchez, Scripta Met. 20, 201 (1986).

90. R.E. Watson and L.H. Bennett, CALPHAD 5 (1), 25 (1980).

91. C. Colinet, A. Pasturel, and P. Hicter, CALPHAD 9 (1), 71 (1985).

92. R.E. Watson and L.H. Bennett, CALPHAD 8 (4), 307 (1984).

93. J. Friedel, in "The Physics of Metals" (Edited by J.M. Ziman), Cambridge Univ. Press, London (1969).

94. C.M. Varma, Sol. St. Comm. 31, pp 295-297 (1979).

95. D.G. Pettifor, Phys. Rev. Lett. 42, 846 (1979).

96. J.C. Slater and G.F. Koster, Phys. Rev. 94, 1498 (1954).

97. R.E. Watson and L.H. Bennett, in "Theory of Alloy Phase Formation" (edited by L.H. Bennett), The Metallurgical Society of AIME, pp 425-449 (1980).

98. J. Friedel, Adv. Phys. 3, 446 (1954).

99. E.N. Economou, in "Green's Functions in Quantum Physics", Springer Series in Solid-State Sciences 7 (1983).

100. M.J. Kelly, Sol. St. Physics 35, Academic Press, pp 295-383 (1980).

101. R. Haydock, Sol. St. Physics 35, Academic Press, pp 215-294 (1980).

102. R. Haydock, V. Heine and M.J. Kelly, J. Phys C5, 2845 (1972).

103. R. Haydock, V. Heine and M.J. Kelly, J. Phys C8, 2591 (1975).

104. R. Haydock and M.J. Kelly, J. Phys. C8, L290 (1975).

105. P. Turchi, F. Ducastelle and G. Treglia, J. Phys. C15, 2891 (1982).

106. N. Beer and D. Pettifor, ψ_k Newsletter N° 4 Oct. 1982 (Daresbury Lab.), 13 (1982).

107. C. Kittel, in "Introduction à la Physique de l'Etat Physique", Dunod Université, Bordas, Paris (1972).

108. R. Nieminen and C. Hodges, J. Phys. F6, 573 (1976).

109. M.O. Robbins, not published.

110. D.M. Ceperley and B.J. Alder, Phys. Rev. Lett. 45, 566 (1980).

111. W.A. Harrison, Electronic Structure and the Properties of Solids, W.H. Freeman and Company, San Francisco, pp 476-550 (1980).

112. L.F. Mattheiss, Phys. Rev. 134, A970 (1964).

113. O.K. Andersen and O. Jepsen, Physica (Utrecht) 91B, 317 (1977).

114. H. Shiba, Progr. Theor. Phys. 46, 77, (1971).

115. A. Bieber and F. Gautier, Physica 107B, 71 (1981).

116. M.O. Robbins and L.M. Falicov, in Alloy Phase Diagrams, Edited by L.H. Bennett, T.B. Massalski, and B.C. Giessen, MRS Symposia Proceedings, Vol.(19),pp 53-66 (1983).

117. V.L. Moruzzi, J.F. Janak, A.R. Williams, in "Calculated Electronic Properties of Metals", Pergamon Press (1978).

118. C. Sigli, M. Kosugi, and J.M. Sanchez, to be published in Physical Review Letters.

119. O. Kubaschewski and T.G. Chart, J. Inst. Met. 93, 329 (1964-1965).

120. S.C. Singhal and W.L. Worrell, Met. Trans. 4, 1125 (1973).

121. S.C. Singhal and W.L. Worrell, in Metallurgical Chemistry, Proceedings of the International Symposium held at Brunal University, July 14-16 1971 (Edited by O. Kubashewski), Her

Majesty's Stationary Office, London, pp. 65-74 (1972).

122. A.T. Aldred and K.M. Myles, Trans. Met. Soc. AIME 230, 736 (1964).

123. S.C. Singhal and W.L. Worrell, Met. Trans. 4, 895 (1973).

124. A.V. Nagender Naidu, A.M. Sriramamurthy, and P. Rama Rao, Bull. Alloy Phase Diag. 5, 289 (1984).

125. A.R. Williams, C.D. Gelatt, and V.L. Moruzzi, Phys. Rev. Lett. 44, 429 (1980).

126. Yu.O. Esin, M.G. Valishev, A.F. Ermakov, O.V. Gel'd, and M.S. Petrushevskii, Russ. J. Phys. Chem. 55, 421 (1981).

127. J.C. Gachon and J. Hertz, CALPHAD 7, 1 (1983).

128. G.A. Levshin and V.I. Alekseev, Russ. J. Phys. Chem. 53, 437 (1979).

129. M.P. Henaff, C. Colinet, A. Pasturel, and K.H.J. Buschow, J. Appl. Phys. 56, 307 (1984).

130. G.A. Levshin, V.I. Alekseev, G.B. Petrov, and V.I. Polikarpov, Dokl. Akad. Nauk SSSR 269, 870 (1983).

131. J.C. Gachon, J. Charles, and J.Hertz, CALPHAD 9, 29 (1985).

132. P. Steiner and S. Hufner, Acta Metall. 29, 1885 (1981)

133. U.V. Choudary, K.A. Gingerich, and L.R. Cornwell, Met. Trans. 8A, 1487 (1977).

134. P.J. Meschter and W.L. Worrell, Met. Trans. 7A, 299 (1976).

135. P.J. Meschter and W.L. Worrell, Met. Trans. 8A, 503 (1977).

136. V. Srikrishnan and P.J. Ficalora, Met. Trans. 5, 1471 (1974).

137. R.S. Carbonara and G.D. Blue, High Temp. Sci. 3, 225 (1971).

138. P. Villars and L.D. Calvert, in " Pearson's Handbook of Crystallographic Data for intermatallic Phases", Volume 3, p.3059, Am. Soc. of Metals, Metals Park (1985).

139. Metal Handbook, Eight Edition, Vol.8, Am. Soc. of Metals, Metals Park (1973).